Using a weather generator to create future daily precipitation scenarios for Sweden

Deliang Chen[1], Christine Achberger[1], Ulrika Postgård[2]
Alexander Walther[1], Yaomin Liao[1,3], Tinghai Ou[1]

[1]Regional Climate Group, Department of Earth Sciences
University of Gothenburg, Sweden

[2]Swedish Rescue Services Agency, Sweden

[3]Beijing Climate Center, China

EARTH SCIENCES CENTRE
UNIVERSITY OF GOTHENBURG
C75 2007
ISSN 1400-383X

Postadress	**Besöksadress**	**Telefon**	**Telefax**	Earth Sciences Centre
Geovetarcentrum	Geovetarcentrum	031-7861951	031-7861986	University of Gotheburg
S-405 30	Guldhedsgatan 5A			S-40530 Göteborg
Göteborg				SWEDEN

CONTENTS

Abstract

Within project 'Extreme rainfall events in Sweden and their importance for local planning' two main tasks have been the focus: a) identifying trends of precipitation extremes in Sweden using daily precipitation observations from 220 stations during the period 1961-2004, and b) projecting future changes in the extremes over the next 100 years by using a weather generator developed for Sweden. Extreme precipitation is expressed in terms of eight indices, which are chosen from a much larger set of possible indices based on the discussion between the authors and the reference group of the project. They describe specific aspects of extreme precipitation considered to be important for Sweden. These also include indices quantifying means as well as dry conditions. All indices are calculated based on daily precipitation from measurements or simulations by the weather generator developed in this project.

The trend analysis has been reported in an earlier report (Achberger and Chen, 2006). One of the main conclusions is that a clear majority of the stations show trends in all indices towards wetter conditions between 1961 and 2004, implying an increase in precipitation in the annual means and extremes. This finding is generally in line with results from other studies concluding that regions at middle and higher latitudes are getting wetter and extremes are becoming more frequent and more intense. Separate trend analysis for the different seasons show that climate mainly gets wetter in winter, spring and summer, while decreasing trends could be observed at many stations in autumn.

The second task of the project includes several steps to obtain future local information about extreme precipitation climates. 1) a stochastic model or weather generator simulating daily precipitation time series for the present climate is developed for each of the 200 Swedish stations. The observed daily precipitation at these stations is used to calibrate the parameters of the model. 2) Present day climate simulation and future projections of daily precipitations for Sweden from two global climate models (GCMs), ECHAM5 and HadCM3, are extracted and used to get weather generator parameters for the present and future climates at the GCMs scale for Sweden. 3) The ratio of the weather generator parameters for the present climate simulated by the GCMs to those calculated for each station falling into the GCM grid box are computed for all the stations. 4) These ratios are assumed to be valid in the future climate, that way the future parameters for each station under the projected future climate by GCMs can be calculated. 5) Using the estimated future parameters, the future daily precipitation at each station can be simulated with help of the weather generator. 6) Finally the simulated daily precipitation for the future is used to compute the eight indices.

By following all the steps above, future extreme precipitation at local scale in Sweden under the SRES A2-scenario is obtained and presented. As expected, the changes vary from station to station within a short distance, further demonstrating the need of downscaling from GCM scale to local scale. However, an overall trend of increased frequencies and intensity of the extremes can still be identified for the majority of the stations studied. The developed downscaling methodology has been relatively simply but useful in deriving local precipitation changes including changes in the extremes for local application.

1. **Introduction**

The impact of climate change on society due to changes in the atmospheric greenhouse gas concentrations is of fundamental importance for the future planning and management. The characteristics of extreme events are part of the climate. As the climate changes, the characteristics of extremes may also change (Beniston and Stephenson, 2004). For many impact applications and decision support systems, extreme events are much more important than the mean climate (Mearns et al., 1984). Change in extremes may be due to the mean effect (e.g. Wigley, 1985), the variance effect (e.g. Katz and Brown, 1992), or a combination of the mean and variance effects (e.g. Brown and Katz, 1995), or the structural change in shape etc (e.g. Beniston, M., 2004).

Extreme climate events can be defined as maxima/minima during a certain period of time, magnitude (a threshold of a variable), rarity, and the size of impacts such as losses. According to the IPCC (2001, p. 790), "An extreme weather event is an event that is rare within its statistical reference distribution at a particular place. Definitions of 'rare' vary, but an extreme weather event would normally be as rare as or rarer than the 10th or 90th percentile. By definition, the characteristics of what is called extreme weather may vary from place to place. An extreme climate event is an average of a number of weather events over a certain period of time, an average which itself is extreme (e.g. rainfall over a season).".

For many applications daily weather data are required. In particular, extreme events over short period are much more important than the mean climate over long period of time. The question of changes in climate and weather extremes is of fundamental interest to the economic well-being of all nations and poses a challenging scientific question to understanding natural and anthropogenic climate variability (IPCC, 2001).

The awareness that global climate change not only leads to changes in the mean climate but may also cause more frequent and more severe weather extremes have triggered an intensive research to answer the question of whether or not the climate is becoming more extreme. This is by no means a surprising development in the light of today's vulnerability against events like heavy rainfalls, drought, hot spells, or storms etc. Any increase in frequency or extent of such events is therefore expected to have profound consequences for economics and societies even in the future.

While an increasing number of climate model studies indicate that rising contents of greenhouse gases in the atmosphere will probably lead to more severe weather conditions in the future, it is of great importance to increase our understanding regarding the occurrence of climate extremes in the recent and more remote past. During the last five to ten years, a large number of studies have therefore been carried out focusing on various aspects of climate extremes (mainly temperature and precipitation) in different regions of the world (e.g. Trenberth, 1999; Easterling et al., 2000; Beniston and Stephenson, 2004). Depending on research tasks, different measures were used to quantify extremes, which not always allow direct comparison of results. A general conclusion of many of these studies is, however, that changes in extreme temperature and precipitation have occurred world-wide during the past century along with the ongoing climate change in terms of the mean temperature. Yet, it is still hard to draw a firm conclusion from these studies, whether these changes are due to natural variability or caused by anthropogenic activity (IPCC, 2001). To mention some examples, Groisman et al. 1999 studied the probability distribution of daily precipitation in eight countries located on different continents and concluded that increased mean precipitation is associated with an increase in heavy rainfalls. In their near-global analysis, Frich et al. 2002 found regions with both negative and positive changes in wet extremes, with parts of Europe having more robust positive changes. On a more regional scale, Moberg and Jones (2005) investigated trends in daily temperature and precipitation extremes across Europe over the past century and found that

both mean precipitation and wet extremes have increased mainly during winter. Also Klein Tank and Können (2003) found an increase in the annual number of moderate and very wet days between 1946 and 1999. According to Haylock and Goodess (2004), inter-annual variability and trends in extreme winter rainfall are to a large extent linked to variations in the North Atlantic Oscillation (NAO). Numerous studies have also been carried out at the national level. Fowler and Kilsby (2003) studied multi-day rainfall events in the UK since 1961 and found significant but regionally varying changes in the 5- and 10-day events which they consider as having important implications for the design and planning of flood control measures. Other examples from central Europe include Schmidli and Frei (2005) who found significant increasing trends in winter and autumn rainfall in Switzerland or Hundecha and Bardossy (2005) who found increasing precipitation extremes across western Germany since 1958. Earlier studies on precipitation extremes in Europe also included data from Nordic countries (e.g., Moberg and Jones, 2005; Klein Tank and Können, 2003; Frich et al., 2002), but the number of Scandinavian stations was generally rather limited, which did not allow spatial variability of rainfall extremes be studied in more detail.

The overall aim of the project "Extreme rainfall events in Sweden and their importance for local planning" supported by Swedish Rescue Services Agency is to identify changes in precipitation extremes in Sweden during the past 44 years and to project their future changes. More specifically, the objectives of the project are twofold: 1) to identify trends of precipitation extremes in Sweden during the period 1961-2004 at all Swedish stations, 2) to develop a weather generator to be used in projecting future changes in the extremes over the next 100 years. This report summarizes the outcomes of the second task of the project focusing on future precipitation extremes derived from local precipitation scenarios covering the 20th century. Results from the first objective are presented in Achberger and Chen (2006).

2 Methods

This section describes the data sets and methods used to estimate precipitation extremes in Sweden, both for future climate conditions as well as for today's climate. Although the main focus is on the methods used to project future local precipitation conditions taking climate change into account, the data set of daily precipitation observations is briefly described in Section 3.1 because the future scenarios of climate change are also calculated for these stations. Furthermore, the calculation of the indices quantifying precipitation extremes for today's climate is briefly described. More detailed information on the indices can be found in Achberger and Chen (2006).

2.1 Station observations and precipitation indices

2.1.1 Station data

Within this study, daily precipitation data in Sweden were used covering the period 1961-2004. In total, daily data from 366 precipitation stations were provided by SMHI (Swedish Meteorological and Hydrological Institute). Due to a rather high fraction of missing days at many stations, a considerable number of stations had to be excluded. It was therefore decided to only include stations having less than 10% missing data, reducing the original number of the total stations to 220. Figure 2.1 shows the location of stations used in the study. Station density varies across the region and is in general lower in the northern half of the country and in the mountainous areas.

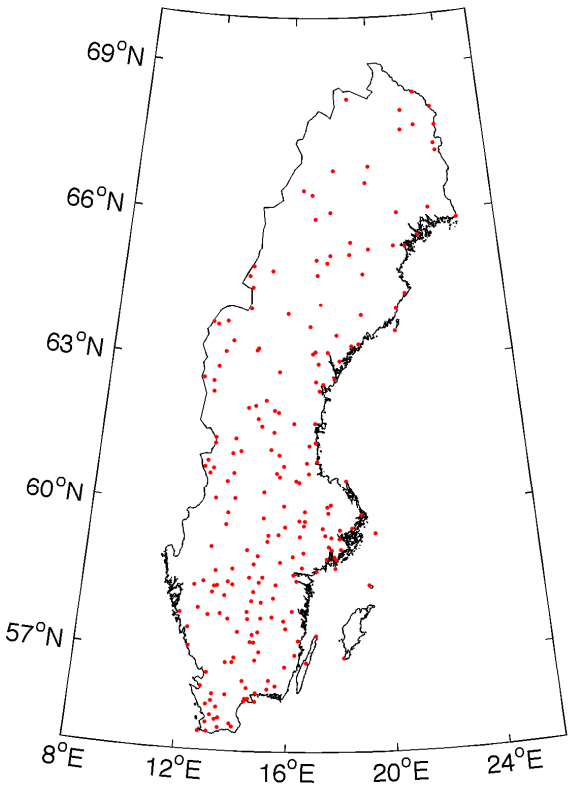

Figure 2.1: Location of the 220 precipitation stations in Sweden used in this study. They all record daily precipitation for the period 1961-2004 and have <10 % missing data.

2.1.2 Precipitation indices

To enable objective quantification and characterization of climate variability and change, The Expert Team on Climate Change Detection Monitoring and Indices (ETCCDMI) has compiled a catalogue of so called climate change indices (Karl et al. 1999, Nicholls and Murray 1999). These indices are calculated from daily observations of the key climate variables temperature and precipitation and describe various statistical properties. They serve as a practical and standardized tool to monitor changes in the statistical properties of the climate focusing on extremes and have already found wide application within the climate research community. Climate change indices quantify rarely occurring temperature and precipitation events as well the mean climate conditions, providing the general climatological background necessary to place extremes into a broader context.

In this study, eight precipitation indices are used to quantify various properties of the past and the future local precipitation climate in Sweden, such as occurrence and magnitude of precipitation extremes. These indices partly belong to the aforementioned climate change indices by Karl et al. (1999) and Nicholls and Murray (1999), however, during the course of the project work, several "own" indices were added which were considered as useful in several practical applications. Table 2.1 lists the various indices and their implication.

Table 2.1: Precipitation indices used in this study.

Index	***Description***	***Implication***
nrain	no of rain days with precipitation>0.1 (%)	precipitation occurence
*pint **	precipitation intensity (rain per rain day, mm/day)	daily intensity on rainy days
*pq90 **	90th percentile of rain day amounts (mm/day)	intermediate precipitation extreme
*pxcdd **	max no. consecutive dry days (days)	measure for risk of dryness
px1d	greatest 1-day total rainfall (mm)	measure of short-term extremes
*px5d **	greatest 5-day total rainfall (mm)	measure of longer-term extremes
exc25	number of days with precipitation $\geq$ 25 mm (days)	rare extreme event
exc40	number of days with precipitation $\geq$ 40mm (days)	very rare extreme event

2.2 Weather generator

Stochastic weather generators (models) were developed and used in estimating the future precipitation conditions at the local scale. A weather generator (WG) is a statistical model that generates sequences of daily weather data resembling the statistical properties of the data to which they have been fit (Hutchinson, 1995). WG are nowadays widely used in many applications since they can provide additional data when the observed climate record is insufficient with respect to length, completeness, or spatial coverage (Wilks, 1999). Since these models are computationally fast and can be set up for different climate variables such as precipitation, temperature and radiation, they have been frequently used. One important application is to translate the coarse information from global climate models (GCM) to the local scale for climate impact studies. This process is usually called downscaling (Hanssen-Bauer et al., 2005). In this study, site-specific WG models for daily precipitation were developed for the 220 sites in Sweden shown in Figure 2.1.

The type of WG used here is a two-state Markov chain model as suggested by Richardson (1981). It simulates precipitation occurrence and precipitation intensity in two separate steps. In the first step it is determined whether a certain day is dry or wet involving two conditional probabilities: *p10* (the

probability of a dry day (0) following on a wet day (1)) and *p01* (the probability of a wet day following on a dry day). In all, the two-state Markov chain uses four conditional probabilities:

P (*wet* |*dry*) = *p01* (2.1)
P (*dry* |*dry*) = *p00*= 1-*p01* (2.2)
P (*dry* |*wet*) = *p10* (2.3)
P (*wet* |*wet*) =*p11*=1-*p10* (2.4)

where *p00* is the probabilites of a dry day following a dry day, and *p11* is the probability of a wet day following a wet day. These four transition probabilities were derived from the daily precipitation observations from 1961 to 2004 individually for each of the 220 sites. In addition, since these parameters vary over the course of the year, *p01, p11, p10* and *p00* were calculated separately for each of the 12 calendar months.

The precipitation amounts for wet days are determined in the second step using a random number generator. To ensure that the simulated precipitation intensities have the same statistical properties as the observed ones, the randomly generated precipitation has to be taken from a distribution resembling the observed precipitation frequency. Typically, the frequency distribution of daily precipitation is strongly "skewed" to the left, which implies that there exist a large number of days with relatively small amounts and a small fraction of days with larger amounts. One distribution function that is often used to describe the empirical frequency distribution of daily precipitation is the Gamma-distribution with shape parameter α and the scale parameter β:

$$f(\chi)=\frac{(\chi/\beta)^{\alpha-1}\exp(-\chi/\beta)}{\beta\Gamma(\alpha)} \qquad \chi,\alpha,\beta>0 \qquad (2.5).$$

The shape parameter indicates the skewness of the distribution whereas the scale parameter is related to the total precipitation amount. Figure 2.2 visualizes the Gamma distribution using different combinations of α and β: in Figure 2.2a) β=5 and α varies between 0.5 and 4; in Figure 2.2b) α=0.8 and β ranges between 4 and 10 (α=0.8 and β=5 are typical values for Swedish precipitation). Clearly, the skewness of the distribution increases with increasing α when β is kept constant, while the growing β moves the distribution "to the right" on the x-axis when keeping α constant. In general, larger α and β implies stronger extremes given that the other parameter is kept constant.

The Gamma-parameter derived from Swedish precipitation observations vary from site to site and over the course of the year. They were therefore, like the transition probabilities, estimated individually for each station and each calendar month.

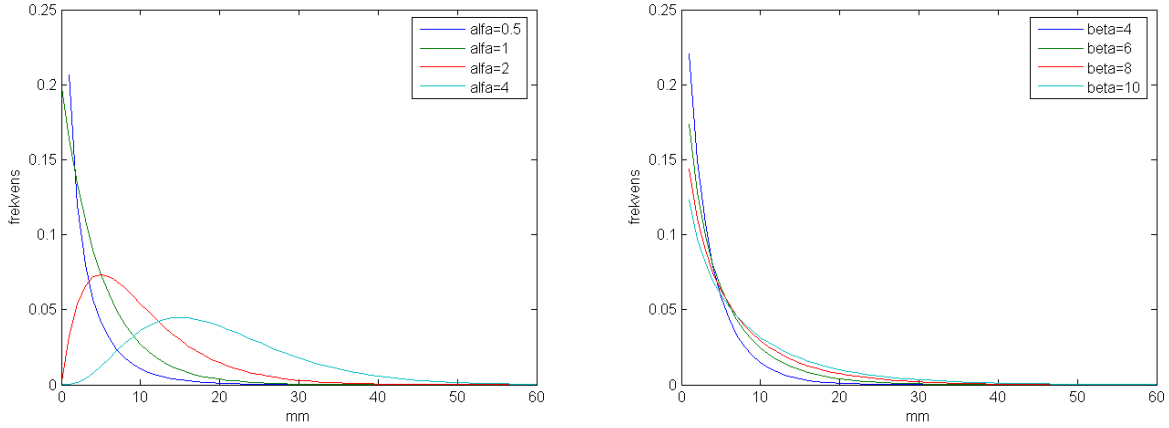

a) b)

Figure 2.2: Gamma distribution using different combinations of the shape parameter α and the scale parameter β. a) β has a constant value of 5 and α varies between 0.5 and 4, b) α has a constant value of 0.8 and β varies between 4 and 10. (α=0.8 and β=5 are typical values for Swedish precipitation.)

When simulating daily precipitation, in the first step it is determined whether a certain day is wet or dry based on the monthly transition probabilities. If a day is simulated as a wet day, the precipitation amount for this day is simulated by means of the parameters of the Gamma-distribution:

$$R = \left[-\frac{RN1^{\frac{1}{\alpha}}}{RN1^{\frac{1}{\alpha}} + RN2^{\frac{1}{1-\alpha}}} \times \ln(RN3) - \ln(RN4) \right] \times \beta \qquad (2.6)$$

where R is the precipitation amount, and RN1, RN2, RN3 and RN4 are random numbers generated by the computer programme.

Prior to the calculation of the local precipitation scenarios for future climate conditions, WG simulations were carried out for each site using the *observed* WG-parameters. This was done to test the functioning of the WG and to evaluate the performance of the WG against observations. The outcome of the evaluation is presented in Section 3.2.

2.3 GCM scenarios

In order to be able to simulate future precipitation conditions at the stations, the parameters of the WG calibrated using the past observations need to be modified to take global climate change into account. The changed parameters should represent the precipitation conditions of the future climate. In the following, the necessary steps to adapt the WG to future climate conditions are described.

In a climate change study, the information about the future climate conditions is usually obtained from climate change scenarios provided from global climate models (GCM). In this study, daily precipitation data from the German GCM ECHAM5 and the English GCM HadCM3 were used to derive the weather generator parameters for the simulation of the future precipitation conditions at the various sites. In Table 2.2, information about the spatial resolution of the GCM's and the time period of the simulation runs are given. The GCM's differ with respect to spatial resolution and time period of the model runs. From each GCM, two model runs are used: one representing today's climate conditions, (the control run), and one for the future climate conditions (the scenario run). The latter runs are based on the IPCC Second Report on Emission Scenarios (SRES) A2-scenarios.

Table 2.2: Global Climate Models (GCM) used in this study. The spatial resolution and the time period of the control run representing today's climate conditions and the scenario simulations for the future are also given.

Climate model	***Spatial resolution***	***Model run***
ECHAM 5 Max-Planck-Institut für Meteorologie, Hamburg	1.8°lon x 1.8°lat	Control run 1961-2000 Scenario run (SRES A2) 2046-2065, 2081-2100
HadCM3 Hadley Centre, Bracknell, UK	3.75°lon x 2.5°lat	Control run 1961-1989 Scenario run (SRES A2) 2070-2099

Due to differences in the spatial resolution of the GCMs, the number of the grid boxes covering Sweden and their location differs considerably between ECHAM5 and HadCM3. The figures below show the location of the GCM grid boxes over Sweden (Figure 2.3a) and the number of stations located within each grid box (Figure 2.3b). Here, the significantly lower spatial resolution of the HadCM3 model is very obvious.

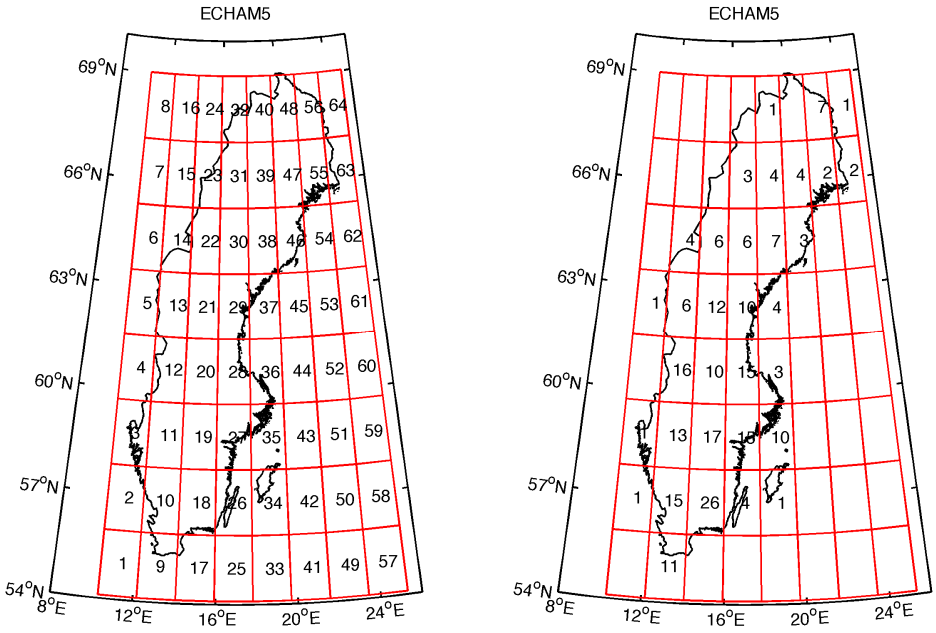

a) b)

Figure 2.3: Layout of the model grid used by ECHAM5. a) Numbering of the ECHAM5 grid boxes over Sweden; b) number of precipitation stations within each grid box (boxes without any number do not have any stations).

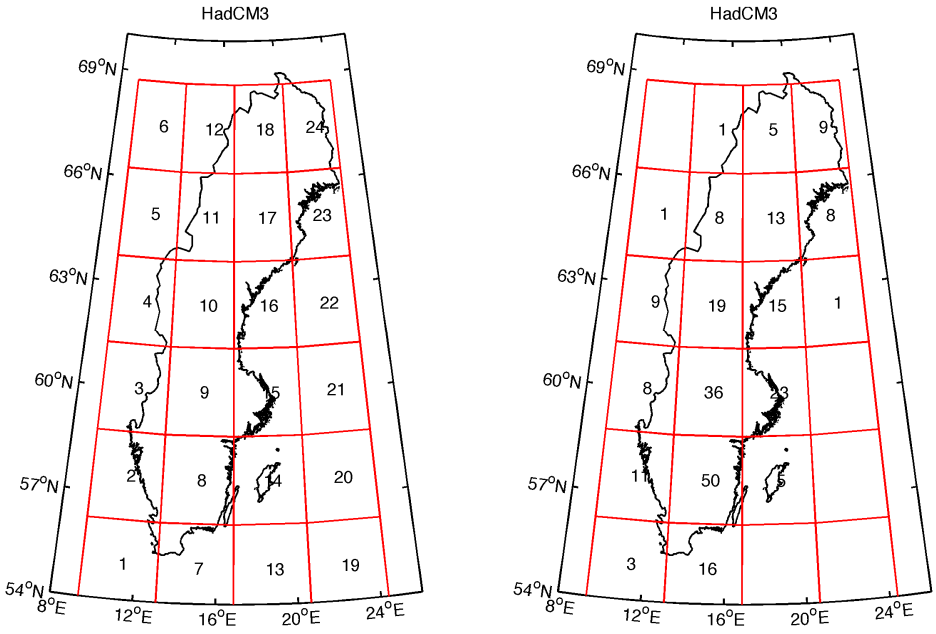

a) b)

Figure 2.4: Layout of the model grid used by HadCM3. a) Numbering of the HadCM3 grid boxes over Sweden; b) number of precipitation stations within each grid box (boxes without any number do not have any stations).

2.4 Downscaling of GCM scenarios by scaling the WG parameters

Since GCMs operate on the global scale, the spatial scale at which information is provided by these models is almost always too coarse to estimate climate changes at the regional and local scale (Benestad et al., 2008). Many practical applications, aiming at studying and estimating the impact of climate change on e.g., ecosystems, societies and different aspects of human life, require information at the regional and local scale. The output from GCMs therefore needs to be post-processed in order to translate the coarse-resolved GCM information to the finer scale, a procedure commonly known as "downscaling" (Benestad et al., 2008). During the past years, many different methods have been developed to downscale climate information from GCMs for northern Europe including Sweden (Hanssen Bauer et al., 2005). One downscaling approach often used in other regions is to apply site-specific WG with parameters modified based on information from GCMs runs to represent future climate conditions at the local scale.

Several approaches have been developed to use a WG to construct local climate change scenarios (e.g. Wilks, 1992; Semenov and Barrow, 1997). In principle, parameters of the WG need to be modified according to the climate change scenario from a GCM to generate local climate under changed climate conditions.

As an example, the weather generator used is firstly calibrated using 'average' weather data for a particular region, roughly corresponding to the size of an appropriate GCM grid box, with the resulting parameters describing the statistical characteristics of that region's weather. This 'average' weather is calculated using a number of stations from within the relevant region. The WG is also calibrated at each of these individual stations.

Then relationship between the parameters of the region and individual stations are established. Secondly, daily GCM data for the grid box corresponding to the area-average weather data are used to obtain corresponding parameters. The relationship between the GCM grid scale parameters an dthe station parameters established using past observations is used to estimate parameters at individual stations for the future climate, which allows the generation of scenarios for each station within the area (e.g. Wilks and Wilby, 1999).

The key to the success of the method is how to reliably estimate the local WG parameters at the stations for the future climate, since the parameters for the present day climate are already known from the past observations. Once the future parameters are available, the calculation of future daily precipitation is straightforward. As there are no 'observations' for the future, we have to rely on the simulations of the GCMs for the future providing WG parameters for the future at the GCM grid scale. Then the next question is how to get local parameters from those at the GCM grid scale.

From simulated present day climate (control run), we can estimate WG parameters for the present climate at the GCM grid scale. These estimates can be compared with those estimated from the observations at the stations if the local parameters can be properly scaled up to the GCM grid scale. If we **ASSUME** that the ratio of the parameters of the future climate at a station to those of the future climate at the GCM grid scale remains the same as the ratio of the parameters at the station of the present day climate to those of the present day GCM simulations, we can estimate the future parameters at the station with help of the GCM simulations for the present day and future climates, together with those estimated from the past observations at the station. The procedure of scaling the WG-parameter is illustrated in Figure 2.5.

Following the procedure outlined in Figure 2.5, daily precipitation data for each GCM grid box over Sweden containing at least one precipitation station has been extracted, both for the control run and

the scenario run. Using these time series of simulated daily precipitation, the transition probabilities and the parameters of the Gamma-distribution were derived in the same way as from station observations. For each GCM this resulted in two sets of WG parameters for each grid box, one for the control run and one for the scenario run. Like for station precipitation, the WG parameters were calculated separately for each calendar month. Then, in the next step, for each station and each month, the ratios *R* were calculated between the WG parameters from the GCM control runs and the observations:

$$R = WG\_observation \Big/ WG\_GCM_{control} \qquad (2.7).$$

This resulted in a set of 72 ratios per station (six WG parameter * 12 months). Finally, the local WG parameters for the future were calculated as:

$$WG\_station_{future} = WG\_GCM_{scenario} * R \qquad (2.8).$$

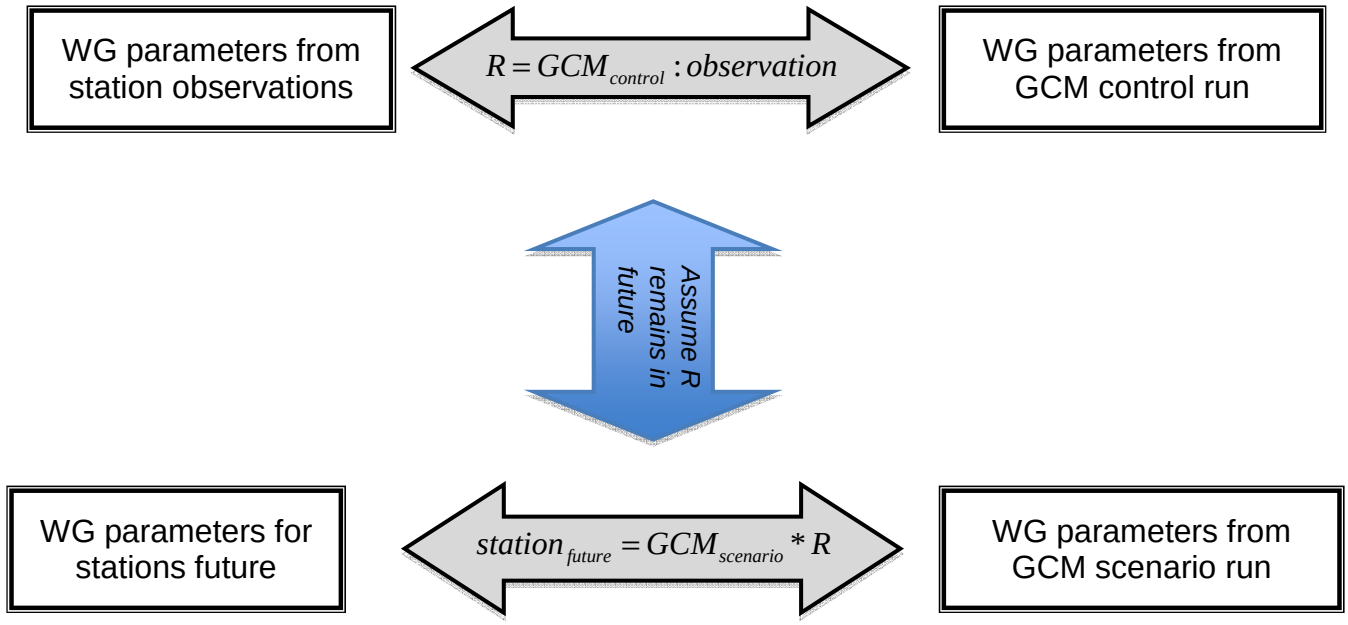

Figure 2.5: Scaling of the WG parameter used in this study assuming that the ratio *R* between the WG parameter from the GCM control run and the observations remains constant in the future.

2.5 Local precipitation scenarios

With the new set of WG-parameters for the changed climate, the future precipitation was simulated at each station. 100 years of daily precipitation were simulated, representing the climate conditions for the years 2081 to 2100 in the case of the ECHAM5-based simulation, and the years 2070-2099 in the case of the HadCM3-based model runs. Even though, the ECHAM5 (HadCM3) time slice only covers 20 (30) years, the weather generator simulated local series for a period of 100 years, in order to achieve higher statistical confidence in the simulated precipitation series. This is especially important when the simulations are used to derive statistics about relatively rare events, i.e., extremes.

All precipitation indices listed in Table 2.1 were calculated from the simulated series at each of the 220 stations in exactly the same ways as was done for the observations. Then, the differences between the observation-based indices and the WG-simulation based indices were calculated at each station, both as annual and seasonal means. The difference in the indices is used to quantify the magnitude of change in precipitation climate at local scale.

3 Results

3.1 Precipitation indices WG parameters derived from station observations

This Section presents precipitation indices and weather generator parameters derived from observations. The various statistics are presented as maps showing the spatial distribution across Sweden, both for annual and seasonal means. Regarding precipitation indices, only two examples are given here. Maps for a large number of different indices can be found in Achberger and Chen (2006).

3.1.1 Selected precipitation indices

a) Regional patterns

The two precipitation indices chosen here are *pint*, representing precipitation intensity during rainy days and *px5d*, quantifying more persistent rain events that increase the risk for flooding.

Annual mean intensities vary between 2.0 and 6.5 mm/day depending on region. The largest mean values are found in the South-West of Sweden, in central Sweden and at some scattered places in the mountainous areas (Figure 3.1). Intensities are generally lower in the South-East of Sweden and in the inner parts of Northern Sweden where *pint* rarely exceeds 4.0 mm/day. Some coastal-near stations along to Baltic Sea Coast in the county of Gävleborg have larger daily intensities, which can probably be explained by the proximity to the Baltic Sea and the shape of the coastline. Calculating pint for different seasons shows a clear seasonal variation with low intensities in winter and the largest amounts during the summer months (Figure 3.2).

The map of the annual *px5d* (Figure 3.3) shows a considerable spatial variation in the precipitation amounts. The regional patterns of *pint* and *px5d* are similar in large parts of Sweden with relatively low values in parts of the counties of Uppsala, Stockholm, Södermanland, Östergötland, Jönköping, Kronoberg, Kalmar, Blekinge, Scania and partly Norrbotten. Higher values of *px5d* can be found at some stations in the counties of Västra Götaland, Värmland, Dalarna and Gävleborg, as well as at some scattered stations in the mountains of the county Jämtland. Index *px5d* is highest during the summer months and the regional differences are smaller compared to other seasons. During autumn, the coastal stations in the county of Gävleborg and some stations in Västra Götaland are the ones with the highest values (Figure 3.4).

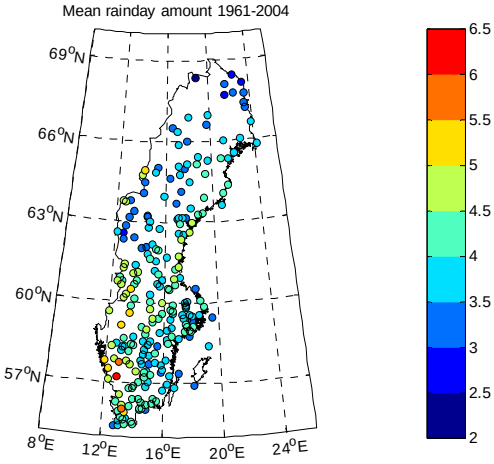

Figure 3.1: Annual mean of *pint* (precipitation intensity during rainy days) in mm/day for the period 1961-2004.

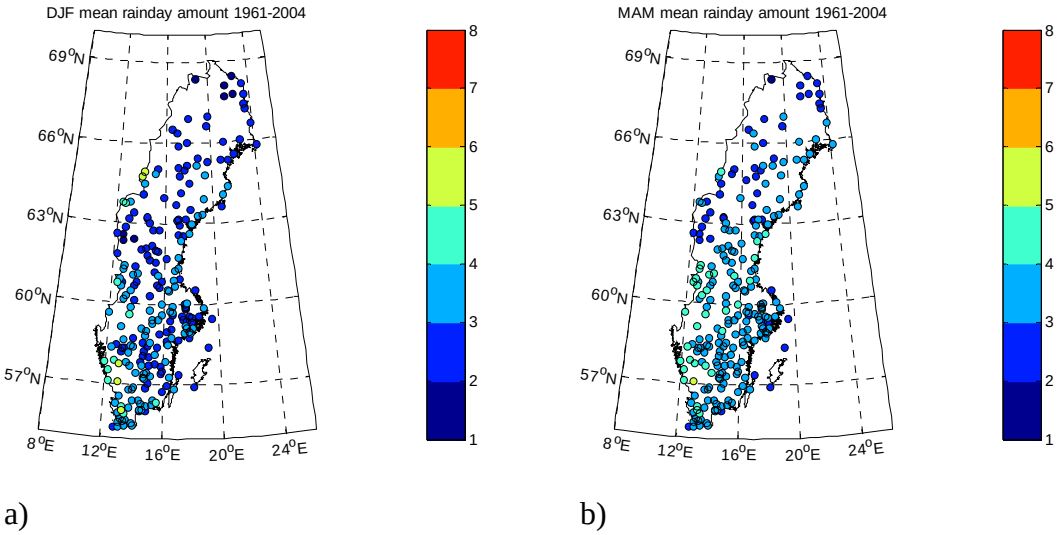

a) b)

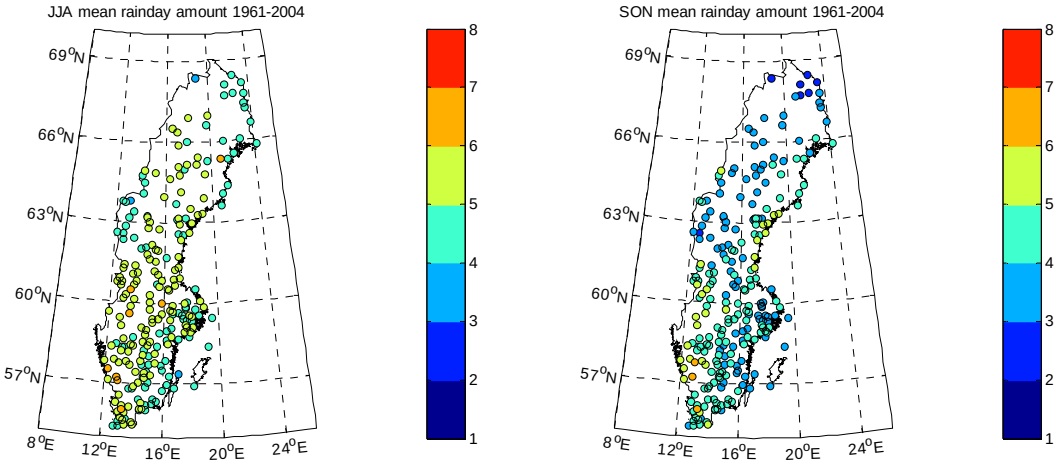

c) d)

Figure 3.2: Seasonal mean of *pint* (precipitation intensity during rainy days) in mm/day for the period 1961-2004. a) winter, b) spring, c) summer, and d) autumn.

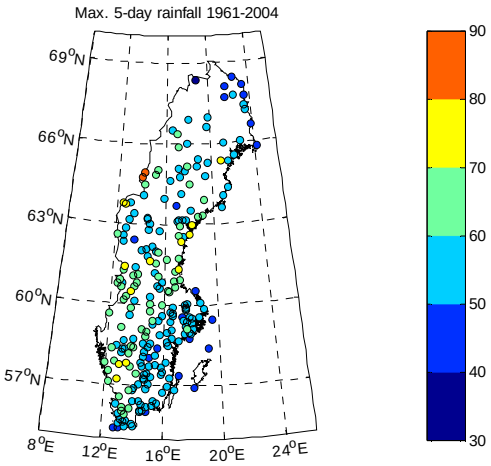

Figure 3.3: Annual mean of *px5d* (largest 5-day accumulated precipitation amount) in mm/5-days for the period 1961-2004.

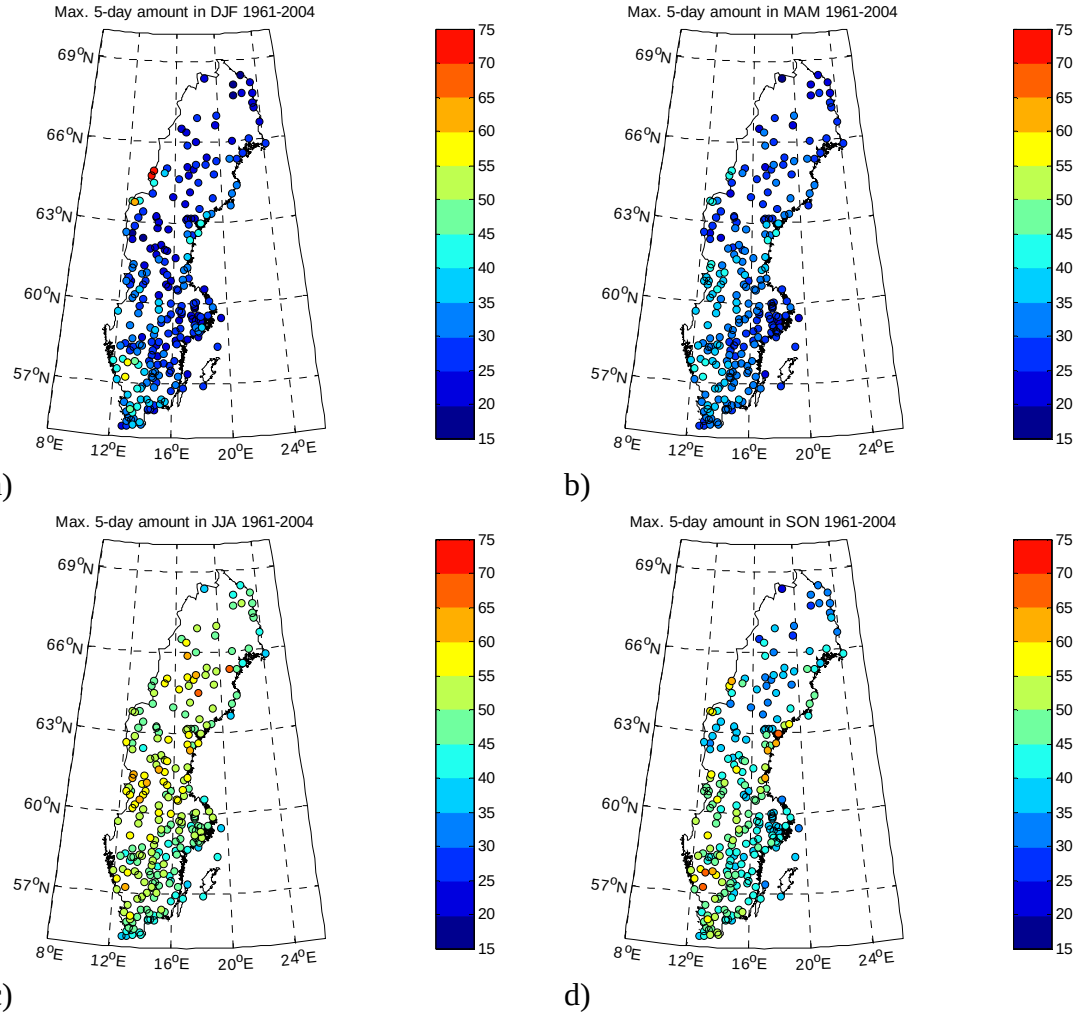

a) b)

c) d)

Figure 3.4: Seasonal mean of *px5d* (largest 5-day accumulated precipitation amount) in mm/5-days for the period 1961-2004. a) winter, b) spring, c) summer, and d) autumn.

3.1.2 Weather generator parameters

a) Spatial distribution of weather generator parameters

To visualize the regional patterns of the weather generator parameters derived from station observations, the transition probabilities *p11* and *p00* as well as α and β of the Gamma-distribution are shown on maps (Figure 3.5 to 3.12). Here, examples are given for four months; January, April, July and October representing the conditions for the four different seasons.

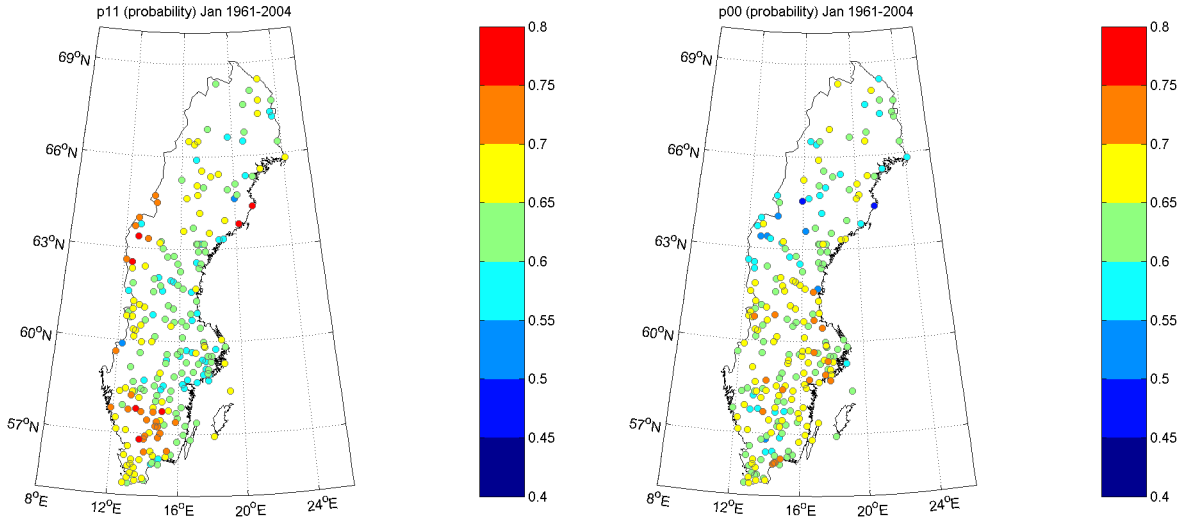

a) b)

Figure 3.5: Transition probabilities in January derived from daily precipitation observations at 220 stations for the period 1961 to 2004. a): *p11*, (probability of a wet day following on a wet day) and; b): *p00* (probability of a dry day following on a dry day).

Figure 3.5a) shows that *p11* exceeds 0.5 during winter at almost all stations, indicating that there is a relatively high fraction of consecutive wet days in January. Regarding the geographical pattern of *p11*, there are several regions with similar transition probabilities, e.g., the Swedish West Coast, central Småland and parts of Svealand. The highest *p11* values are found in central Småland and at some stations in the mountains, which presumably is an effect of the more pronounced topography in these parts of Sweden. For *p00*, the values are in general lower than *p11*. There is a general decreasing trend from South to North, indicating that consecutive dry days occur more often in Southern Sweden than in Northern Sweden.

Regarding April, *p11* is slightly lower than during winter implying fewer occasions with consecutive wet days (Figure 3.6). In parallel, *p00* is increasing from January to April.

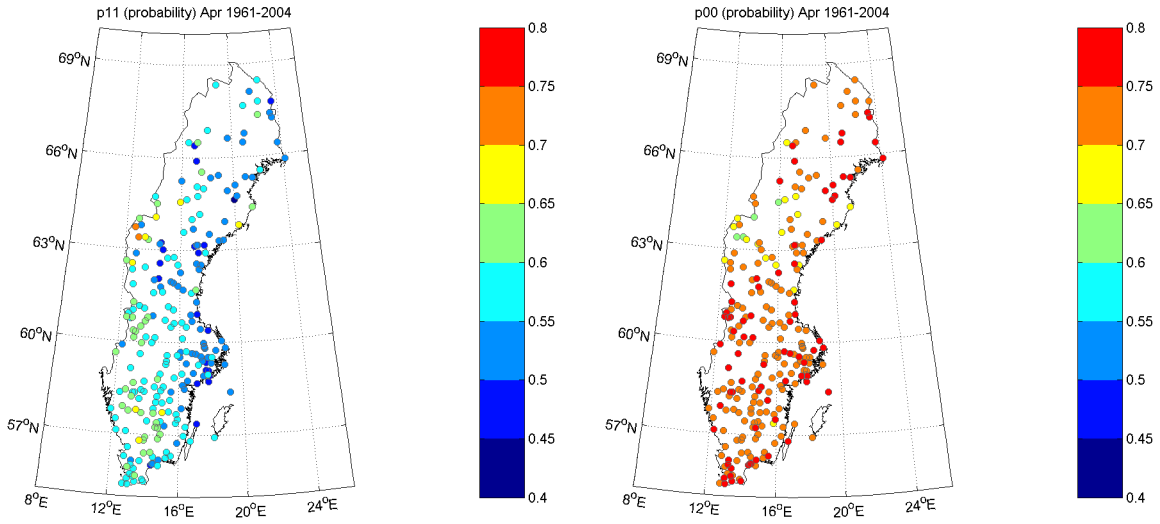

Figure 3.6: Transition probabilities in April derived from daily precipitation observations at 220 stations for the period 1961 to 2004. a): *p11*, (probability of a wet day following on a wet day) and; b): *p00* (probability of a dry day following on a dry day).

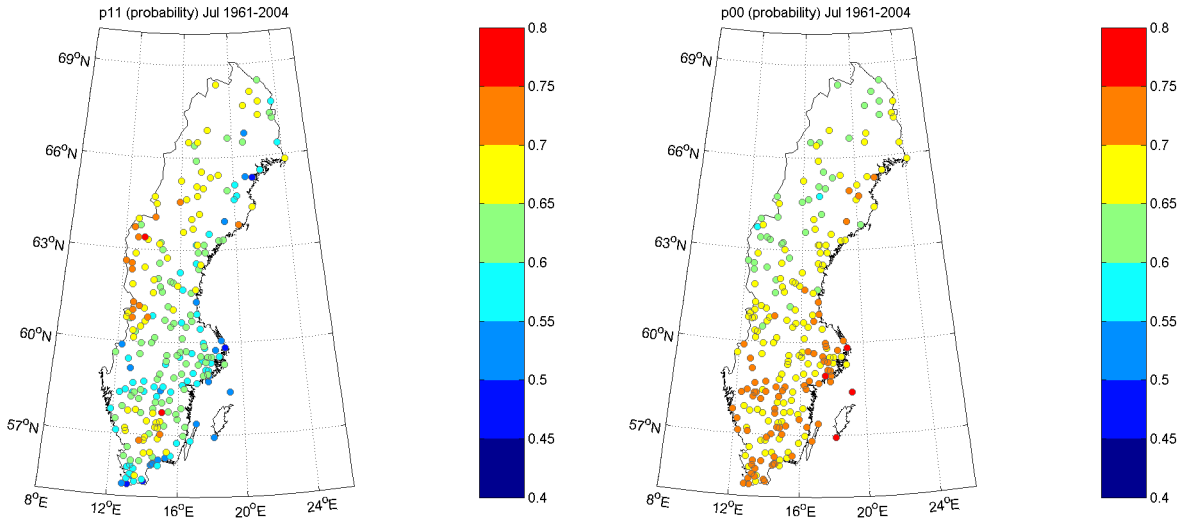

a) b)

Figure 3.7: Transition probabilities in July derived from daily precipitation observations at 220 stations for the period 1961 to 2004. a): *p11*, (probability of a wet day following on a wet day) and; b): *p00* (probability of a dry day following on a dry day).

Even during summer, the spatial pattern of *p00* and *p11* is similar to the winter and spring pattern (Figure 3.7). The probability *p11* is generally higher than in April and increases from South to North. Consecutive wet days are therefore more usual during summer than during spring but less frequent than during winter. Even in summer, there are regions with rather similar *p11* (Figure 3.7a): coastal-near stations often have *p11*>0.55, while *p11*>0.65 is typical for central Småland, mountainous regions and parts of Norrland. In July, the decreasing trend in p00 from South to North is very obvious (Figure 3.7b), implying more occasions with consecutive dry days in Southern Sweden. The generally high values of *p00* in the whole of Sweden clearly decrease towards the summer.

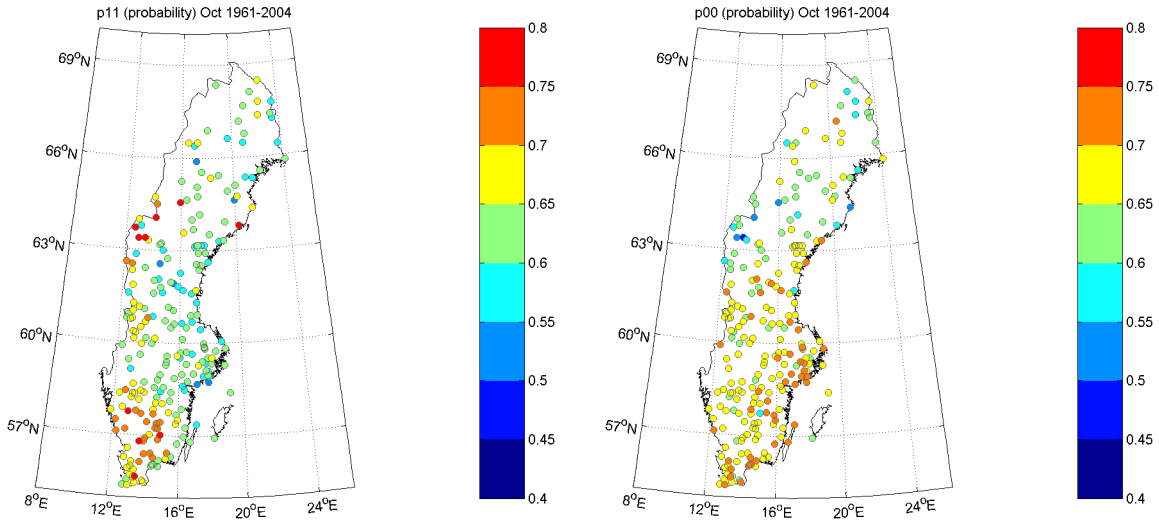

Figure 3.8: Transition probabilities in October derived from daily precipitation observations at 220 stations for the period 1961 to 2004. a): *p11*, (probability of a wet day following on a wet day) and; b): *p00* (probability of a dry day following on a dry day).

The autumn pattern of *p11* and *p00* are very similar to the corresponding winter patterns (Figure 3.8 a), however, during autumn dry periods are more frequent in Southern Sweden than during winter. From the maps, the general conclusion can be drawn that the geographical distribution of the transition probabilities are quite stable over the course of the year. Only the values of the probabilities change with season.

Figure 3.9 to 3.12 below show the distribution of the Gamma-parameters across Sweden for January, April, July and October. The January values for α vary between 0.6 and 1.3, but are generally slightly lower in Southern Sweden compared to α in the northern part of the country. Regarding the spatial variability, in January and April there is a considerably larger variability in α compared to July and October, when α only ranges between 0.6 and 0.9. Despite the large-scale spatial trend with slightly higher α-values in northern Sweden in winter, it is difficult to distinguish other homogeneous areas. The values for β in January are on average lower than in July, indicating that precipitation amounts are in general lower during winter than during summer. In spring and autumn, the β-values range between the summer and winter values. There is relatively little spatial variability in all four months, making it difficult to distinguish larger, homogeneous regions. Generally, from the maps of α and β it can be concluded that the parameters clearly vary with season. Typically, α is higher and β is lower during autumn and winter, while the conditions are reversed in spring and summer.

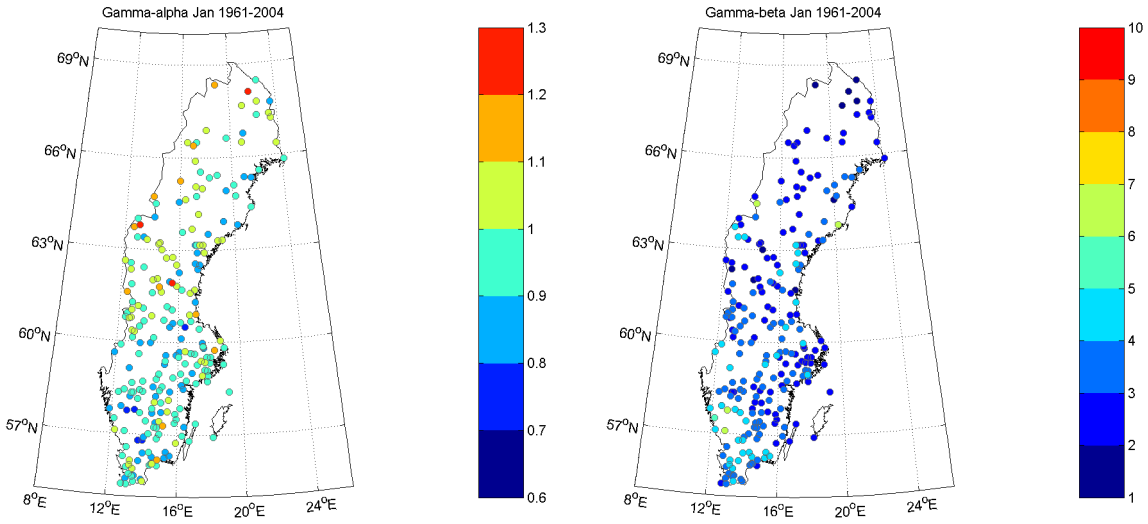

a) b)

Figure 3.9: Gamma parameters for January derived from daily precipitation observations at 220 stations for the period 1961 to 2004. a) Gamma α; b) Gamma β.

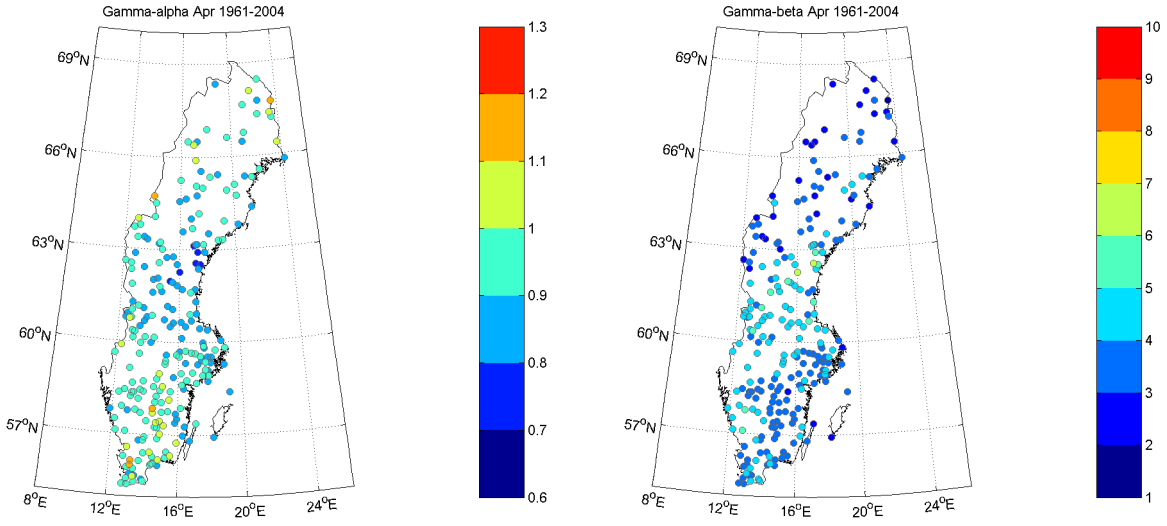

a) b)

Figure 3.10: Gamma parameters for April derived from daily precipitation observations at 220 stations for the period 1961 to 2004. a) Gamma α; b) Gamma β.

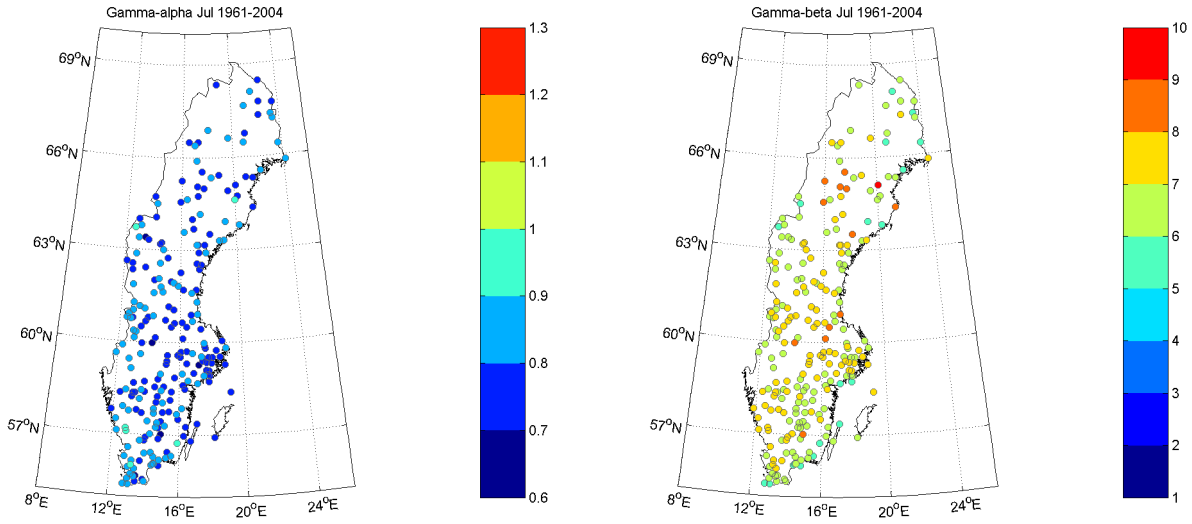

a) b)

Figure 3.11: Gamma parameters for July derived from daily precipitation observations at 220 stations for the period 1961 to 2004. a) Gamma α; b) Gamma β.

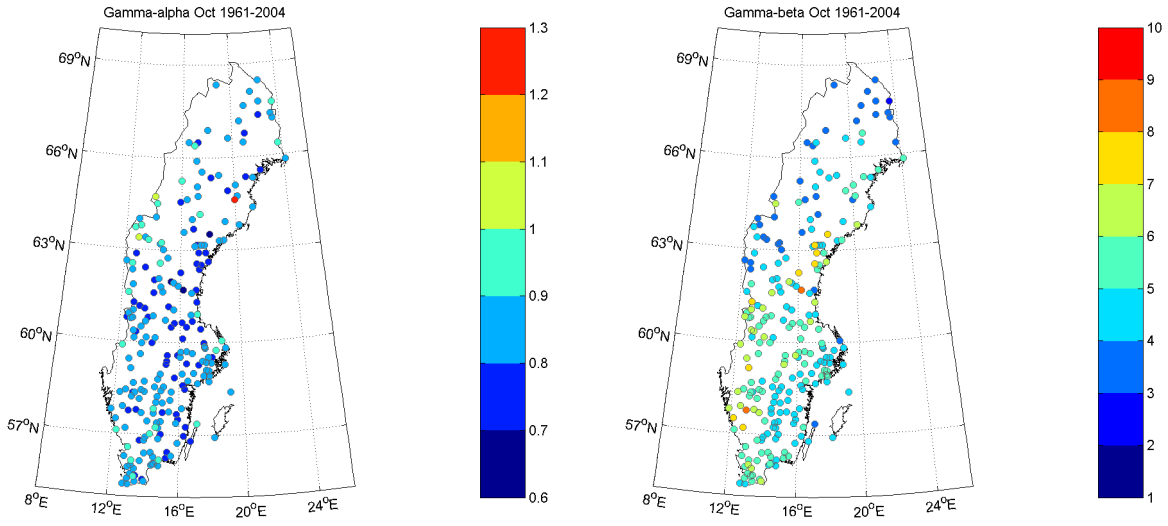

a) b)

Figure 3.12: Gamma parameters for October derived from daily precipitation observations at 220 stations for the period 1961 to 2004. a) Gamma α; b) Gamma β.

b) Seasonal distribution of weather generator parameters

The monthly variability in the WG-parameters is given in the Figures 3.13 and 3.14. They show the average over all stations for each month together with the spread in the values indicated by the length of the bars (ranging between -1 and +1 standard deviation). There is a very distinct yearly pattern in the transition probabilities with high *p00* and low *p11* during spring and summer. The variability between the stations is rather constant from month to month, however, it is slightly larger for *p11* than for *p00*.

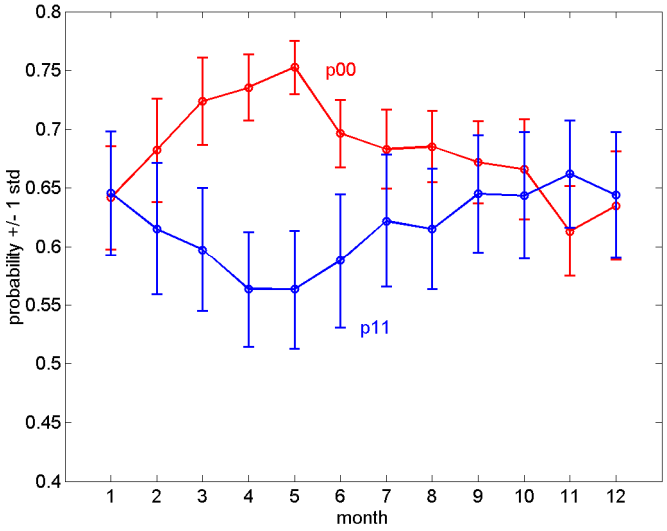

Figure 3.13: Monthly transition probabilities *p00* (probability of a dry day following on a dry day) and *p11* (probability of a wet day following on a wet day) averaged over all stations for the period 1961 to 2004. The length bars indicate the spread around the mean ranging in the interval +/- 1 standard deviation.

Even the Gamma parameters show a clear seasonal cycle (Figure 3.14) characterized by higher α and lower β in autumn and winter (vice versa in spring and summer). The distinct seasonal cycle in the WG-parameters clearly shows the need to develop the models in such a manner, that the seasonal variations in the precipitation frequency distribution and the stochastic properties of daily precipitation are taken into account to be able to achieve realistic simulation results.

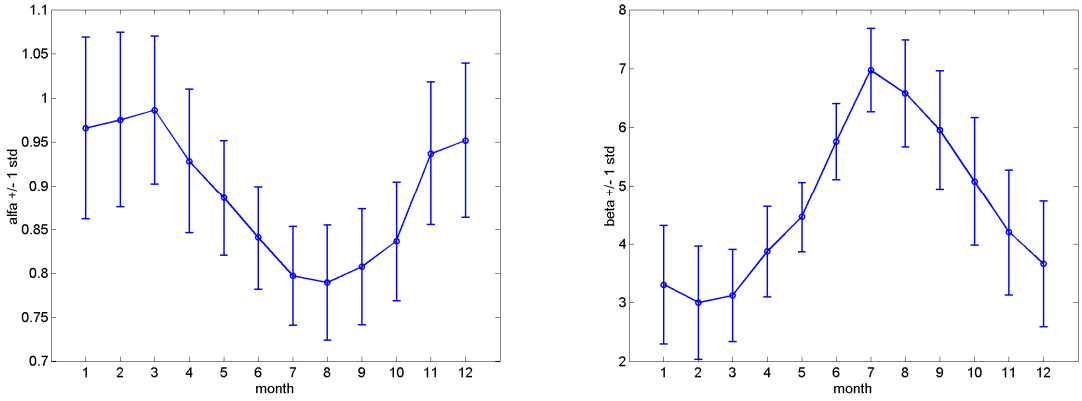

a) b)

Figure 3.14: Monthly Gamma parameters averaged over all stations for the period 1961 to 2004. a) Gamma α, b) Gamma β. The length of the bars indicate the spread around the mean ranging in the interval +/- 1 standard deviation.

3.2 Performance of weather generator

In order to assess the quality and performance of the weather generator, the simulation results need to be compared against observations to reveal both differences and agreements between simulated and observed series. Regarding precipitation simulations with a weather generator, a random number generator creates the daily precipitation intensities with statistical properties corresponding to the observations. Therefore, the temporal development from day to day differs always between simulations and observations. The evaluation must therefore be based on some statistical quantities that are derived both from the observations and the simulations. Comparing statistics such as the annual and monthly precipitation total, the number of rainy days, the number of days over some certain precipitation intensity or various measures quantifying extremes allows quantifying to which degree observations and simulations agree or disagree regarding precipitation intensity, frequency and extremes.

For the purpose of model evaluation, simulations covering a time period of 100 years have been made for each station using the WG parameters derived from the observations for the years 1961-2004. Then, the various statistics mentioned above were derived from the simulated 100 years and compared with the corresponding observed statistics for 1961-2004. To visualize the results, a number of scatter plots were made by plotting the simulation-derived statistics against the one from observations (Figure 3.15 to 3.X). In addition, a number of precipitation indices characterizing extremes were derived from the simulations and the difference between these and the corresponding observed indices were plotted on maps to show if the performance of the WG depends on region.

3.2.1 Annual and monthly total precipitation

Simulated annual total is plotted against observed annual precipitation in Figure 3.15, and Figure 3.16 shows scatter plots for the monthly totals. In these plots, each dot corresponds to one station. The agreement is perfect if all dots lie on the 1:1-line and decreases with increasing distance from the 1:1-line. Generally, simulated and observed annual totals agree relatively well (Figure 3.15), but the simulations tend to systematically overestimate annual totals at a large number of stations (dots lie above the line). This is also the case for the monthly scatter plots (Figure 3.16), however, the degree to which the simulations deviate from the observations varies from month to month. The differences are larger during summer and autumn.

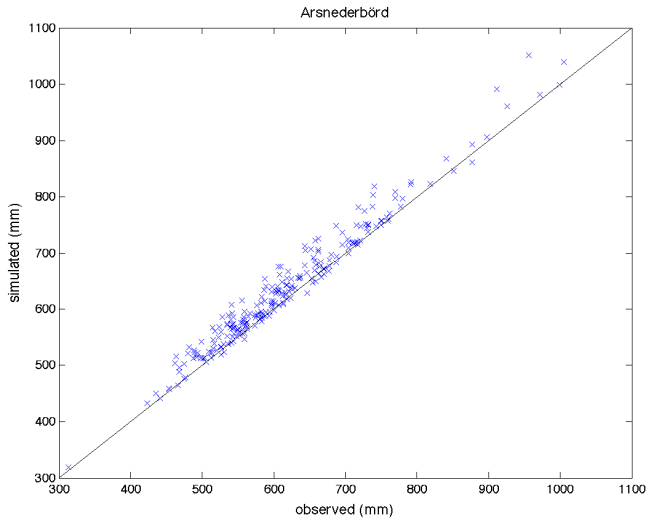

Figure 3.15: Annual precipitation total derived from WG-simulations over 100 years plotted against observed annual totals for the period 1961-2004. Each dot represents one station.

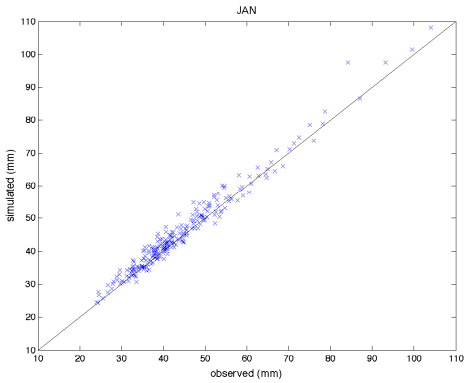
JAN
simulated (mm)
observed (mm)
10 20 30 40 50 60 70 80 90 100 110

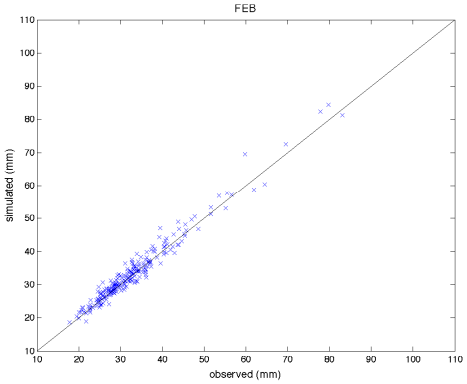
FEB
simulated (mm)
observed (mm)
10 20 30 40 50 60 70 80 90 100 110

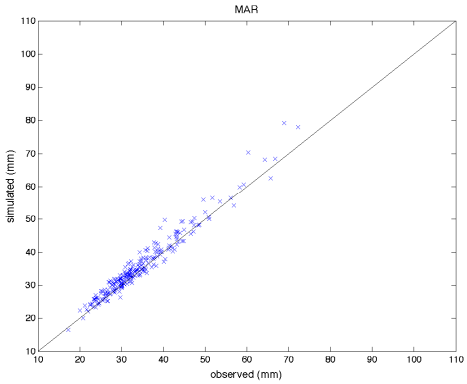
MAR
simulated (mm)
observed (mm)
10 20 30 40 50 60 70 80 90 100 110

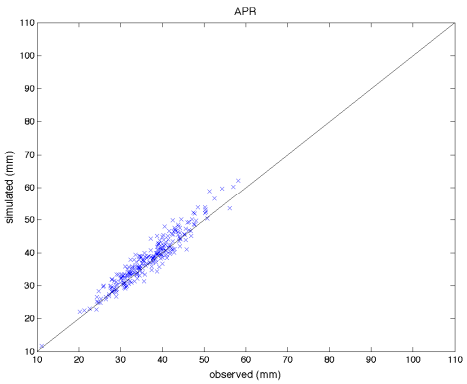
APR
simulated (mm)
observed (mm)
10 20 30 40 50 60 70 80 90 100 110

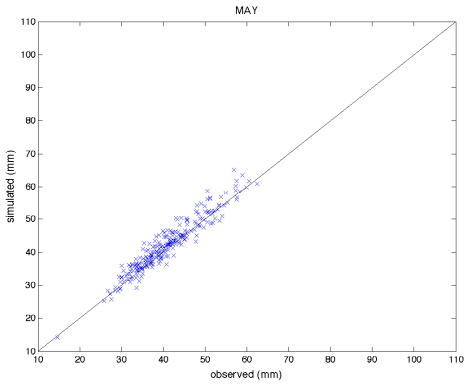
MAY
simulated (mm)
observed (mm)
10 20 30 40 50 60 70 80 90 100 110

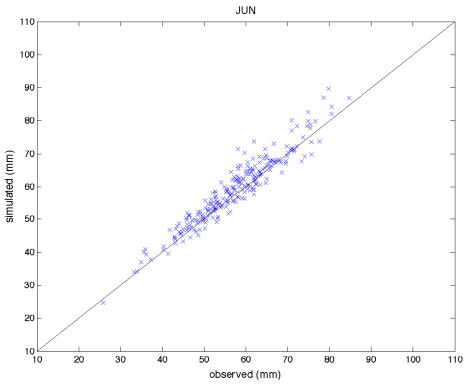
JUN
simulated (mm)
observed (mm)
10 20 30 40 50 60 70 80 90 100 110

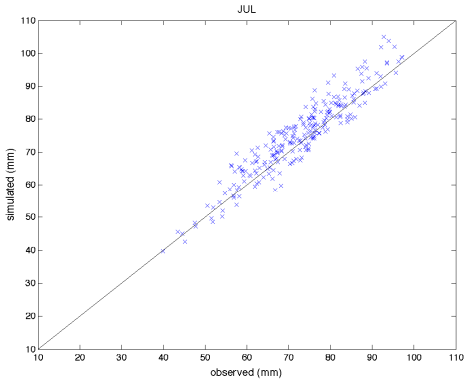
JUL
simulated (mm)
observed (mm)
10 20 30 40 50 60 70 80 90 100 110

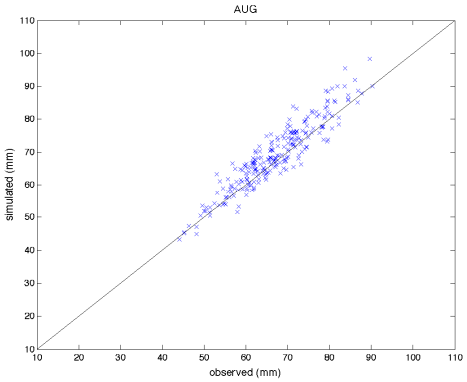
AUG
simulated (mm)
observed (mm)
10 20 30 40 50 60 70 80 90 100 110

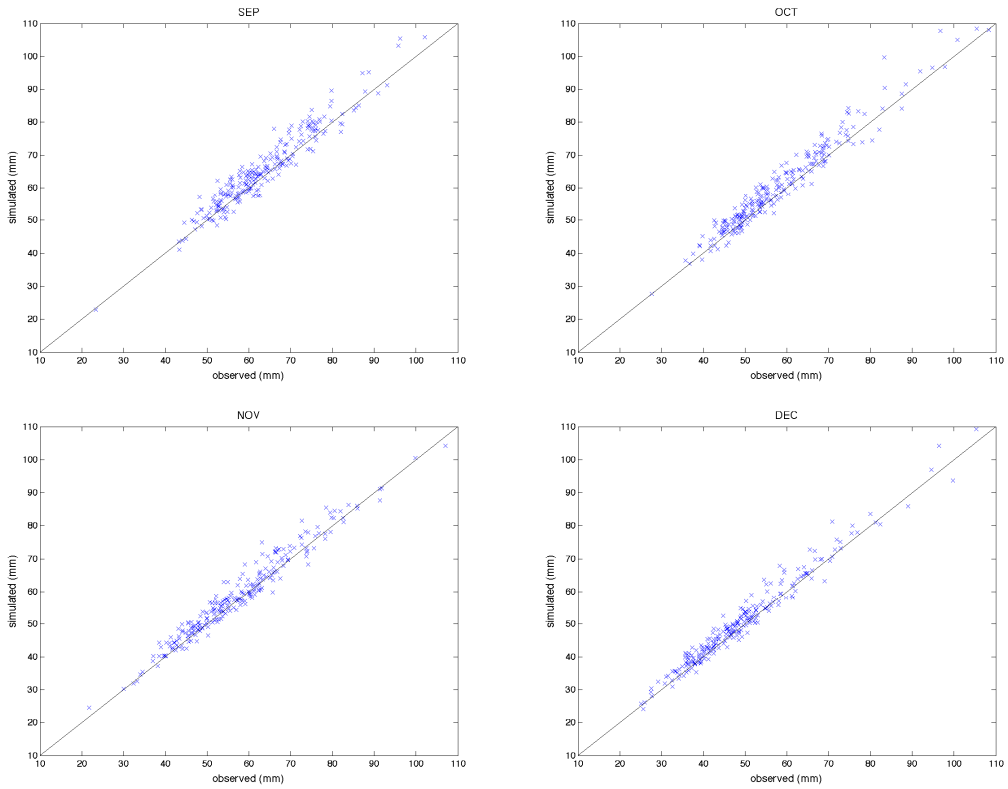

Figure 3.16: Monthly precipitation totals derived from WG-simulations over 100 years plotted against observed monthly precipitation totals for the period 1961-2004. Each dot represents one station.

3.2.2 Number of days with precipitation

Figure 3.17 shows the number of wet days per year derived from the simulations plotted against the number of wet days from the observations. There is a systematic overestimation of the number of wet days in the simulations at almost all stations.

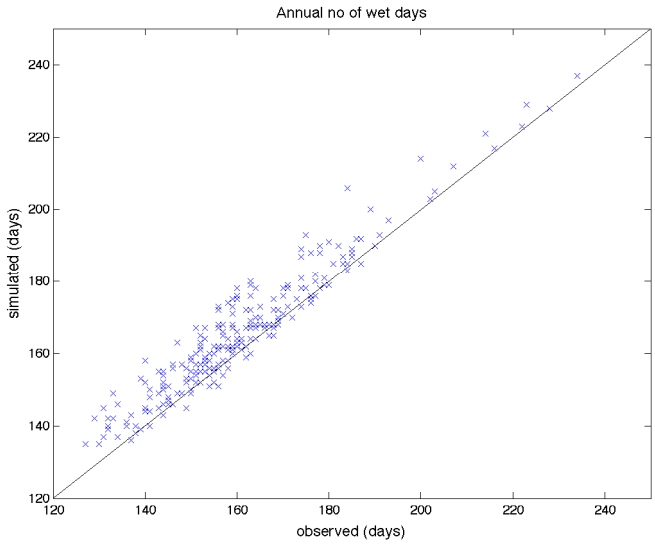

Figure 3.17: Annual *Nrain* (number of days with precipitation per year) derived from WG-simulations over 100 years plotted against *Nrain* derived from observations for the years 1961 to 2004. Each dot corresponds to one station.

The scatter plots in Figure 3.18 show the simulated and observed number of days with precipitation simulated for each calendar month. Like in the previous figure, the number of wet days is systematically overestimated in the various months. Since the same combination of simulated and observed number of wet days occur at several stations (for instance 12 observed and 14 simulated wet days), each dot in the monthly scatter plots may represent more than one station. Therefore, the *bias* was calculated in addition quantifying the systematic difference between observations and simulations. It is simply calculated as simulation minus observation. Positive and negative deviations can in principal cancel out resulting in a bias close to zero. If the simulated values are systematically larger (smaller) than the observed ones, the *bias* is positive (negative). Figure X shows the *bias* for each month, showing that the simulations overestimates the number of days with precipitation by 0.2 to 0.5 days on average in all months despite in January.

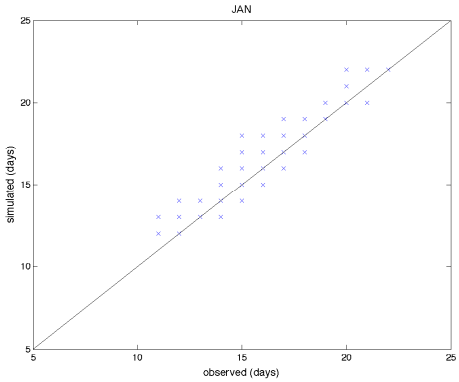
JAN
simulated (days)
observed (days)
5
10
15
20
25

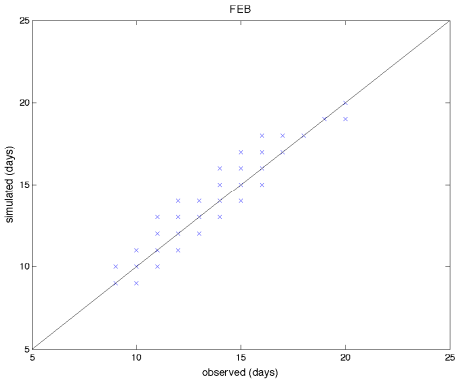
FEB
simulated (days)
observed (days)
5
10
15
20
25

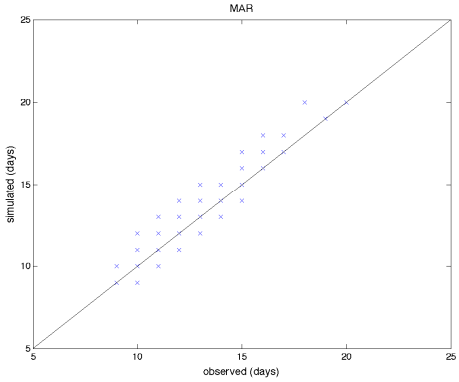
MAR
simulated (days)
observed (days)
5
10
15
20
25

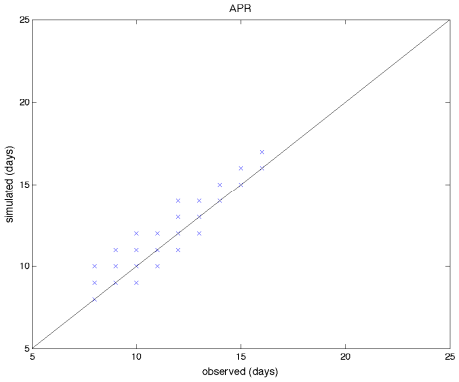
APR
simulated (days)
observed (days)
5
10
15
20
25

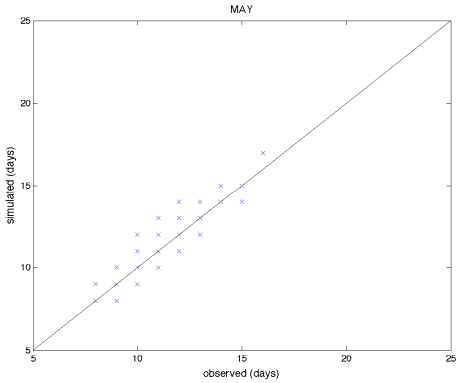
MAY
simulated (days)
observed (days)
5
10
15
20
25

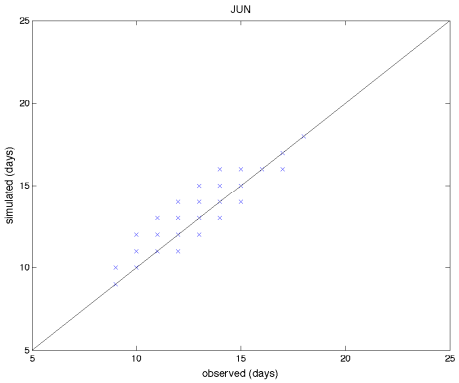
JUN
simulated (days)
observed (days)
5
10
15
20
25

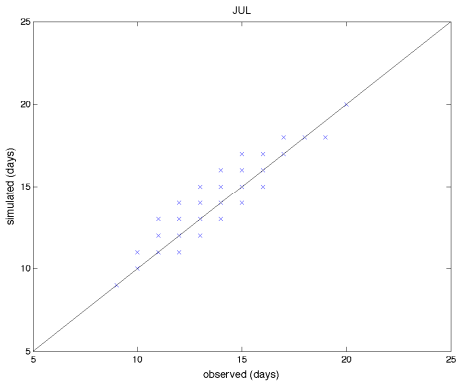
JUL
simulated (days)
observed (days)
5
10
15
20
25

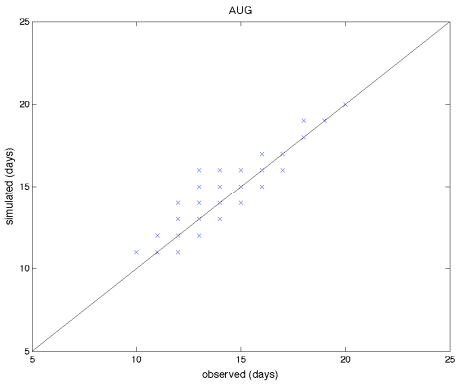
AUG
simulated (days)
observed (days)
5
10
15
20
25

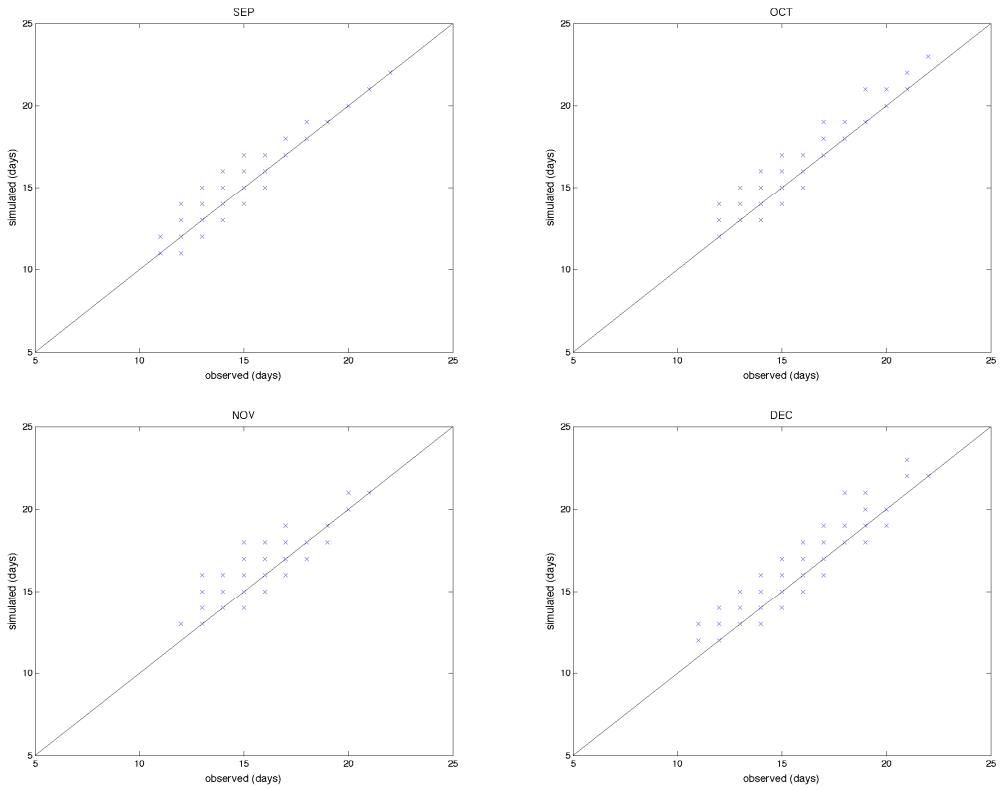

Figure 3.18: Monthly *Nrain* (number of days with precipitation per year) derived from WG-simulations over 100 years plotted against *Nrain* derived from observations for the years 1961 to 2004. Each dot corresponds to one station.

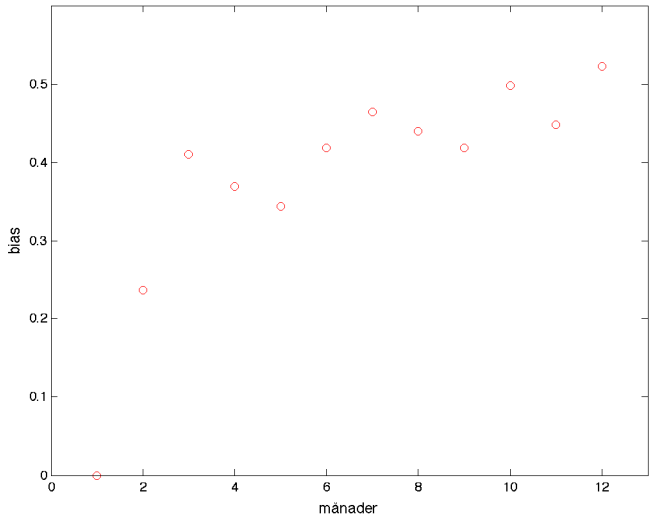

Figure 3.19: Monthly *bias* in *Nrain* (number of days with precipitation) derived from WG-simulations over 100 and observations for the period 1961 to 2004.

3.2.3 Precipitation extremes

a) Scatter plots

For the validation of the extremes, the number of days exceeding 40 mm per year (*exc40*) is used. Figure 3.20 shows the simulated *exc40* plotted against the observed *exc40*. The observed *exc40* ranges between 0.05 and 0.4 at the various stations (implying that the recurrent period ranges between 20 and 2.5 years), while for the simulations *exc40* lies in the interval 0 to 0.35 (i.e., the shortest recurrent period is 2.8 years). The figure shows that the WG is able to simulate these strong precipitation events but tends to underestimate the frequency of those days.

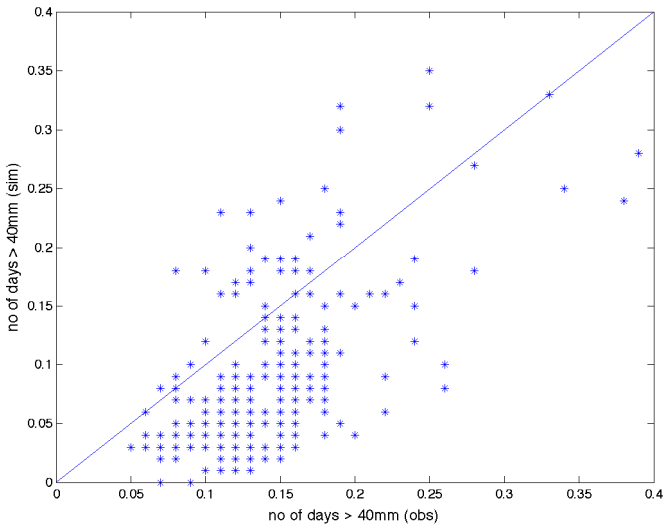

Figure 3.20: Annual *exc40* (number of days exceeding 40 mm per year) derived from WG-simulations over 100 years plotted against *exc40* derived from observations for the years 1961 to 2004. Each dot corresponds to one station.

Due to the rather rare occurrence of *exc40*, the validation of the extremes is based on a small sample size (small number of days). To achieve a more complete validation of extremes, monthly maximum precipitation from simulations and observations were plotted against each for each calendar month (Figure 3.21). There are partly rather big deviations between simulations and observations. The simulations both overestimate and underestimate the observed monthly maximum precipitation. Underestimation is especially pronounced during summer (July and August). Figure 3.22 and 3.23 quantify the difference between simulations and observations by means of the correlation coefficient (Figure 3.22) and the *bias* (Figure 3.23) for the different months. The correlation is largest in winter (0.5-0.6) and drops below 0.2 towards summer. The *bias* reveals that the simulations systematically underestimate observed monthly maximum precipitation, especially during summer.

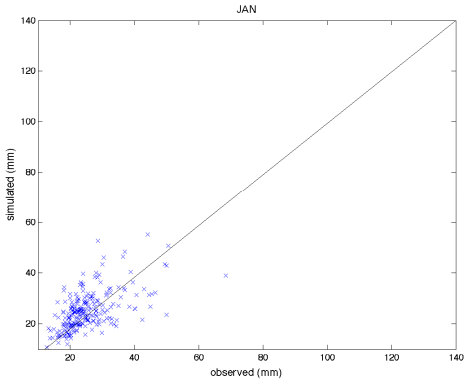
JAN
simulated (mm)
observed (mm)

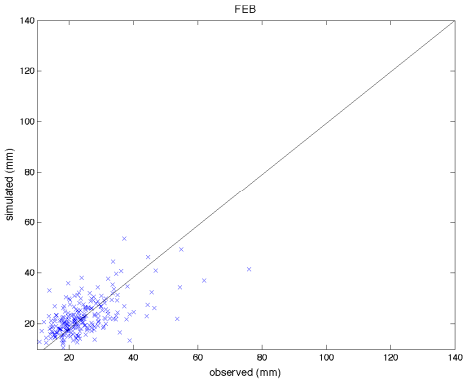
FEB
simulated (mm)
observed (mm)

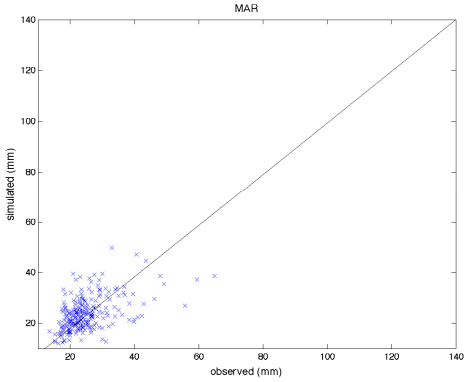
MAR
simulated (mm)
observed (mm)

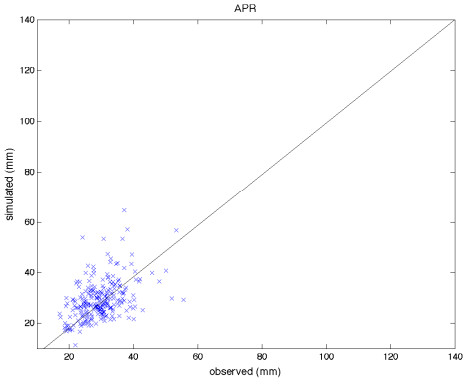
APR
simulated (mm)
observed (mm)

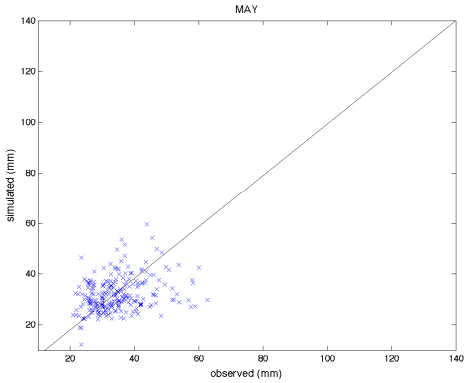
MAY
simulated (mm)
observed (mm)

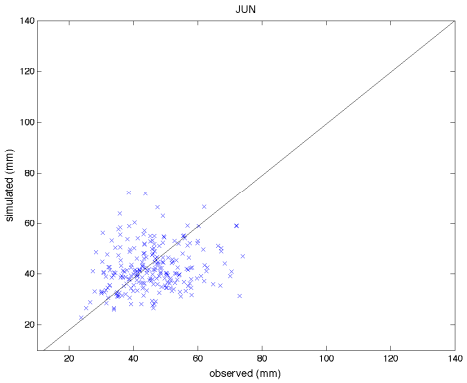
JUN
simulated (mm)
observed (mm)

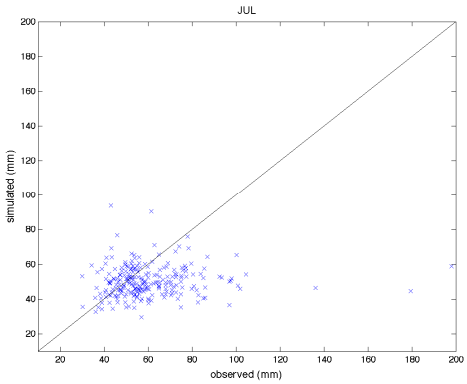
JUL
simulated (mm)
observed (mm)

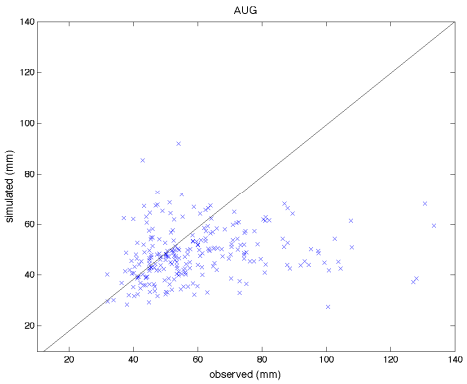
AUG
simulated (mm)
observed (mm)

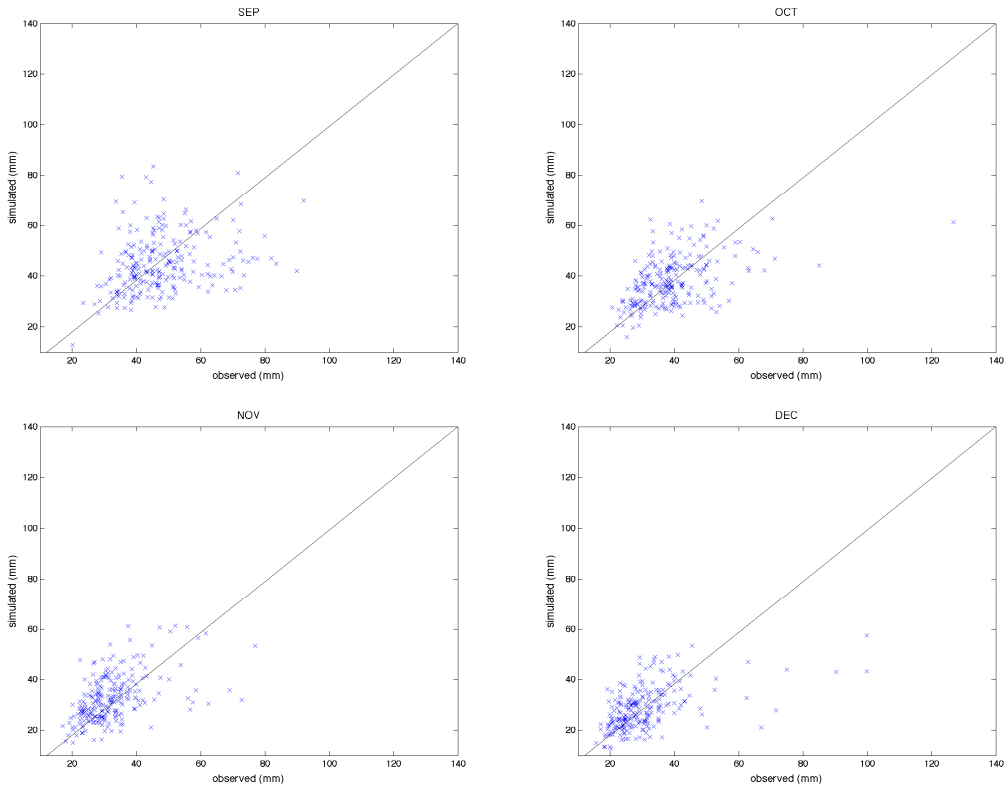

Figure 3.21: Monthly maximum precipitation derived from WG-simulations over 100 years plotted against observed monthly maximum precipitation derived from observations for the years 1961 to 2004 for different months. Each dot corresponds to one station.

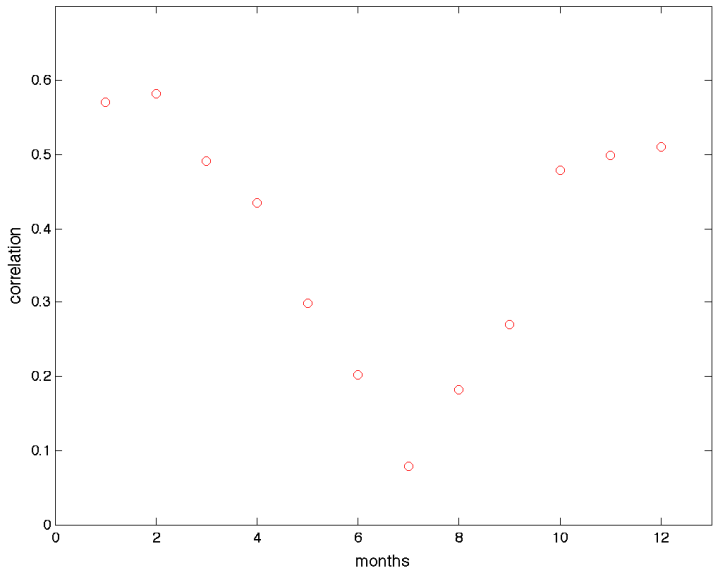

Figure 3.22: Correlation coefficient between observed (1961-2004) and simulated (WG-simulation over 100 years) monthly maximum precipitation in different months. The correlation coefficients are derived by correlating simulated and observed monthly maximum precipitation at the various stations separately in each month.

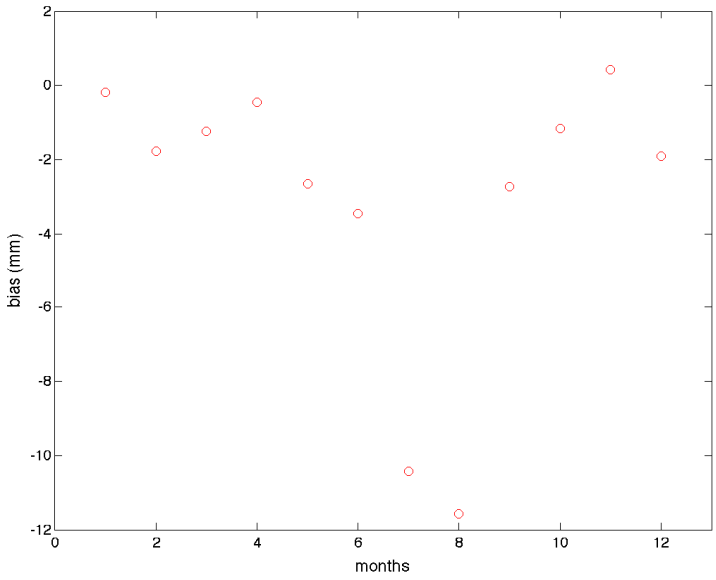

Figure 3.23: *Bias* between observed (1961-2004) and simulated (WG-simulation over 100 years) monthly maximum precipitation in different months. The bias is calculated as the difference between simulated and observed monthly maximum precipitation at the various stations separately in each month.

b) Spatial distribution

The diagrams in the previous section do not reveal whether there exist regional differences in the performance of the WG simulations. Therefore, a number of precipitation indices quantifying extremes were calculated from both the simulations and the observations, and the differences between them were plotted on maps (Figure 3.24 to 3.28). All maps consider differences in annual mean values.

Differences between simulations and observations are small at the majority of the stations. The simulations both overestimate and underestimate the observed indices. Furthermore, it can be concluded that the simulations work equally well in all regions of Sweden, since there are no clear spatial differences in the deviations across Sweden.

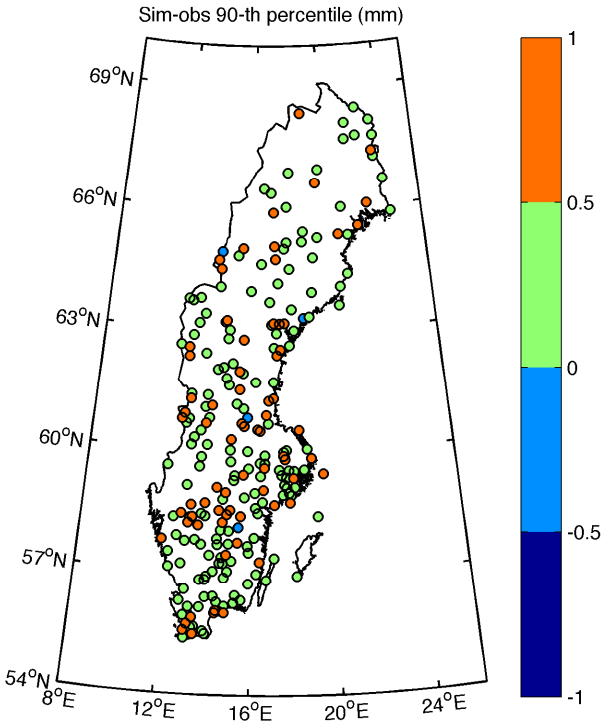

Figure 3.24: Deviations in annual *p90* (90-th percentile) in mm between simulated (WG-simulation over 100 years) and observations (for the period 1961 to 2004). The deviations are calculated as 'simulation minus observation'.

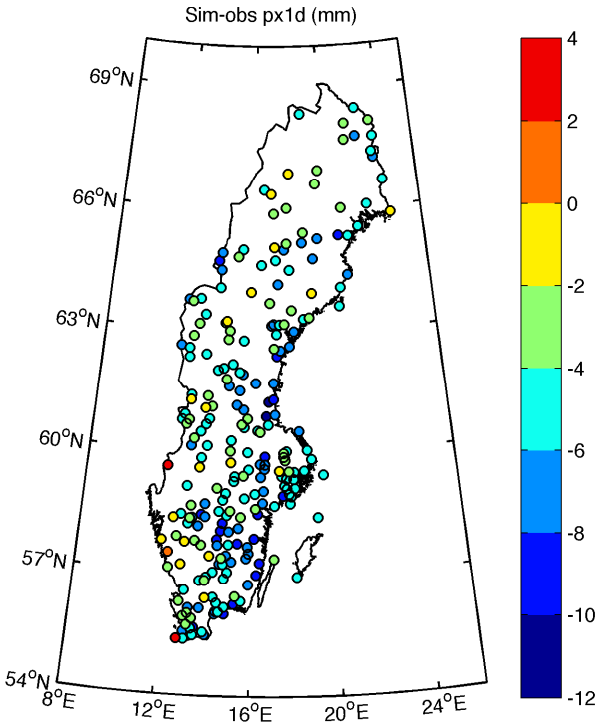

Figure 3.25: Deviations in annual *px1d* (greatest one day precipitation amount) in mm/day between simulated (WG-simulation over 100 years) and observations (for the period 1961 to 2004). The deviations are calculated as 'simulation minus observation'.

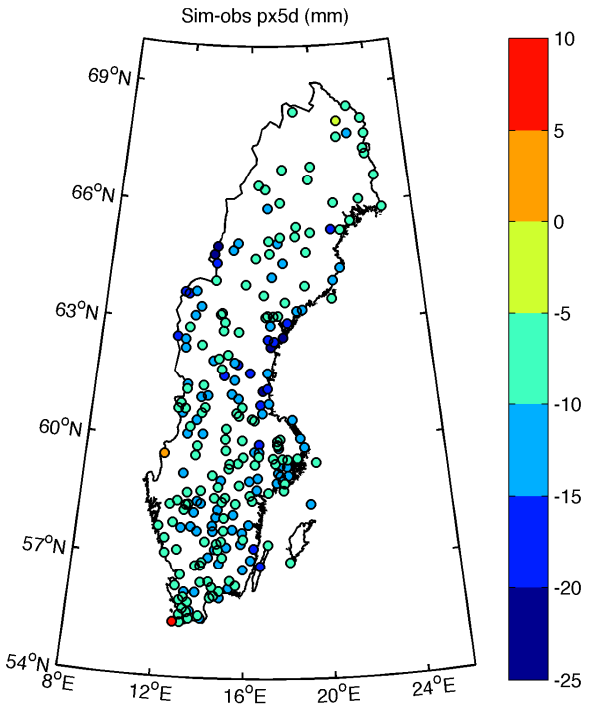

Figure 3.26: Deviations in annual *px5d* (greatest 5-day precipitation amount) in mm/5 days between simulated (WG-simulation over 100 years) and observations (for the period 1961 to 2004). The deviations are calculated as 'simulation minus observation'.

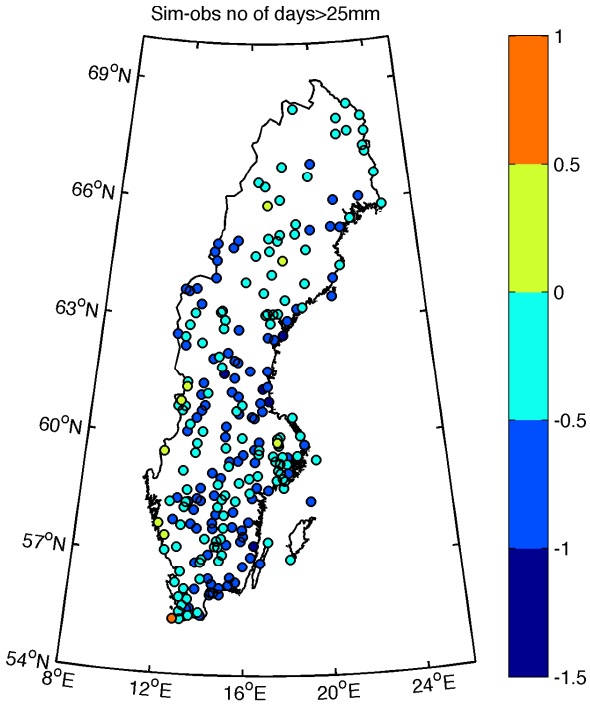

Figure 3.27: Deviations in annual *exc25* (number of days >25 mm) in days between simulated (WG-simulation over 100 years) and observations (for the period 1961 to 2004). The deviations are calculated as 'simulation minus observation'.

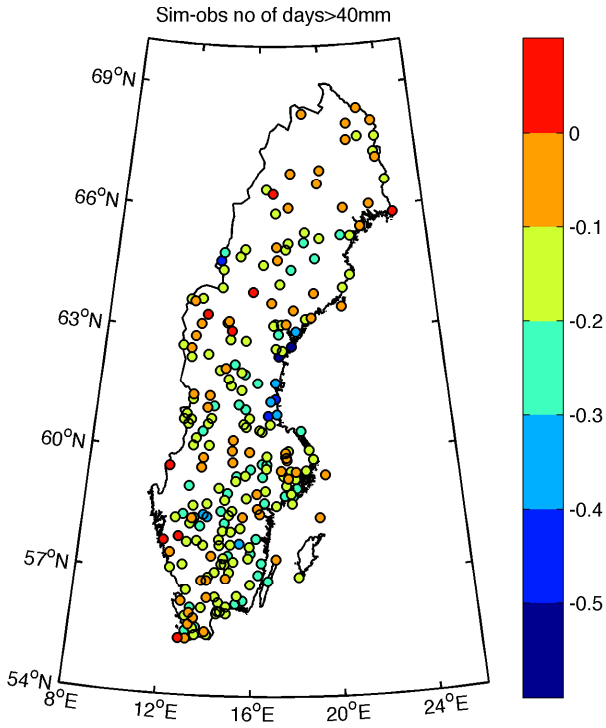

Figure 3.28: Deviations in annual *exc40* (number of days >40 mm) in days between simulated (WG-simulation over 100 years) and observations (for the period 1961 to 2004). The deviations are calculated as 'simulation minus observation'.

3.3 GCM precipitation scenarios for Sweden

This Section evaluates daily precipitation from the ECHAM5 and the HadCM3 control runs by comparing the simulations with observed precipitation. In addition, results from the scenario runs are given to show the magnitude of the change in the precipitation climate suggested by the GCM scenario runs. To be able to compare the GCM grid box values with station observations, the precipitation observations have been 'gridded' prior to the comparison. For each GCM grid box, a new daily precipitation series has been calculated by averaging over all stations located in one GCM grid box. Depending on GCM, their spatial resolution and the location of the grid boxes, the number of precipitation stations used to calculate the observed grid box values varies considerably (Figures 2.3b) and 2.4b)). For ECHAM5, this can vary between 26 stations (grid box 18) and one station (grid boxes 2, 5, 34, 40, 64), for HadCM3, 50 stations are at most located in one box (grid box 8) and three boxes have only one station (grid box 5, 12, 22). These differences have to be kept in mind when evaluating the control runs.

For the comparison, mean annual precipitation, and the indices *Nrain* and *pint* (Figures 3.29 to 3.31) have been calculated from the gridded observations and from the both control runs and scenario runs. In addition, histograms have been plotted showing the frequency distribution of the various precipitation series for each grid box (the results are only shown for two grid boxes per GCM). Note that the results from the gridded observations are different for ECHAM5 and HadCM3 because of differences in the spatial resolution of the GCMs and hence grid box location as well as differences in the time period used.

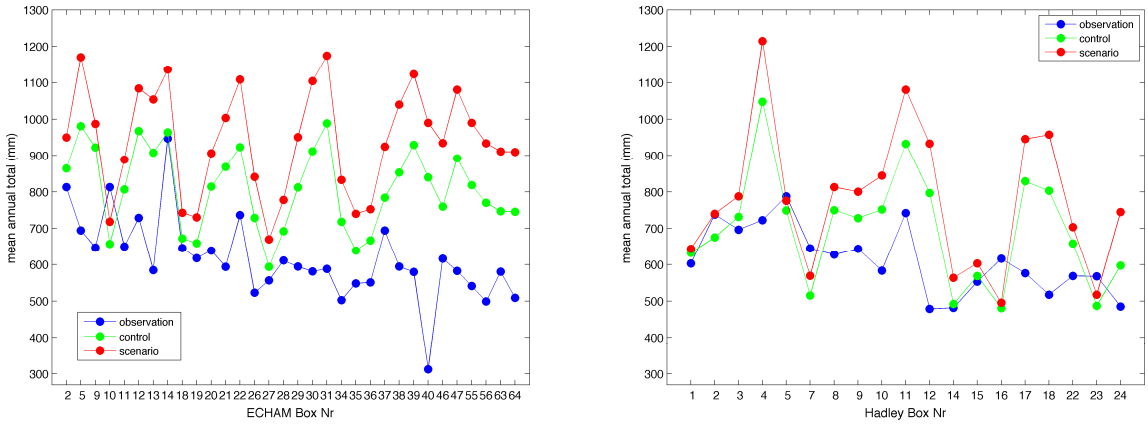

a) b)

Figure 3.29: Mean annual total precipitation in mm calculated for the various grid boxes of a) ECHAM5, b) HadCM3. The various data sets used cover different time periods: ECHAM5 control: 1961-2000, ECHAM5 scenario 2081-2100; HadCM3 control 1961-1989, HadCM3 scenario 2070-2099.

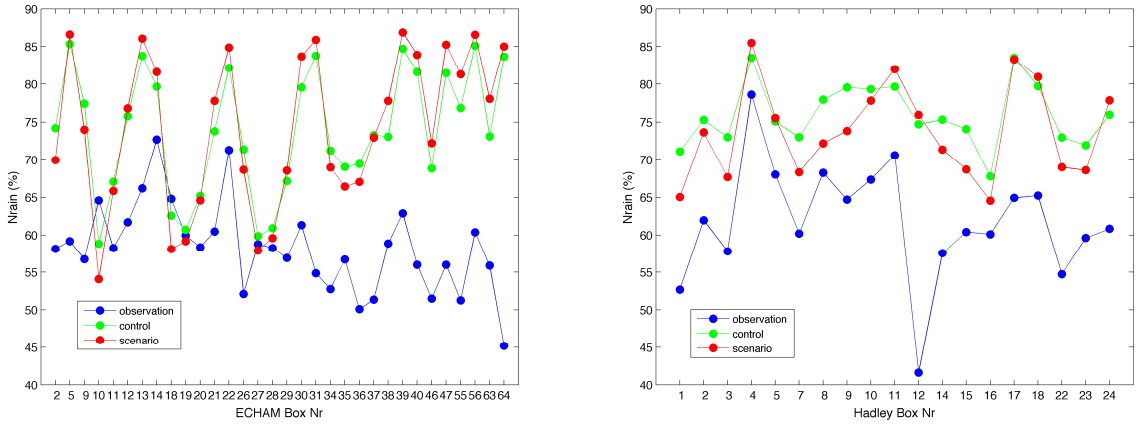

a) b)

Figure 3.30: *Nrain* (number of days with precipitation here expressed in %) calculated for the various grid boxes of a) ECHAM5, b) HadCM3. The various data sets used cover different time periods: ECHAM5 control: 1961-2000, ECHAM5 scenario 2081-2100; HadCM3 control 1961-1989, HadCM3 scenario 2070-2099.

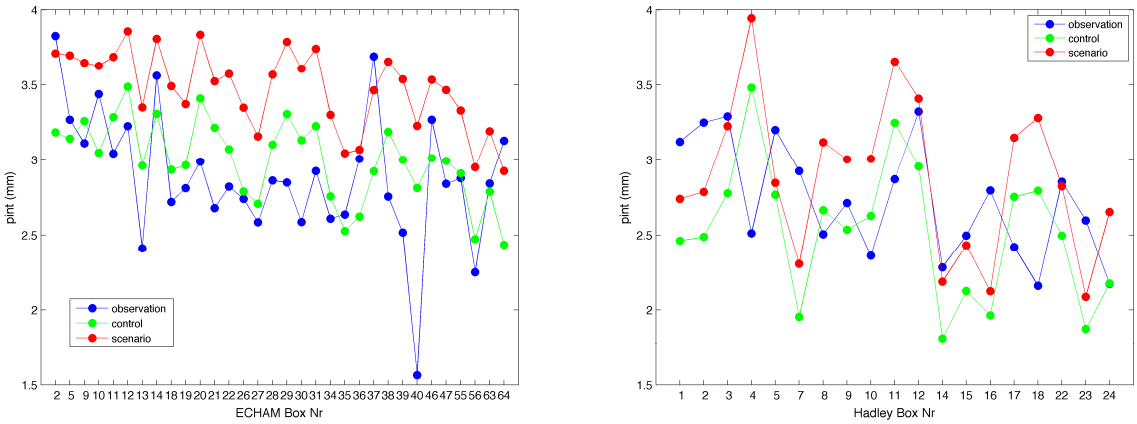

a) b)

Figure 3.31: *pint* (precipitation intensity on rainy days, in mm/day) calculated for the various grid boxes of a) ECHAM5, b) HadCM3. The various data sets used cover different time periods: ECHAM5 control: 1961-2000, ECHAM5 scenario 2081-2100; HadCM3 control 1961-1989, HadCM3 scenario 2070-2099.

From Figure 3.29, it can be seen that the ECHAM5 and HadCM3 control runs produce annual totals that are considerably higher than the observed annual precipitation amounts. Regarding ECHAM5, all simulated annual totals are higher than the corresponding observed grid box mean despite grid box number 10. These differences can to a large part be related to the differences in observed and simulated *Nrain* (Figure 3.30a)). While *Nrain* from the gridded observations range between 45 and 75%, *Nrain* from the ECHAM5 control rum lies between 65 and 85%. The differences in precipitation intensity are less systematic (Figure 3.31a)) as there are a number of grid boxes where the observed *pint* is higher than *pint* from the control run. Comparing annual total, *Nrain* and *pint* from the HadCM3 control run with the observations, similar results obtained.

To show the magnitude of the change in the future precipitation climate, annual total, *Nrain* and *pint* from the simulation runs are also given in Figure 3.29 to 3.31. Both GCMs suggest higher annual totals in all boxes, however, the magnitude of the increase varies with grid box. ECHAM5 suggests a stronger increase in central and Northern Sweden, for HadCM3 the geographical pattern in the changes is not clear. Changes in *Nrain* are both positive and negative in both GCMs depending on grid box. Precipitation intensities, however, are in all grid boxes clearly higher in the scenario runs.

In addition to the comparisons above, the frequency distribution of daily precipitation intensities obtained from the observations, the control and scenario run from the both GCMs have been plotted for each GCM grid box. Here, the results are shown for two ECHAM5 boxes (Figures 3.32) and two HadCM3 boxes (Figures 3.33). These boxes have been selected based on the number of stations stations located in the boxes: ECHAM5 box 18 and HadCM3 box 8 both contain the highest number of stations; ECHAM5 box 64 and HadCM3 box 12 contain only one station each). Differences between the frequency distribution of the control run occur in all grid boxes of both GCMs and are difficult to generalize. Regarding the frequencies of stronger daily intensities above >15 mm, the fraction is very small in the control simulations. Also the fraction of such events in the gridded observations of ECHAM5-box 18 and HadCM3-box 8 is small, which is due to the averaging over several stations. Regarding the distribution obtained from the scenario runs, both GCMs suggests small increases in frequencies mainly >5-7 mm. This finding applies also for the grid boxes not shown here.

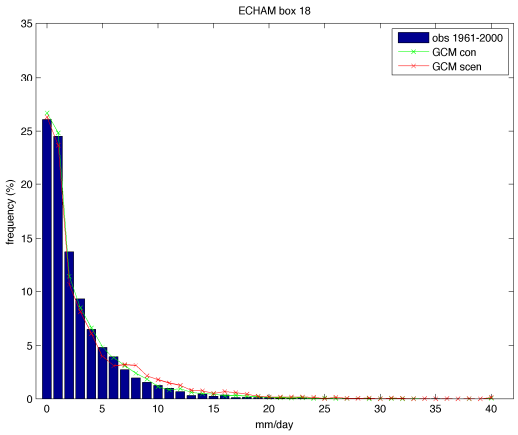

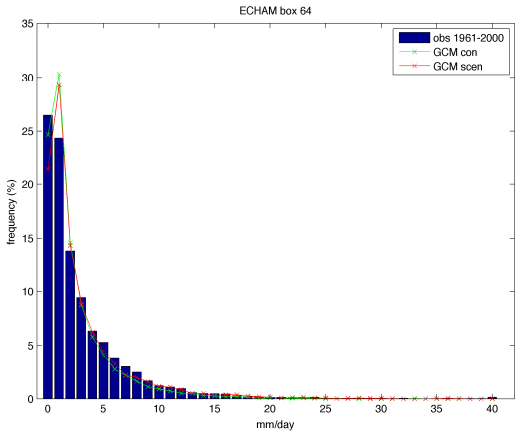

a) b)

Figure 3.32: Frequency distribution of daily precipitation intensities derived from observations (1961-2004), the ECHAM5 control (1961-2001) and scenario (2081-2100) run for two grid boxes. a) grid box 18, b) grid box 64. The numbering of the boxes refers to Figure 2.3.

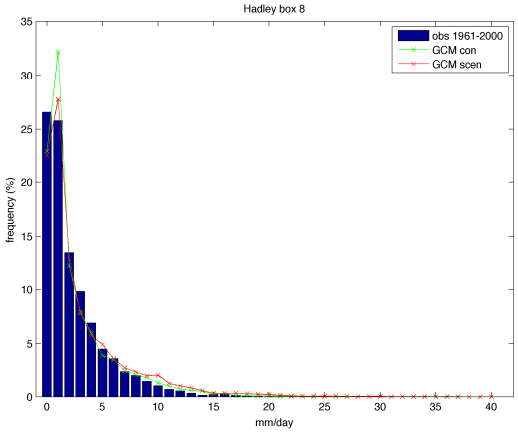

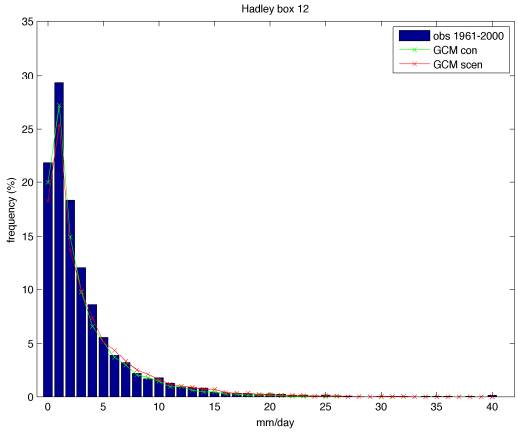

a) b)

Figure 3.33: Frequency distribution of daily precipitation intensities derived from observations (1961-2004), the HadCM3 control (1961-1989) and scenario (2070-2099) run for two grid boxes. a) grid box 8; b) grid box 12. The numbering of the boxes refers to Figure 2.3.

3.4 Changes in weather generator parameters

In order to relate the changes in the precipitation climate at the local scale to changes suggested by the GCM, the changes in the WG-parameters are presented here. The differences between control and scenario run are visualized by means of scatter plots, where the values of the control runs are plotted against the vales of the scenario run. Here, the changes in the four months January, April, July and October are shown representing the different seasons.

3.4.1 Gamma parameters

Changes in the ECHAM5 Gamma parameters (Figure 3.34) shows a slight decrease in α in almost all grid boxes in January, July and October and an increase in β in almost all grid boxes in all four months. The pattern of the changes in the Gamma parameters suggested by HadCM3 (Figure 3.35) is in general similar to the changes by ECHAM, however, in HadCM3 α decreases mainly in January, April and October. In addition, the changes of β in HadCM3 are smaller compared to ECHAM5.

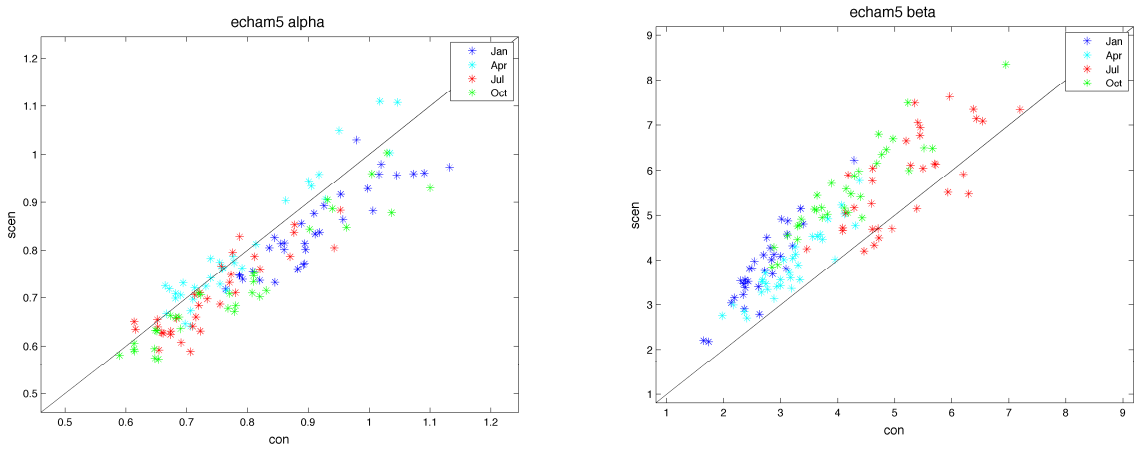

a) b)

Figure 3.34: Scatter plots of the changes in the WG-parameters derived from ECHAM5 for January, April, July and October. On the x-axis, the values for the control run are given, the y-axis shows the values for the scenario run. Each '*' represents one GCM-box. Panel a) Gamma α, panel b) Gamma β.

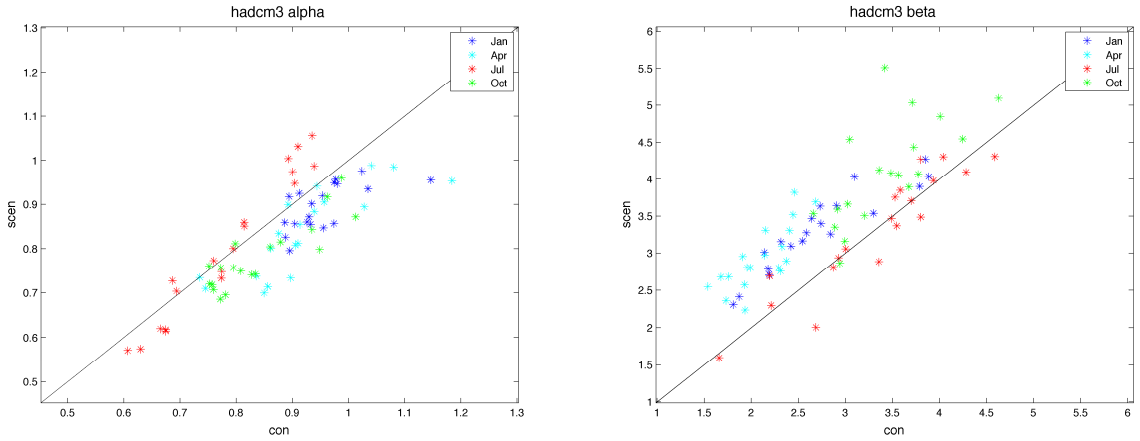

a) b)

Figure 3.35: Scatter plots of the changes in the WG-parameters derived from HadCM3 for January, April, July and October. On the x-axis, the values for the control run are given, the y-axis shows the values for the scenario run. Each '*' represents one GCM-box. Panel a) Gamma α, panel b) Gamma β.

What does a decrease in α and an increase in β imply for the distribution of daily precipitation in the future? Since parameter α measures the skewness of the Gamma distribution, smaller values of α imply decreasing skewness. Parameter β on the other hand is related to the total precipitation amount, and larger β thus means an increase in precipitation amount. As an example, Figure 3.36 illustrates how changes in Gamma α and β influence the frequency distribution of daily precipitation. The values of the Gamma parameters refer to ECHAM5 box no 18 for July. It implies a slight decrease in days with precipitation up to about 6 mm, while the number of days with amounts above 6 mm is slightly increasing. The fraction of days with heavy precipitation (> 20 mm) is small in both runs, but increases in the future (Figure 3.36c)). Thus, there exist a clear link between the changes in the Gamma parameters at GCM scale and the increasing precipitation amounts at local scale as expressed by various precipitation indices.

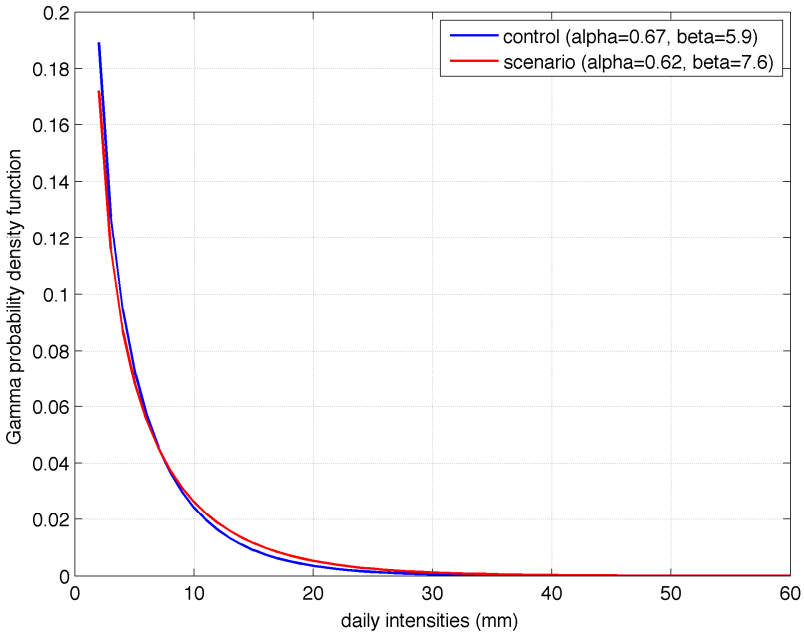

a)

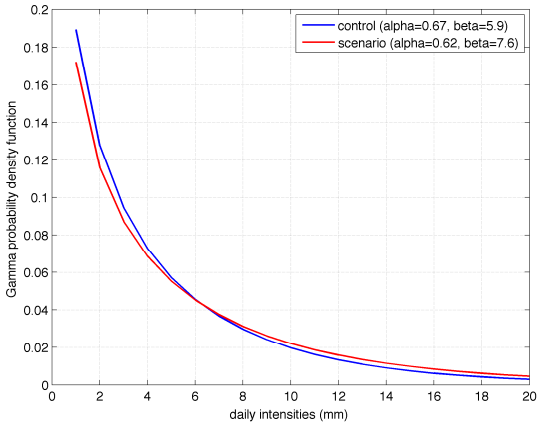

b)

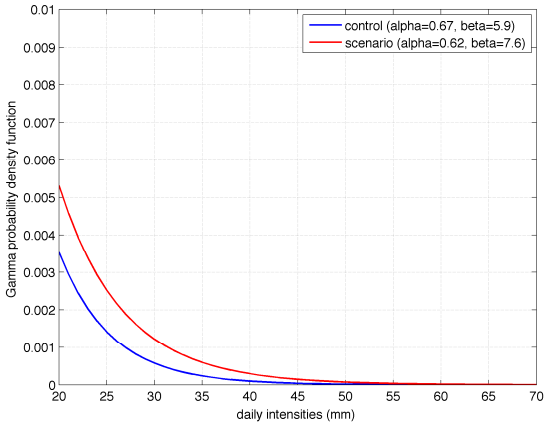

c)

Figure 3.36: Frequency distribution of daily precipitation intensities in July for ECHAM5 box 18 in the control and the scenario run. Panel a) displays the whole range of daily intensities; panel b) enlarges the distribution of intensities up to 20 mm; panel c) shows daily intensities above 20 mm.

3.4.2 Transition probabilities

Compared to the changes in the Gamma parameters, changes in the transition probabilities are less systematic and more difficult to generalize (Figure 3.37 and 3.38). Although the suggest changes differ more between the two GCMs, some regular changes do appear. The ECHAM5 simulated changes in *p01* (transition from dry to wet) and *p11* (transition from wet to wet) have a fairly clear trend towards increased *p01* in July and October and decreased *p01* in January and April (the conditions are reversed for *p11*,). In HadCM3, on the other hand, *p10* (transition from wet to dry) and *p00* (transition from dry to dry) are the probabilities with rather systematic changes: *p01* decreases in all four months, while *p00* increases. In contrast to the changes in the Gamma parameters, that easily could be related to changes in precipitation intensities, the implication of the combined changes in the four transition probabilities on the future precipitation occurrence (i.e., distribution of wet and dry days, wet and dry spell length) is more intricate.

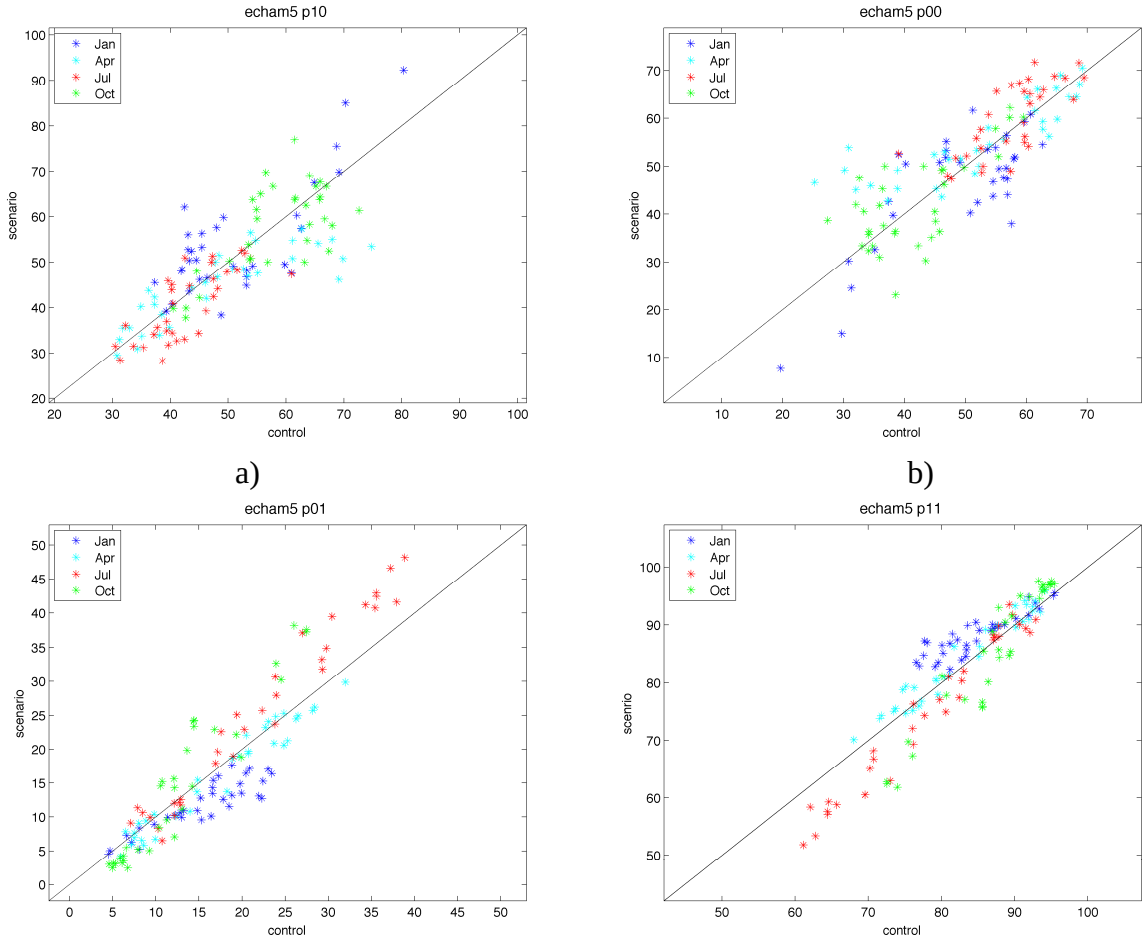

Figure 3.35: Scatter plots of the changes in the transition probabilities derived from ECHAM5 for January, April, July and October. On the x-axis, the values for the control run are given, the y-axis shows the values for the scenario run. Each '*' represents one GCM-box. Xa) *p10* (wet to dry), Xb) *p00* (dry to dry), Xc) *p01* (dry to wet) and Xd) *p11* (wet to wet).

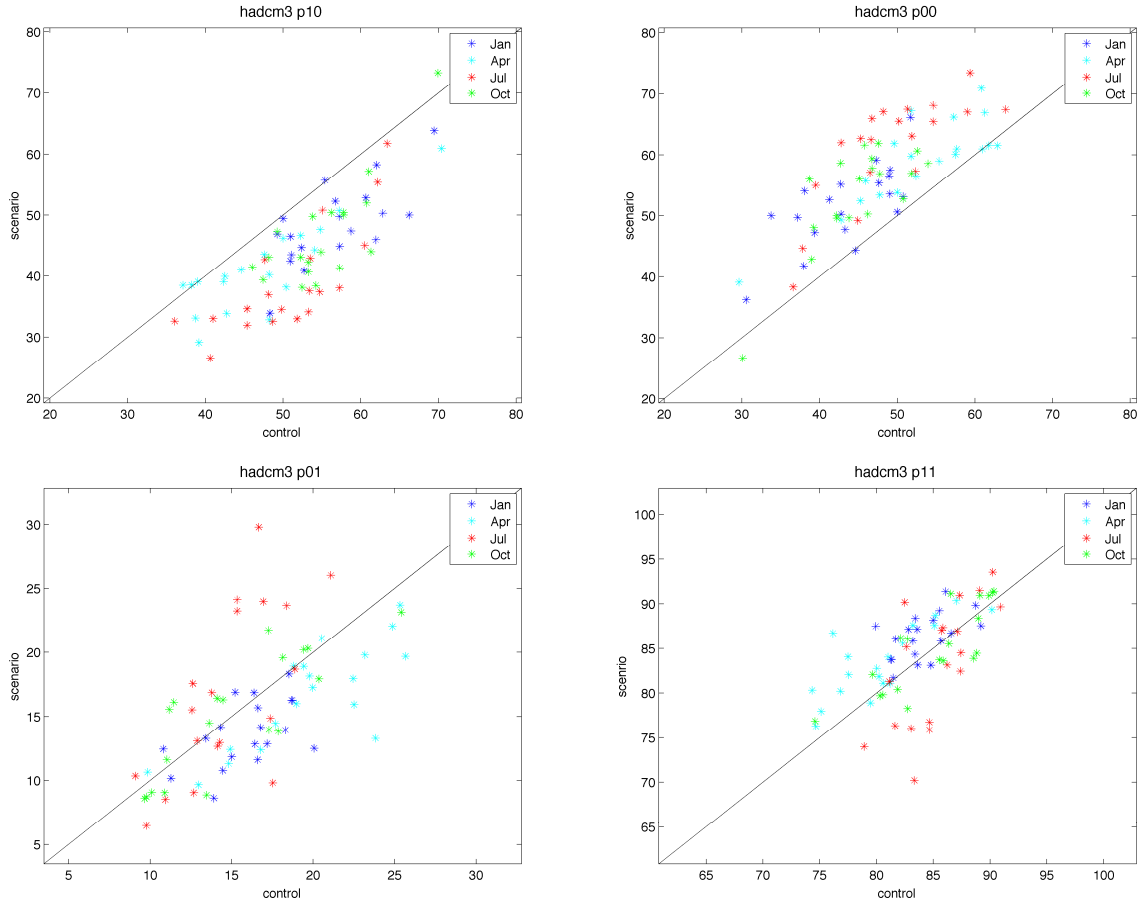

Figure 3.37: Scatter plots of the changes in the transition probabilities derived from HadCM3 for January, April, July and October. On the x-axis, the values for the control run are given, the y-axis shows the values for the scenario run. Each '*' represents one GCM-box. a) *p10* (wet to dry); b) *p00* (dry to dry); c) *p01* (dry to wet) and d) *p11* (wet to wet).

There is nevertheless a rather obvious link between the decrease in *Nrain* in summer comprising almost the whole of Sweden (Figure X) and the systematic decrease in *p11* and increase in *p00* in all or almost all grid boxes of both GCMs (Figure 3.35 and 3.36). In the same way, for the WG-simulations based on ECHAM5, the increase in winter *Nrain* taking place in almost all parts of Sweden despite some coastal regions can be related to the systematic increase in *p11* and decrease in *p00* in the various grid boxes. Also, the HadCM3-based WG-simulations suggest increasing winter *Nrain* in large parts of Sweden, however, the magnitude of the local changes is smaller compared to ECHAM5. This might be explained by the combined effect of the increase in both *p11* and *p00* in the HadCM3 boxes partly counteracting each other.

3.5 Local daily precipitation scenarios

The results from the simulations of the future precipitation changes at local scale are presented by means of maps for annual and seasonal changes at each station. All changes are calculated as the difference between scenario simulations based on the ECHAM5- and HadCM3-derived WG parameters and observations, (i.e. scenario simulation minus observation). In addition, Table X and X give the fraction of stations having positive (or negative changes). The magnitude of the changes at the various stations were divided into seven classes: three classes for positive and negative changes respectively, and one class for "no change". Positive changes indicating wetter climate conditions are given with green to blue colour tones in the maps, the yellow to red colour tones indicate changes towards drier climate. (The maps for *pxcdd* are the only exception where positive (negative) changes imply drier (wetter) conditions.). Stations without any change are symbolized with "x". In addition, Table 3.1 and 3.2 give the fraction of stations in the seven classes for changes at the annual and seasonal scale respectively.

3.5.1 Annual change

In general, at the majority of the stations a change towards wetter climate condition can be expected (Figure 3.38 to 3.45 and Table 3.1). The magnitude of the changes and their geographical distribution depend on the GCM used. Both models estimate that the number of wet days per year in the future decreases with up to 30 days in Southern and central Sweden compared to today's climate conditions. Along the coast in Northern Sweden, the HadCM3-based simulations suggest a decrease of up to 14 days. Precipitation intensities increase at all stations (with up to 6.4 mm/day) independently of the GCM used (Figure 3.39), together with the moderate extremes (*p90*) rising with up to 11.8 mm (Figure 3.40). The HadCM3-based simulations result in a larger number of stations with precipitation changes located in the highest positive interval (Table 3.1) compared to the ECHAM5-based scenarios. For the indices *px1d* (Figure 3.41) and *px5d* (Figure 3.42), the HadCM3 simulations suggest an increase at the majority of the stations, while the ECHAM5 simulations show a decrease of *px1d* at many stations located in Southern and central Sweden. Also, the number of days exceeding 25 mm/day increases in general with 0.1 to 5 days per year in the future climate (Figure 3.43). In addition, extremes with daily intensities exceeding 40 mm/day will become more frequent in the future (with 0.1 to 1.1 days/year) according to the HadCM3 simulations (Table 3.1, Figure 3.44). In contrast, simulations based on ECHAM5 suggest a decrease in *exc40* at around 50 % of the stations. Different results are also obtained for the longest dry spell: according to the HadCM3-scenarios, *pxcdd* increases at the greater part of the stations (Figure 3.45), while the ECHAM5-based simulations propose a decrease in *pxcdd* at many stations.

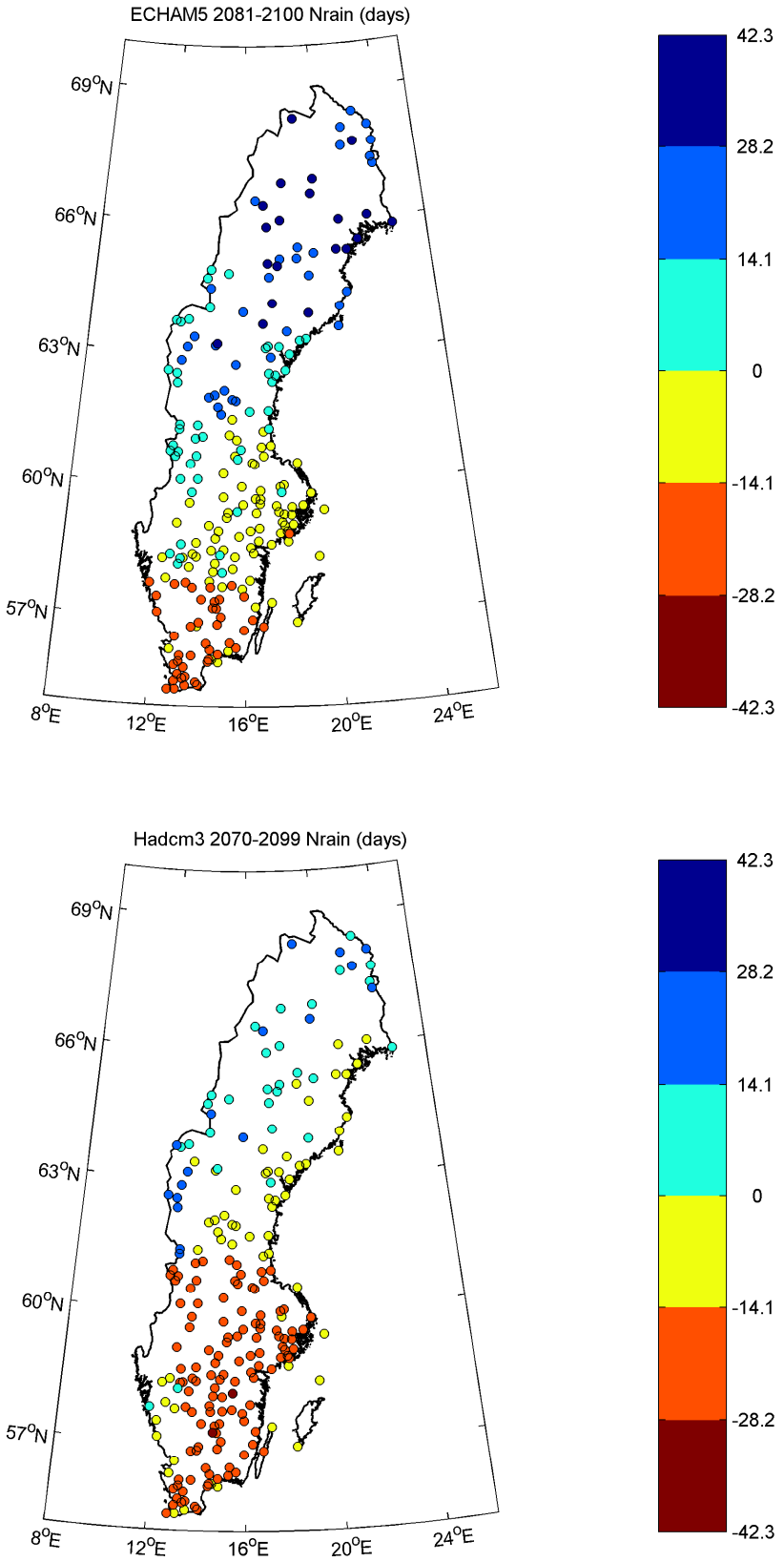

Figure 3.38: Annual changes in *Nrain* (in days) at 220 stations in Sweden derived from WG-simulations based on the ECHAM5 scenario run for the years 2081 to 2100 (upper panel) and the HadCM3 scenario run for the years 2070 to 2099 (lower panel). The annual changes are calculated as 'future simulated climate minus observation'.

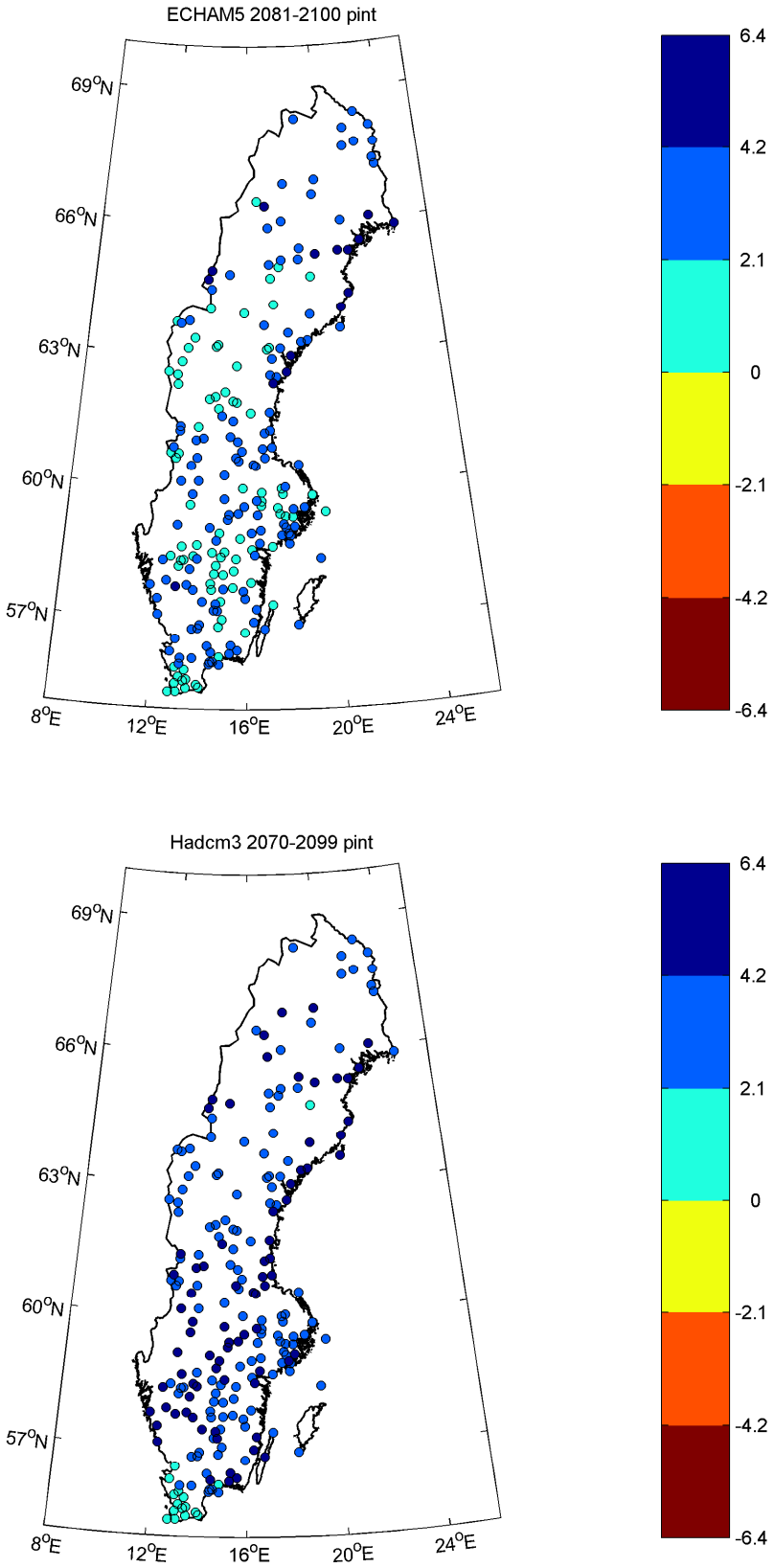

Figure 3.39: Annual changes in *pint* (in mm) at 220 stations in Sweden derived from WG-simulations based on the ECHAM5 scenario run for the years 2081 to 2100 (upper panel) and the HadCM3 scenario run for the years 2070 to 2099 (lower panel). The annual changes are calculated as 'future simulated climate minus observation'.

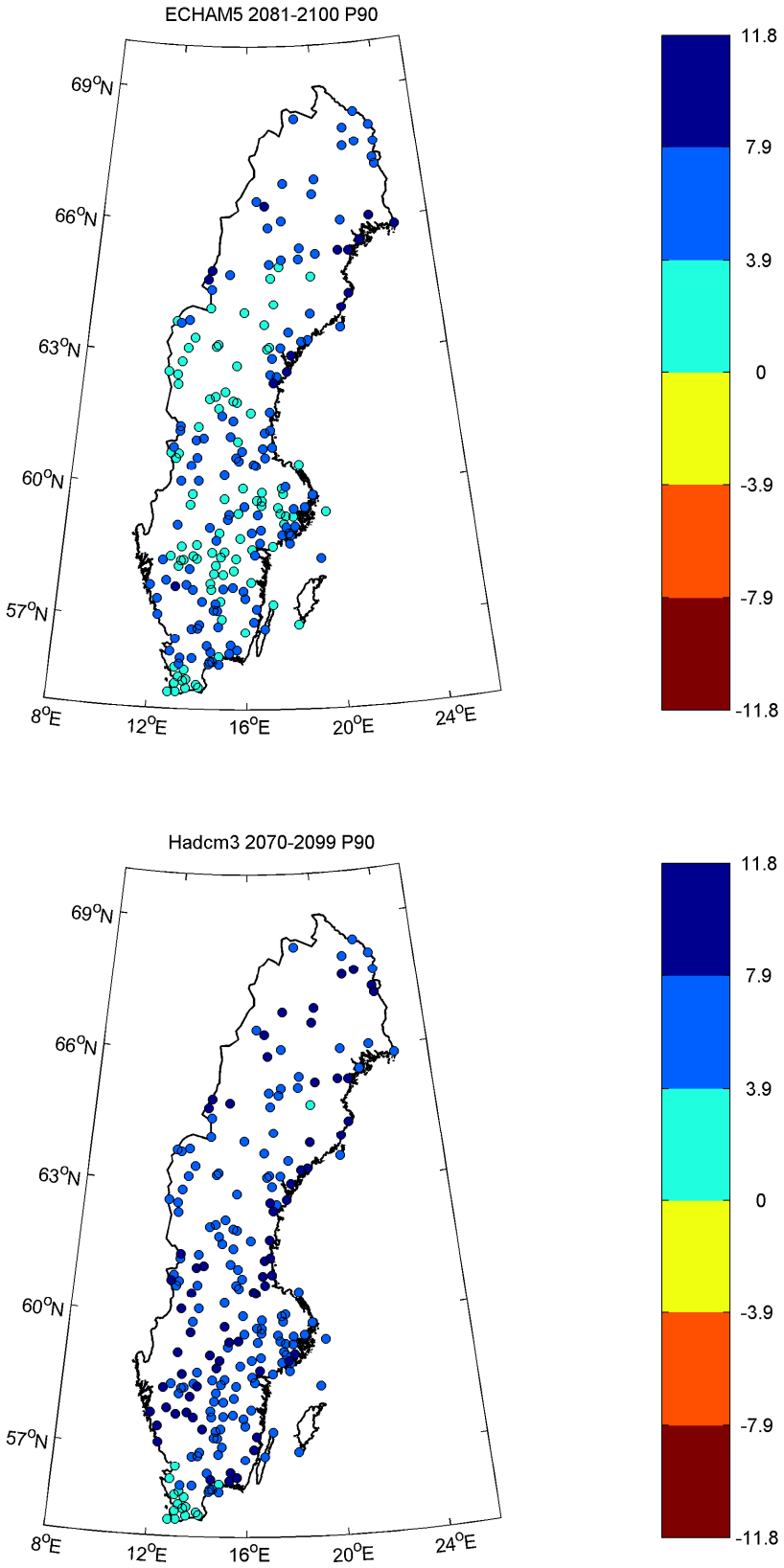

Figure 3.40: Annual changes in *p90* (in mm) at 220 stations in Sweden derived from WG-simulations based on the ECHAM5 scenario run for the years 2081 to 2100 (upper panel) and the HadCM3 scenario run for the years 2070 to 2099 (lower panel). The annual changes are calculated as 'future simulated climate minus observation'.

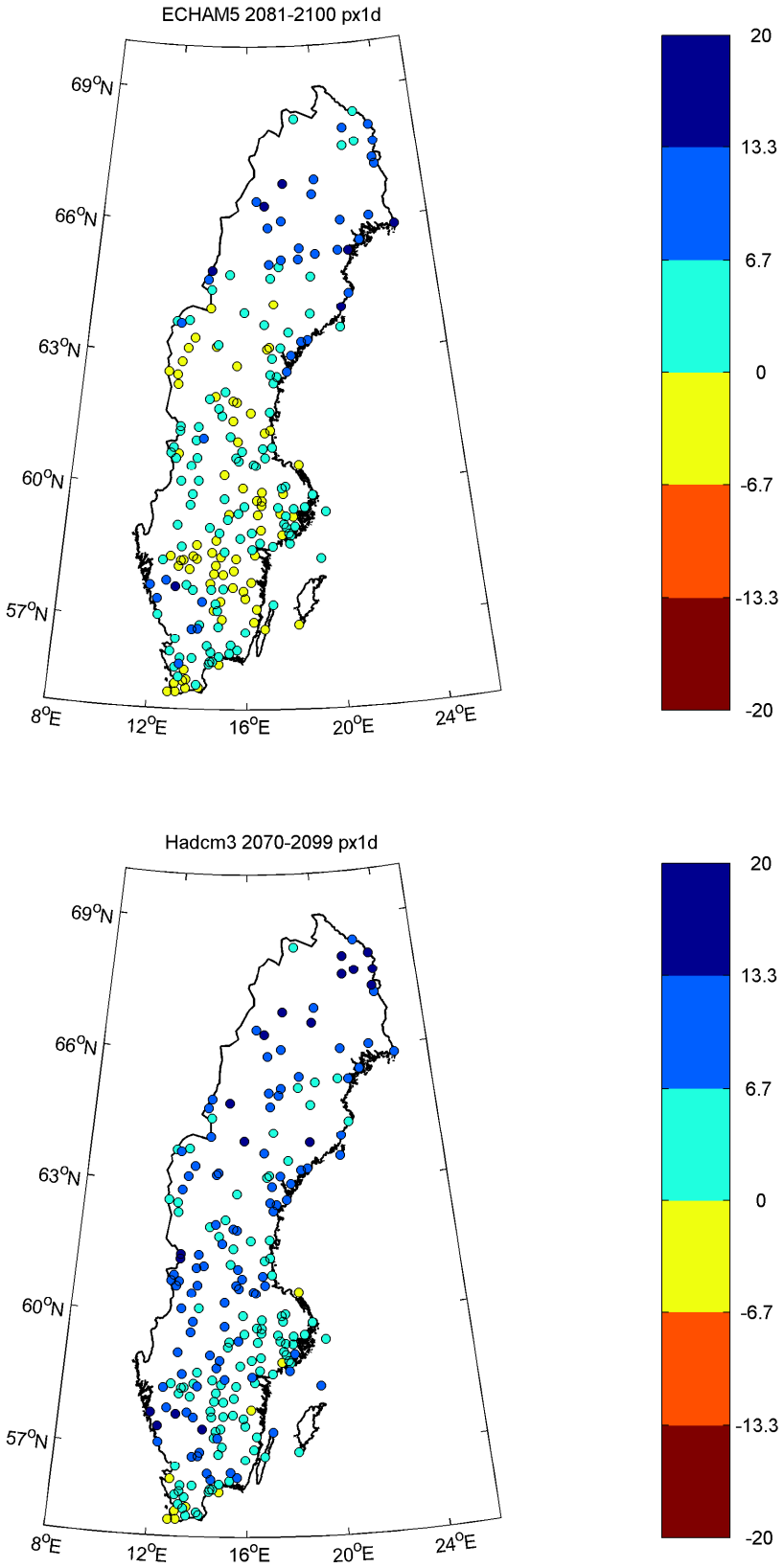

Figure 3.41: Annual changes in *px1d* (in mm) at 220 stations in Sweden derived from WG-simulations based on the ECHAM5 scenario run for the years 2081 to 2100 (upper panel) and the HadCM3 scenario run for the years 2070 to 2099 (lower panel). The annual changes are calculated as 'future simulated climate minus observation'.

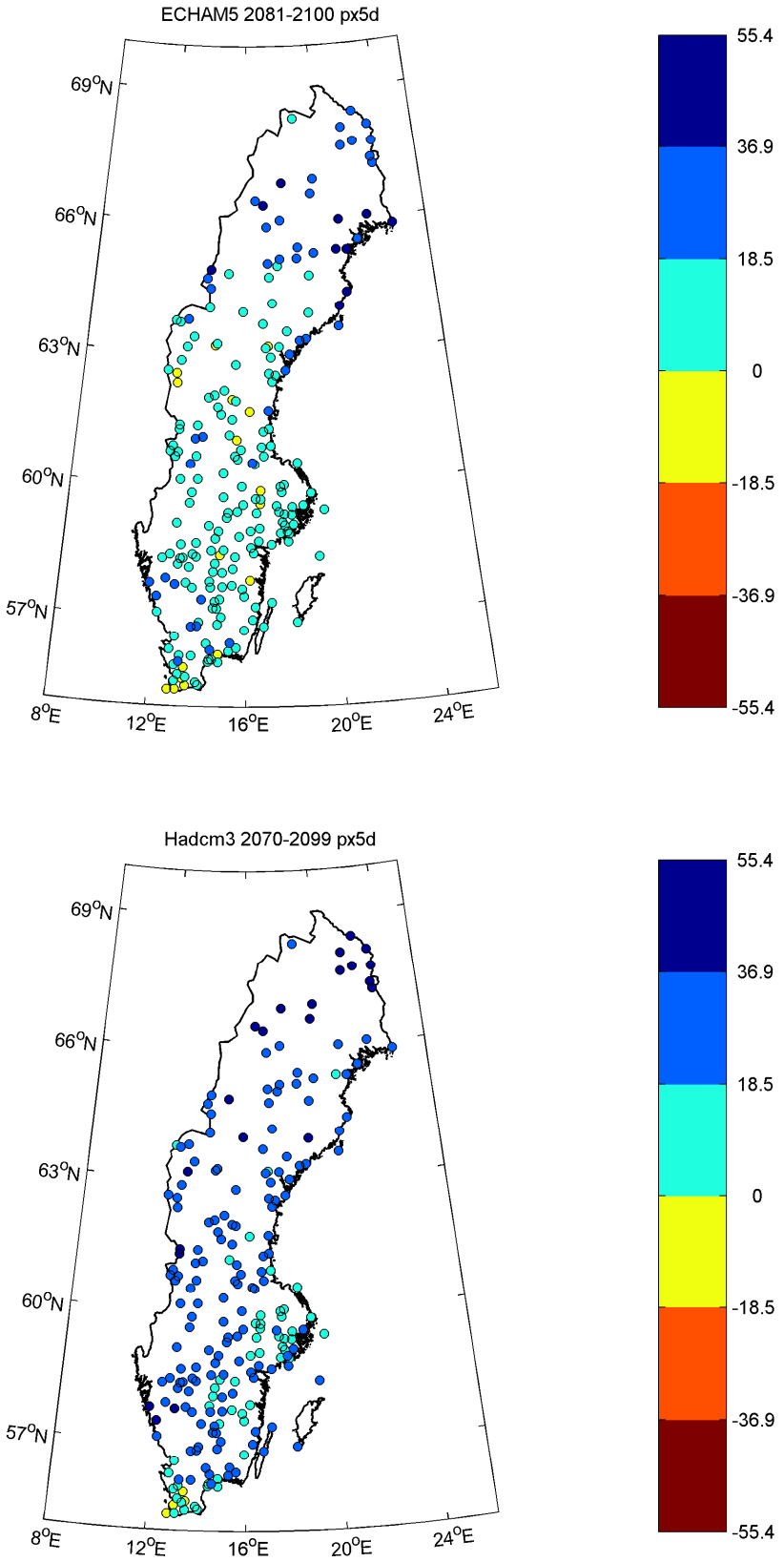

Figure 3.42: Annual changes in *px5d* (in mm/5 days) at 220 stations in Sweden derived from WG-simulations based on the ECHAM5 scenario run for the years 2081 to 2100 (upper panel) and the HadCM3 scenario run for the years 2070 to 2099 (lower panel). The annual changes are calculated as 'future simulated climate minus observation'.

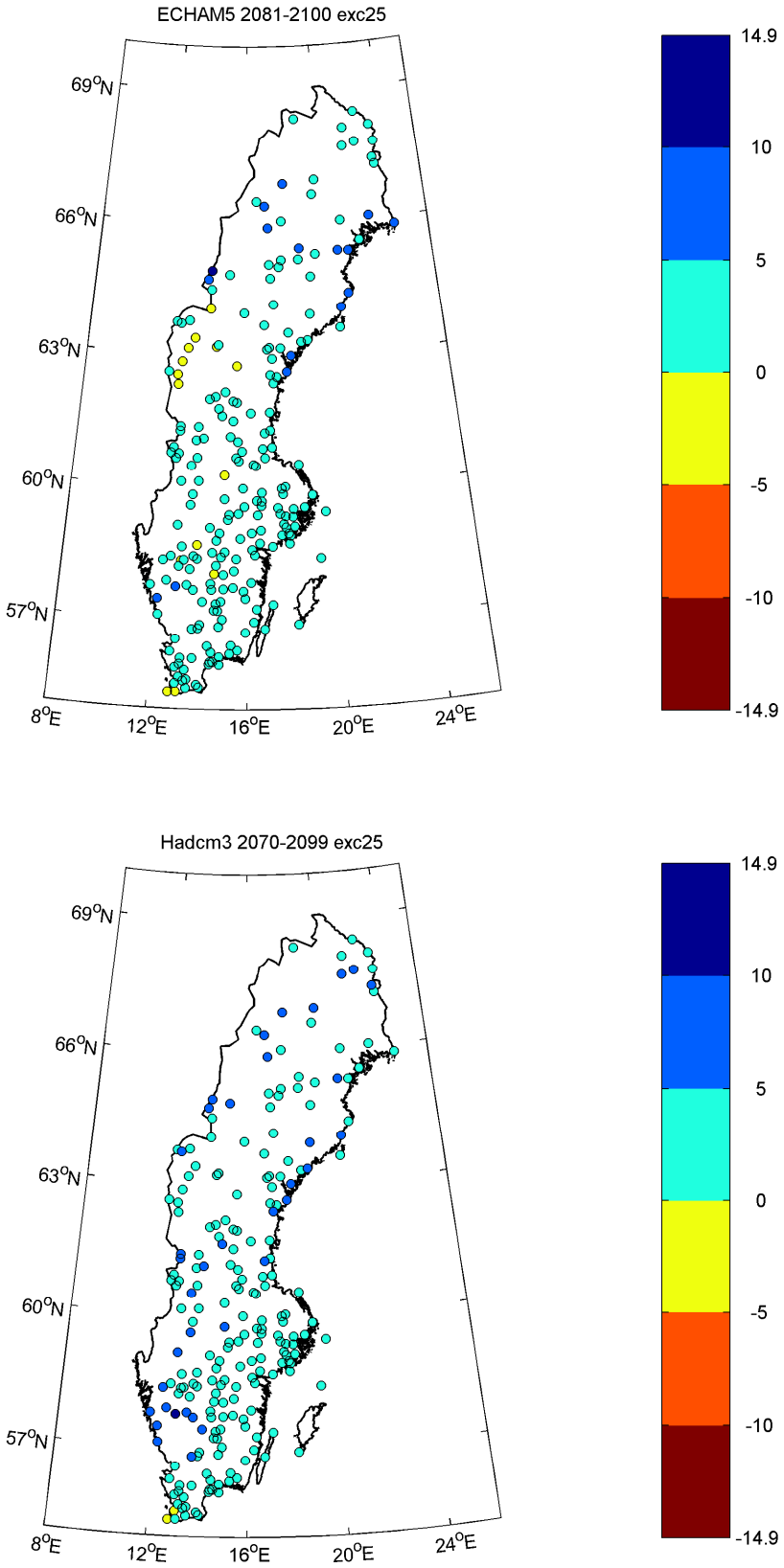

Figure 3.43: Annual changes in *exc25* (in days) at 220 stations in Sweden derived from WG-simulations based on the ECHAM5 scenario run for the years 2081 to 2100 (upper panel) and the HadCM3 scenario run for the years 2070 to 2099 (lower panel). The annual changes are calculated as 'future simulated climate minus observation'.

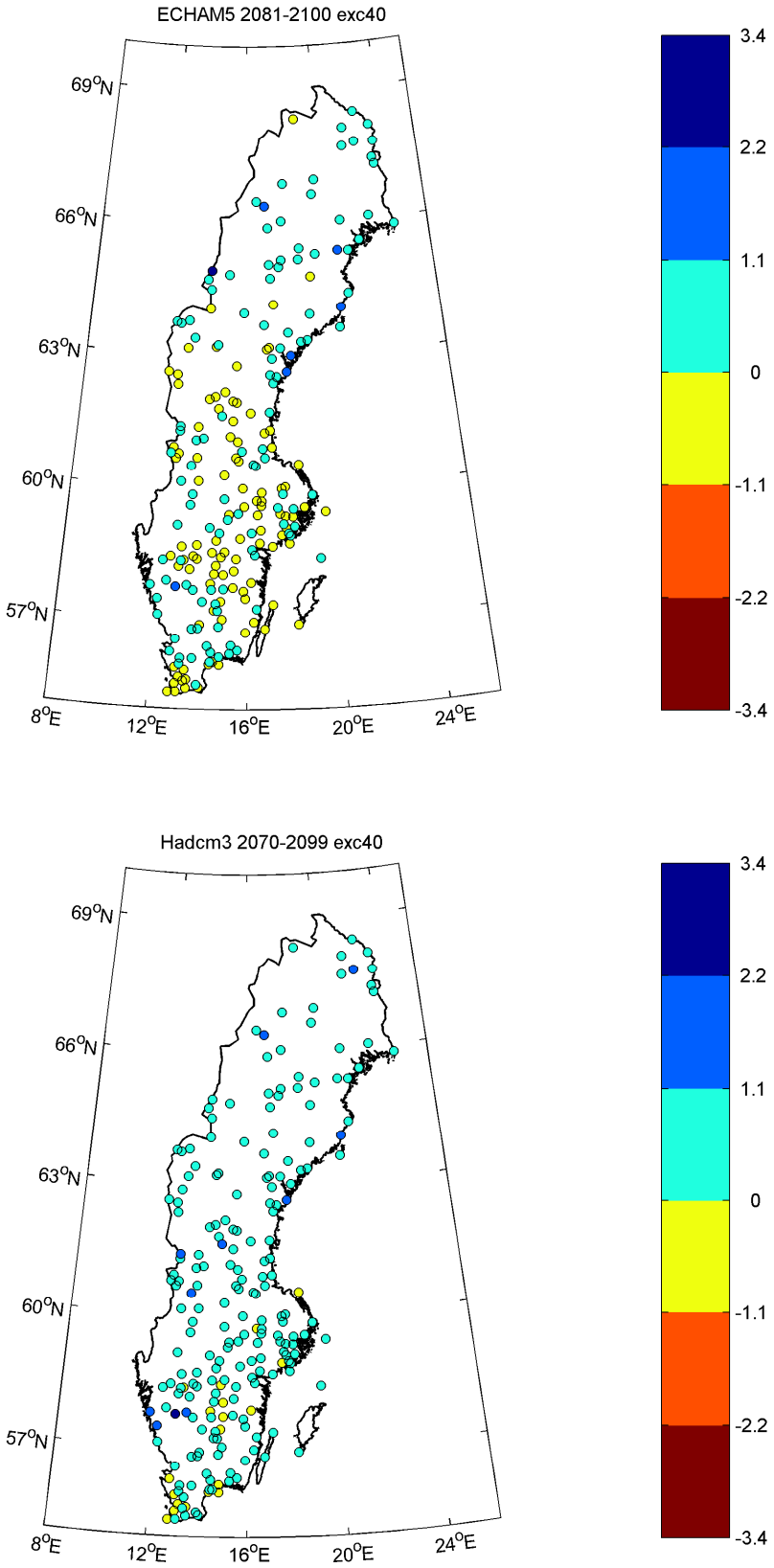

Figure 3.44: Annual changes in *exc40* (in mm) at 220 stations in Sweden derived from WG-simulations based on the ECHAM5 scenario run for the years 2081 to 2100 (upper panel) and the HadCM3 scenario run for the years 2070 to 2099 (lower panel). The annual changes are calculated as 'future simulated climate minus observation'.

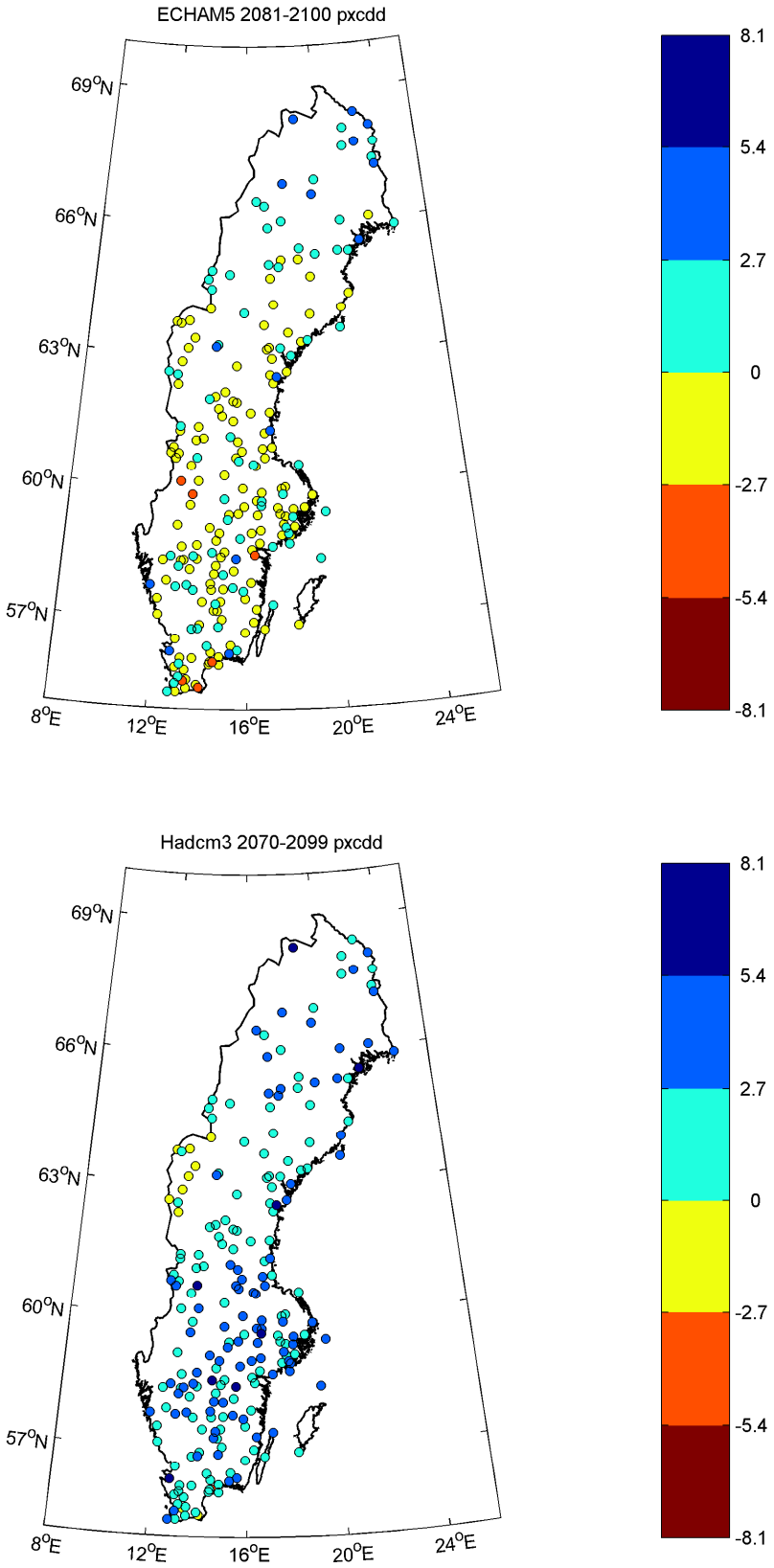

Figure 3.45: Annual changes in *pxcdd* (in days) at 220 stations in Sweden derived from WG-simulations based on the ECHAM5 scenario run for the years 2081 to 2100 (upper panel) and the HadCM3 scenario run for the years 2070 to 2099 (lower panel). The annual changes are calculated as 'future simulated climate minus observation'.

Table 3.1: Fraction of stations (%) with positive, zero or negative annual changes in the precipitation indices derived from WG-simulations based on the HadCM3 and ECHAM5 scenario climate. The magnitude of the change is divided into seven classes; three classes for negative and positive changes respectively, one class for zero change. The size of the '-' and '+' symbols indicate the various classes, the corresponding intervals and their unit are given in the row for each index.

Index and fraction of staton (%)	**–**	**–**	**-**	no change	+	+	+
***Nrain* (days)**	**<-28.2 – -42.3**	**<-28.2 – -14.1**	**<0 – -14.1**	**0**	**>0 – 14.1**	**>14.1 – 28.2**	**>28.2 – 42.3**
HadCM3	1	53	26	0	13	8	0
ECHAM5	0	20	35	0	21	15	9
***pint* (mm)**	**<4.2 – -6.4**	**<-2.1 – -4.2**	**<0 – -2.1**	**0**	**>0 – 2.1**	**>2.1 – 4.2**	**>4.2 – 6.4**
HadCM3	0	0	0	0	7	58	35
ECHAM5	0	0	0	0	38	55	7
***pq90* (mm)**	**<-7.9 – -11.9**	**<-3.9 – -7.9**	**<0 – -3.9**	**0**	**>0 – 3.9**	**>3.9 – 7.9**	**>7.9 – 11.9**
HadCM3	0	0	0	0	8	62	30
ECHAM5	0	0	0	0	41	53	6
***px1d* (mm/day)**	**<-13.3 – -20**	**<-6.7 – -13.3**	**<0 – -6.7**	**0**	**>0 – 6.7**	**>6.7 – 13.3**	**>13.3 – 20**
HadCM3	0	0	5	0	47	40	8
ECHAM5	0	0	33	0	48	16	3
***px5d* (mm/5 days)**	**<-55.4 – -36.9**	**<-36.9 – -18.5**	**<0 – -18.5**	**0**	**>0 – 18.5**	**>18.5 –36.9**	**>36.9 – 55.4**
HadCM3	0	0	12	0	24	64	10
ECHAM5	0	0	8	0	68	19	5
***exc25* (days)**	**<-15 – -10**	**<-10 – -14.9**	**<0 – -5**	**0**	**>0 – 5**	**>5 – 10**	**>10 – 15**
HadCM3	0	1	1	0	83	16	0
ECHAM5	0	0	6	0	85	6	3
***exc40* (days)**	**<-2.2 – -3.4**	**<-1.1 – -2.2**	**<0 – -1.1**	**0**	**>0 – 1.1**	**>1.1 – 2.2**	**>2.2 – 3.4**
HadCM3	0	0	9	0	86	5	0
ECHAM5	0	0	46	0	51	3	0
***pxcdd* (days)**	**<-5.4 – -8.1**	**<-2.7 – -5.4**	**<0 – -2.7**	**0**	**>0 – 2.7**	**>2.71 – 5.4**	**>5.4 – 8.1**
HadCM3	0	0	5	0	54	37	4
ECHAM5	0	3	58	0	32	7	0

3.5.2 Seasonal change

To study the magnitude and spatial distributions of the precipitation changes over the course of the year, the changes in each precipitation index between today's climate and the future conditions were calculated separately for winter (December, January, February), spring (March, April, May), summer (June, July, August) and autumn (September, October, November). Like for the annual changes, the results are presented as maps (Figure 3.46 to 3.53). Table 3.2 and Figure 3.54 present the fraction of stations having positive, negative or zero change.

Generally, all precipitation indices despite *Nrain* and *pxcdd* point toward wetter conditions at the majority of all stations and in the different seasons. This is in line with the positive changes at annual scale. The magnitude of the changes varies depending on season, region and GCM used. Compared to the changes in the other indices, the magnitude and the sign of the changes in *Nrain* (Figure 3.46) are to a larger extent dependent on season. The changes are spatially more homogeneous resulting in clear geographical patterns. In winter, the frequency of wet days increase in almost all parts of Sweden as suggested by all local scenarios. Towards spring, large parts of Southern and central Sweden experience a slight decrease in *Nrain*, the remaining regions are characterized by a slight increase. In summer, the frequency of wet days drops everywhere except in northernmost (ECHAM5) and North-West (HadCM3) Sweden. The decrease is especially pronounced in Southern Sweden. In autumn, less wet days are expected in the South-Easterly half of the country according to the ECHAM5-based scenarios. The HadCM3-based simulations suggest a decrease everywhere except in the North-West of Sweden. Regarding the indices *pint* and *p90*, the local scenarios based on the both GCMs produce very similar results, suggesting higher precipitation intensities on rainy days and increased moderate extremes at all stations (very few exceptions occur) in all seasons (Figure 3.47 and 3.48).

Changes in *px1d* and *px5d* (Figure 3.49 and 3.50) are mainly towards stronger intensities at the majority of the stations in spring and winter, however, according to the ECHAM5-based simulations, the maximum one-day and five-days amounts decrease at many stations in Southern and central Sweden in summer and autumn. The majority of stations will experience a slight increase in the number of days exceeding 25 mm/day according to the HadCM3-based local scenarios in all seasons. In winter, however, many stations located in Northern Sweden will not experience any change. Index *exc25* (Figure 3.51) also slightly increases in winter and spring in the ECHAM5-based simulations, whereas *exc25* in Southern Sweden decreases at many stations in summer. In autumn many stations in Southern Sweden are without any change. For the strongest extremes, *exc40*, a rather heterogeneous picture emerges with positive, negative and zero changes occurring in all seasons (Figure 3.52). Especially the ECHAM5-based simulations estimate at many stations either a drop in the number of days exceeding 40 mm or zero change in winter, spring and autumn. According to HadCM3, *exc40* increases at the greater part of the stations in spring, summer and autumn, while *exc40* remain unchanged at many stations in winter. For *pxcdd*, positive as well as negative changes occur in all seasons both in the HadCM3- and the ECHAM5-based simulations (Figure 3.53). Especially the ECHAM-based local scenarios suggest a decrease in the number of consecutive dry days in autumn and winter, a raise in *pxcdd* occur mainly in summer at stations located in Southern Sweden. According to the local scenarios using HadCM3, *pxcdd* mainly increases in all seasons despite in winter when the fraction of stations with negative changes is relatively high.

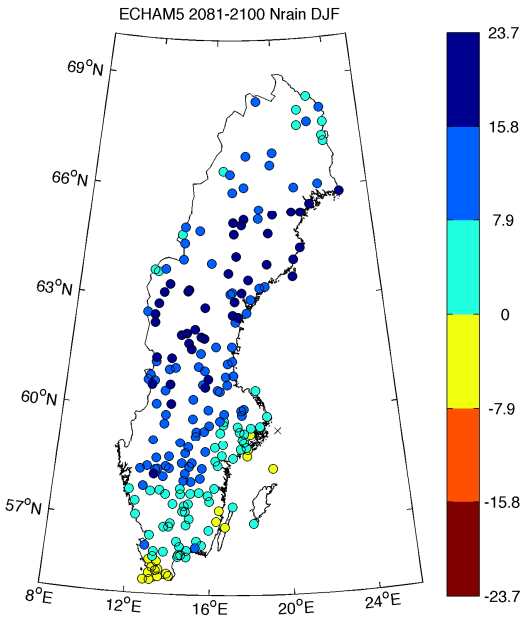
ECHAM5 2081-2100 Nrain DJF
69°N
66°N
63°N
60°N
57°N
8°E
12°E
16°E
20°E
24°E
23.7
15.8
7.9
0
-7.9
-15.8
-23.7

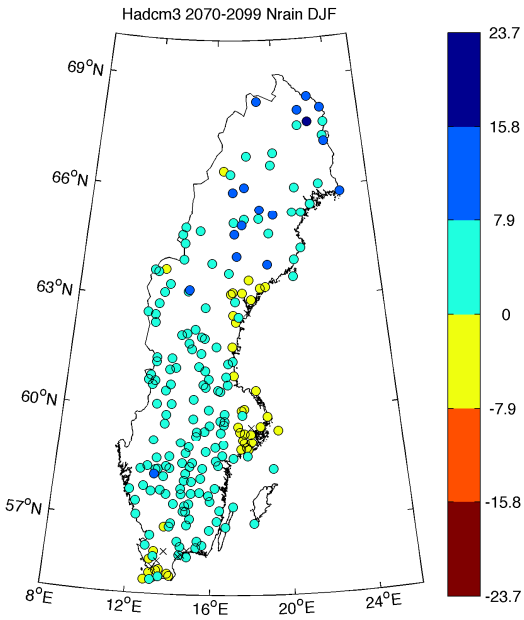
Hadcm3 2070-2099 Nrain DJF
69°N
66°N
63°N
60°N
57°N
8°E
12°E
16°E
20°E
24°E
23.7
15.8
7.9
0
-7.9
-15.8
-23.7

a)

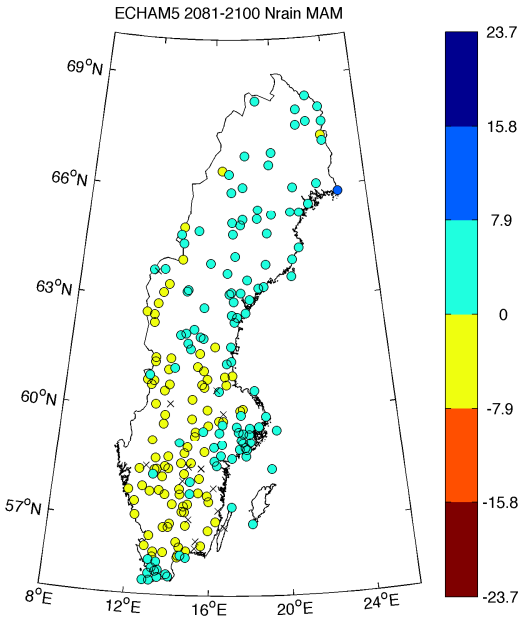
ECHAM5 2081-2100 Nrain MAM
69°N
66°N
63°N
60°N
57°N
8°E
12°E
16°E
20°E
24°E
23.7
15.8
7.9
0
-7.9
-15.8
-23.7

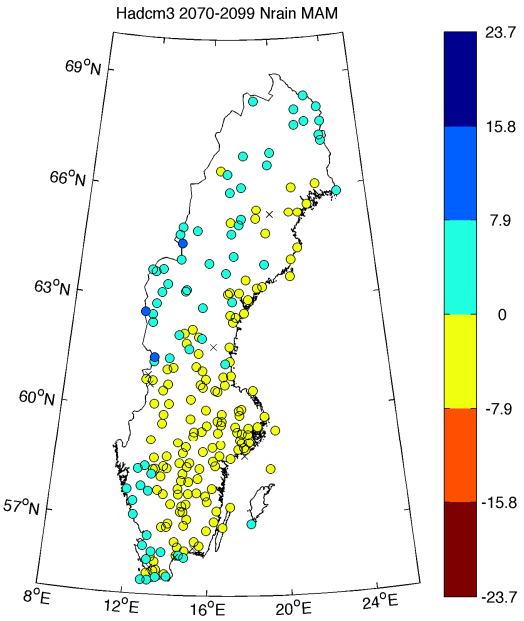
Hadcm3 2070-2099 Nrain MAM
69°N
66°N
63°N
60°N
57°N
8°E
12°E
16°E
20°E
24°E
23.7
15.8
7.9
0
-7.9
-15.8
-23.7

b)

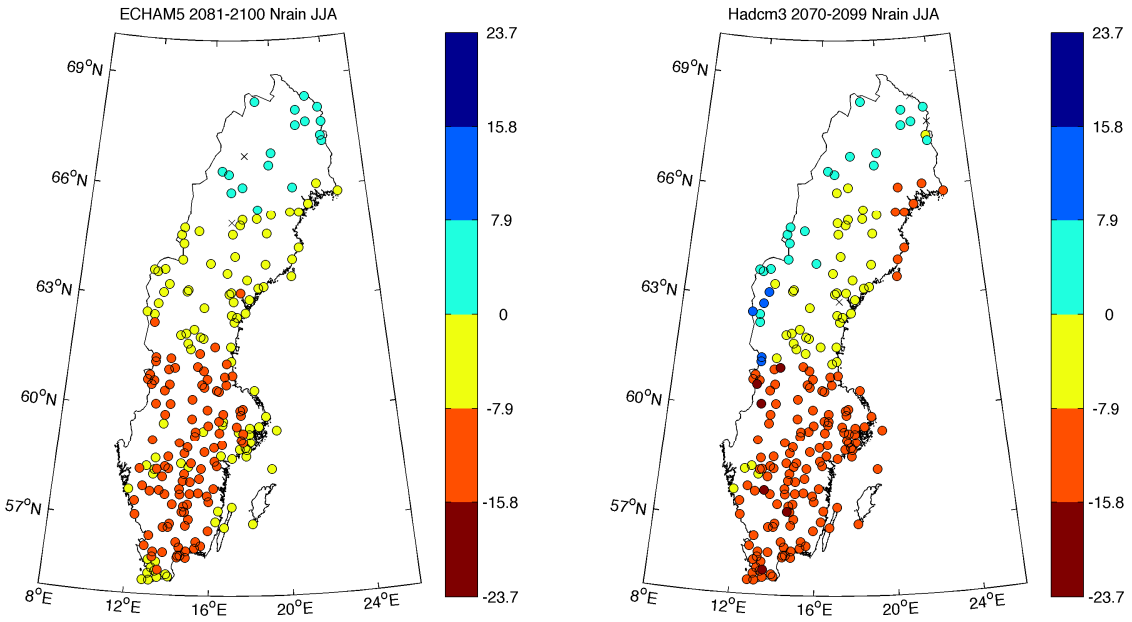

c)

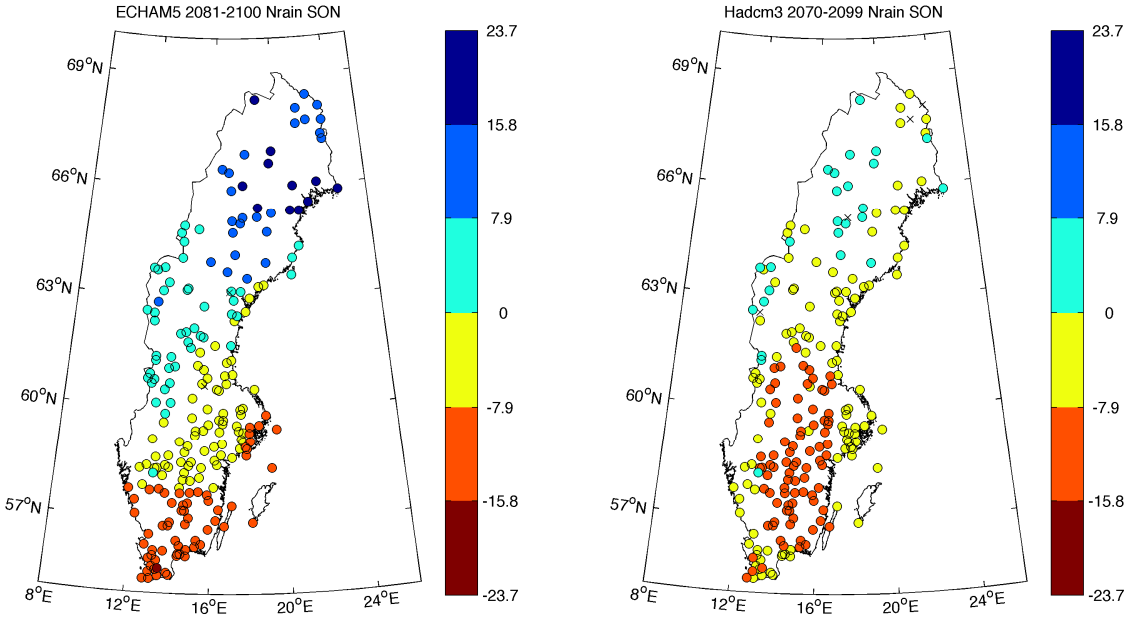

d)

Figure 3.46: Seasonal changes in *Nrain* (in days) at 220 stations in Sweden derived from WG-simulations based on the ECHAM5 scenario run for the years 2081 to 2100 (left column) and the HadCM3 scenario run for the years 2070 to 2099 (right column). The annual changes are calculated as 'future simulated climate minus observation'. Panel a): winter, b) spring, c) summer, d) autumn.

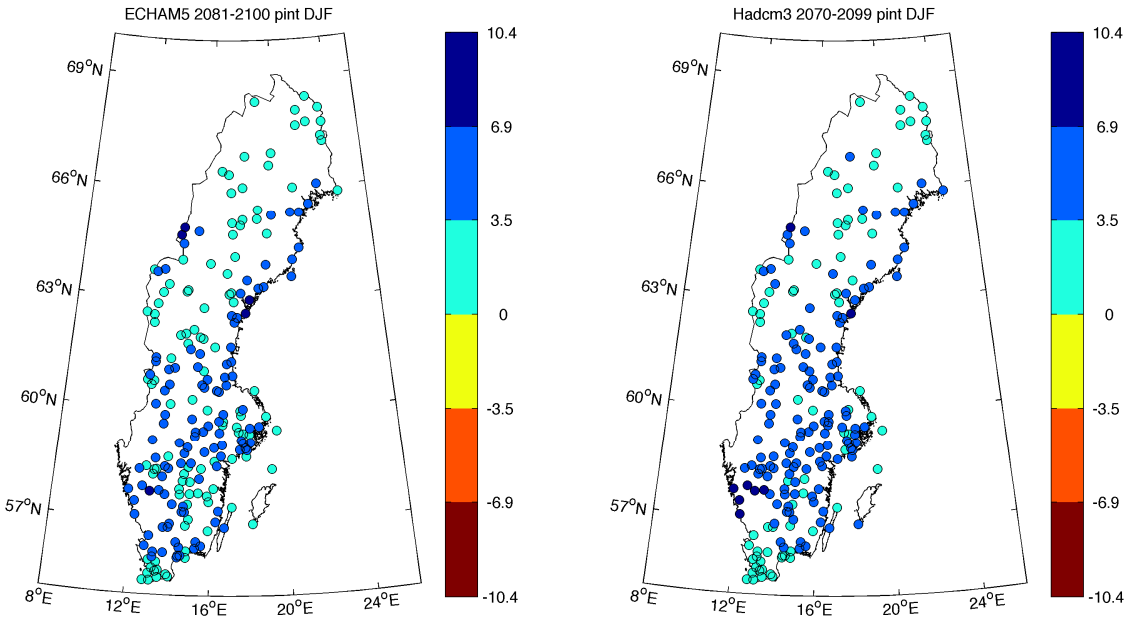
ECHAM5 2081-2100 pint DJF
Hadcm3 2070-2099 pint DJF
69°N
66°N
63°N
60°N
57°N
8°E
12°E
16°E
20°E
24°E
10.4
6.9
3.5
0
-3.5
-6.9
-10.4

a)

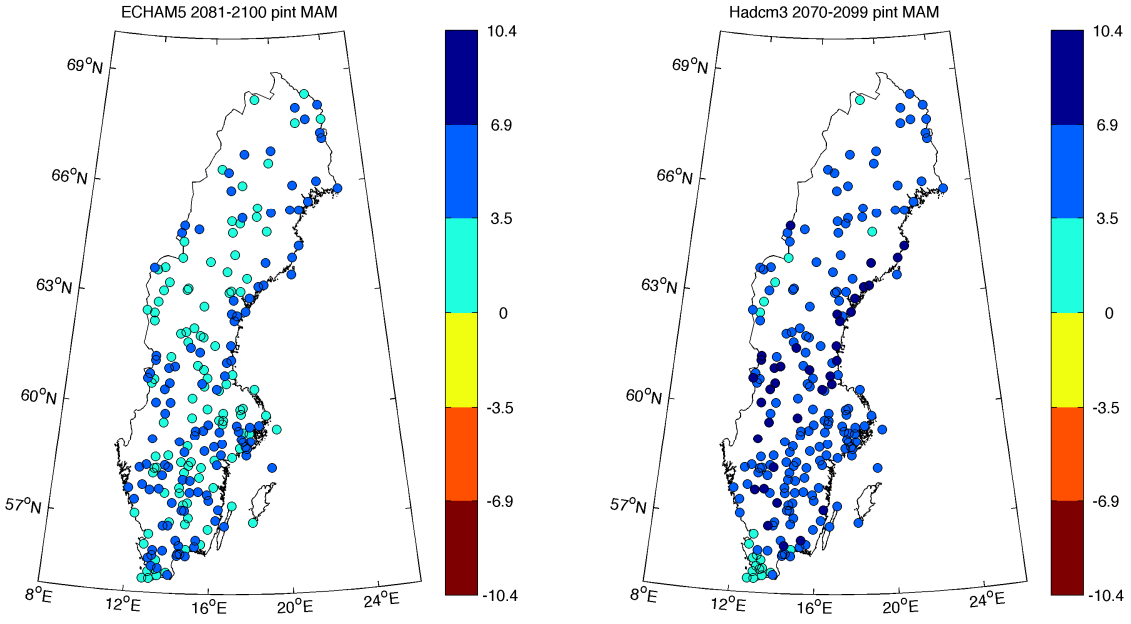
ECHAM5 2081-2100 pint MAM
Hadcm3 2070-2099 pint MAM
69°N
66°N
63°N
60°N
57°N
8°E
12°E
16°E
20°E
24°E
10.4
6.9
3.5
0
-3.5
-6.9
-10.4

b)

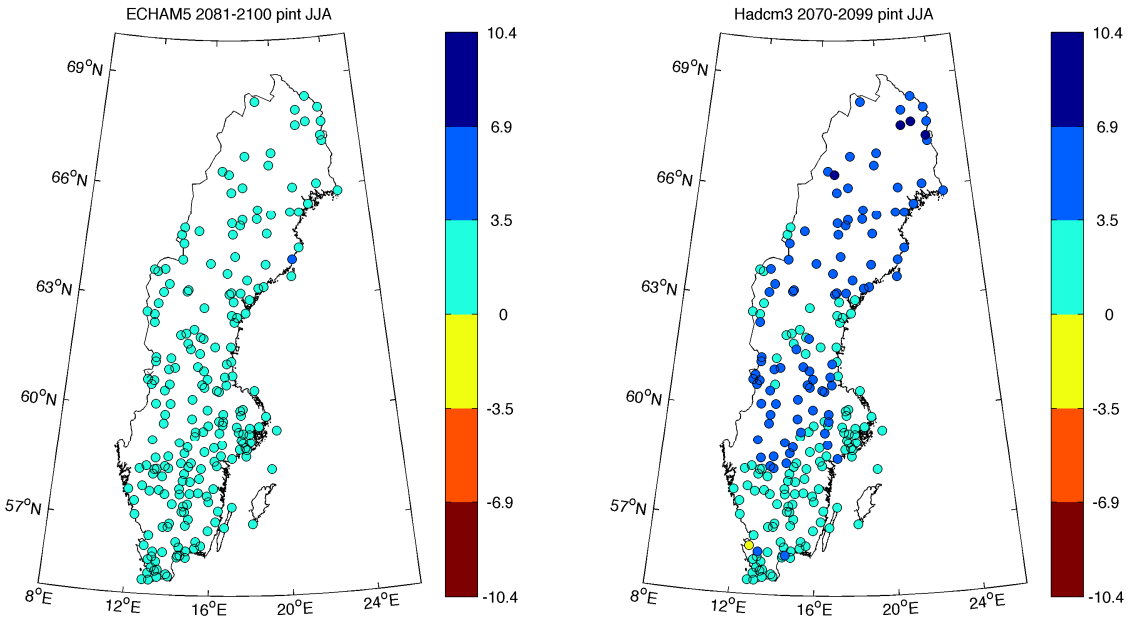

c)

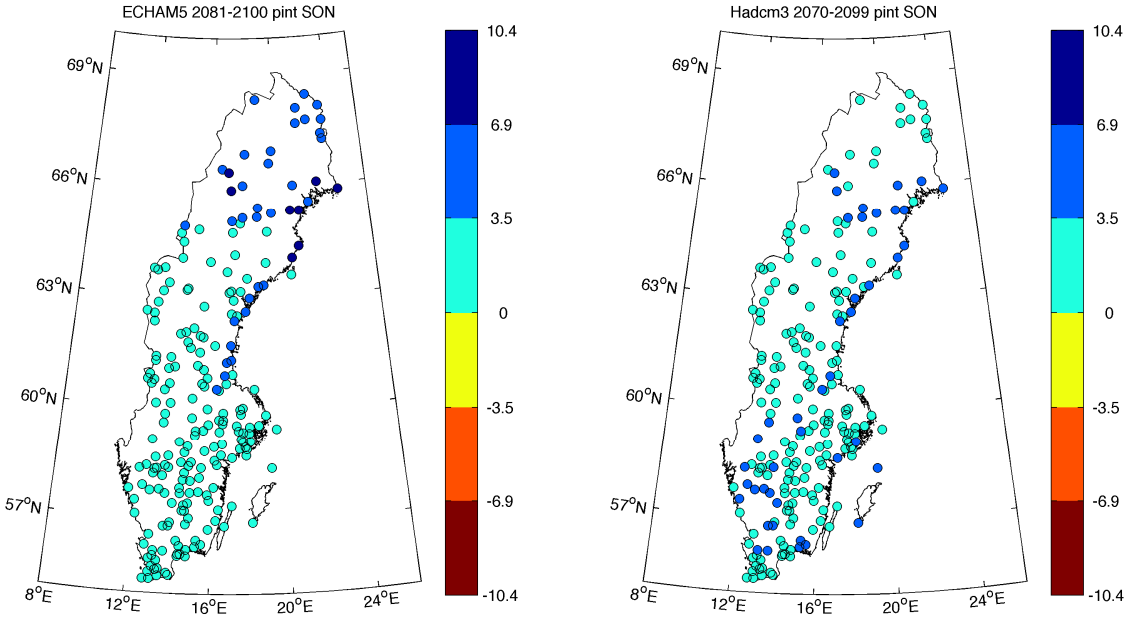

d)

Figure 3.47: Seasonal changes in *pint* (in mm) at 220 stations in Sweden derived from WG-simulations based on the ECHAM5 scenario run for the years 2081 to 2100 (left column) and the HadCM3 scenario run for the years 2070 to 2099 (right column). The annual changes are calculated as 'future simulated climate minus observation'. Panel a): winter, b) spring, c) summer, d) autumn.

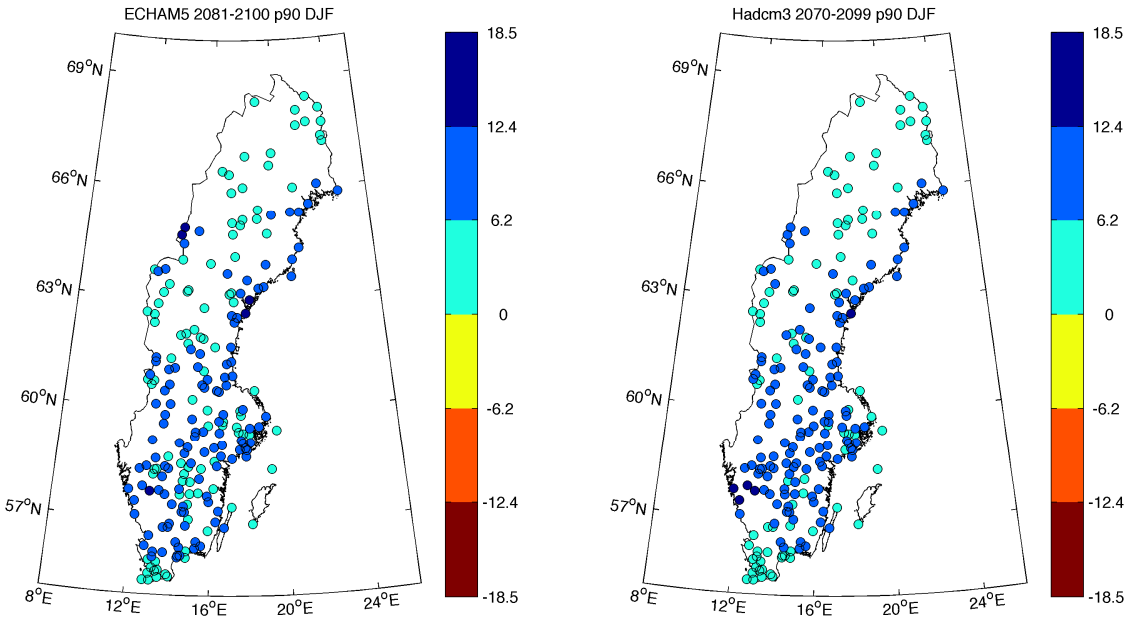
ECHAM5 2081-2100 p90 DJF
Hadcm3 2070-2099 p90 DJF
69°N
66°N
63°N
60°N
57°N
8°E
12°E
16°E
20°E
24°E
18.5
12.4
6.2
0
-6.2
-12.4
-18.5

a)

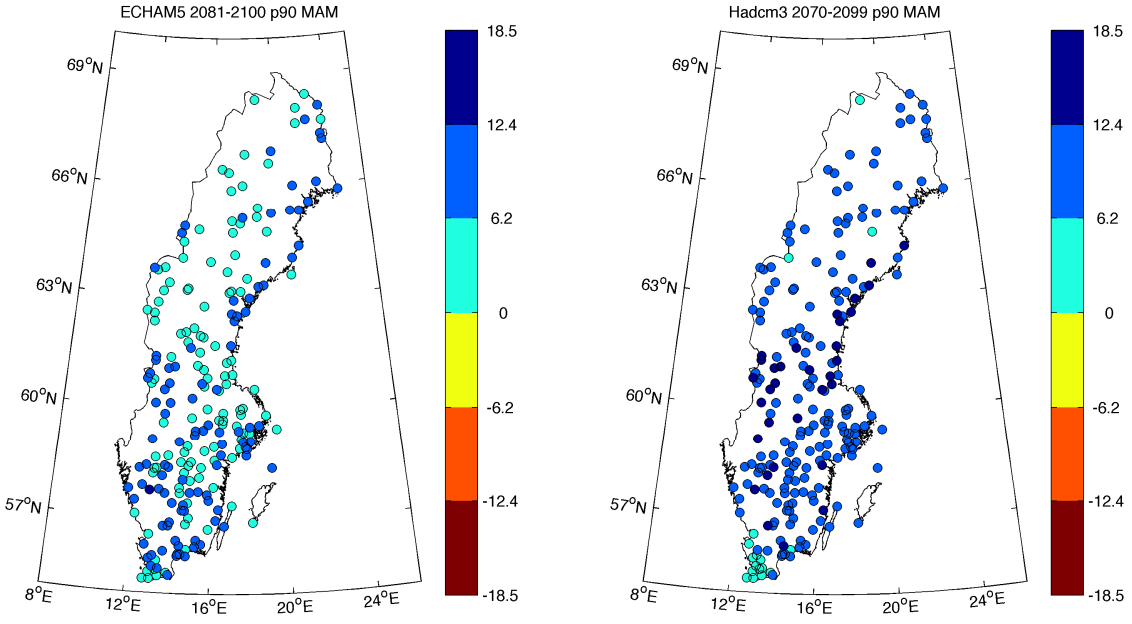
ECHAM5 2081-2100 p90 MAM
Hadcm3 2070-2099 p90 MAM
69°N
66°N
63°N
60°N
57°N
8°E
12°E
16°E
20°E
24°E
18.5
12.4
6.2
0
-6.2
-12.4
-18.5

b)

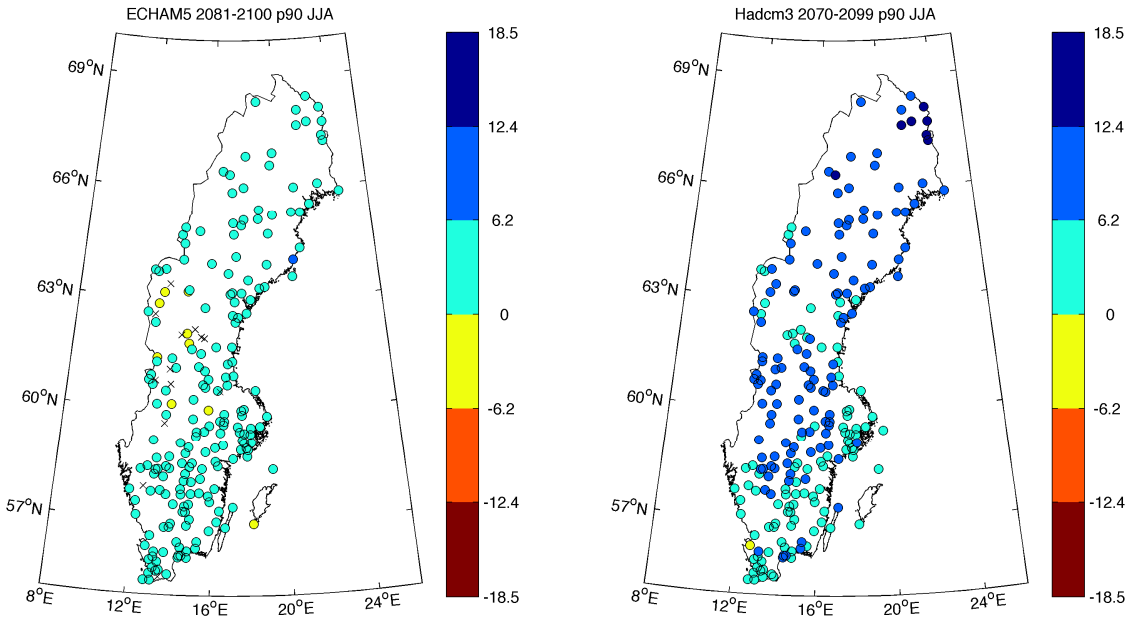

c)

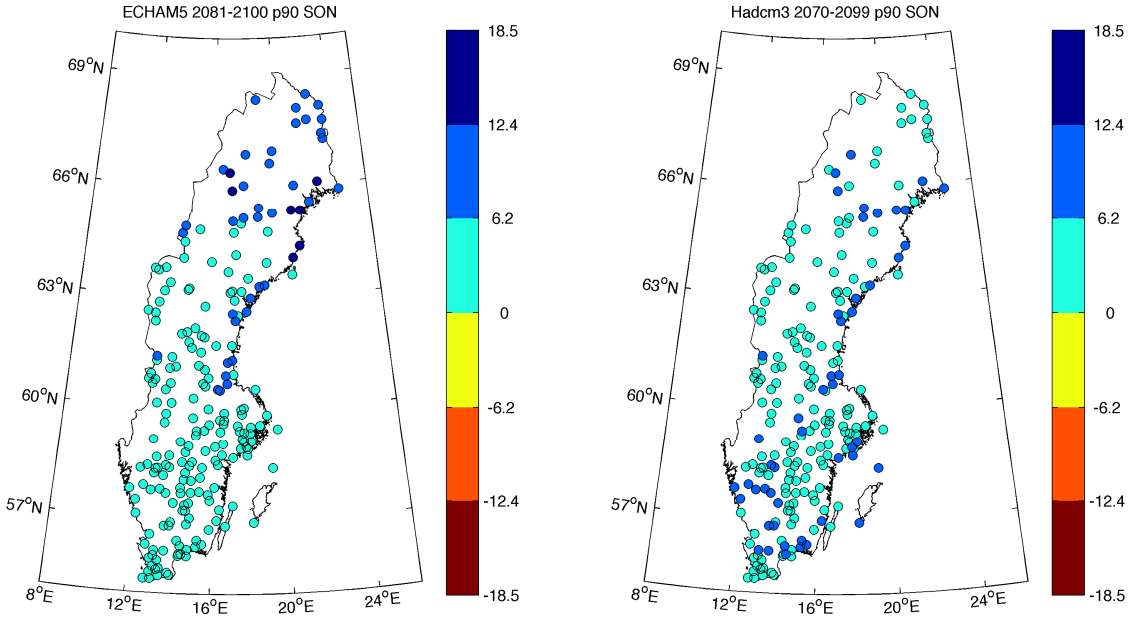

d)

Figure 3.48: Seasonal changes in *p90* (in mm) at 220 stations in Sweden derived from WG-simulations based on the ECHAM5 scenario run for the years 2081 to 2100 (left column) and the HadCM3 scenario run for the years 2070 to 2099 (right column). The annual changes are calculated as 'future simulated climate minus observation'. Panel a): winter, b) spring, c) summer, d) autumn.

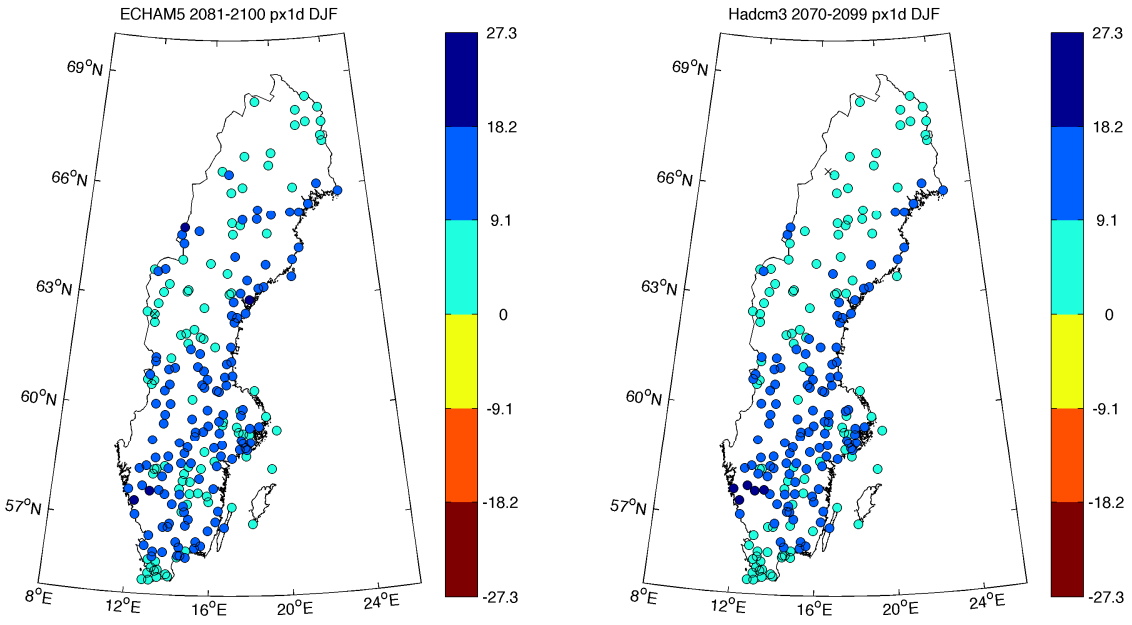
ECHAM5 2081-2100 px1d DJF
Hadcm3 2070-2099 px1d DJF
69°N
66°N
63°N
60°N
57°N
8°E
12°E
16°E
20°E
24°E
27.3
18.2
9.1
0
-9.1
-18.2
-27.3

a)

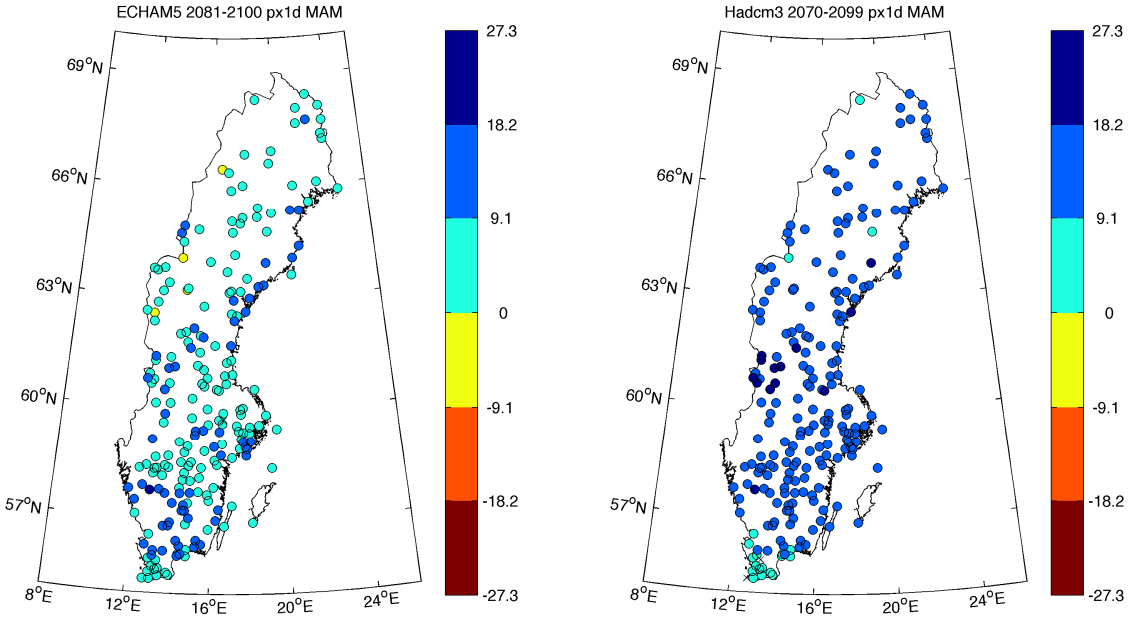
ECHAM5 2081-2100 px1d MAM
Hadcm3 2070-2099 px1d MAM
69°N
66°N
63°N
60°N
57°N
8°E
12°E
16°E
20°E
24°E
27.3
18.2
9.1
0
-9.1
-18.2
-27.3

b)

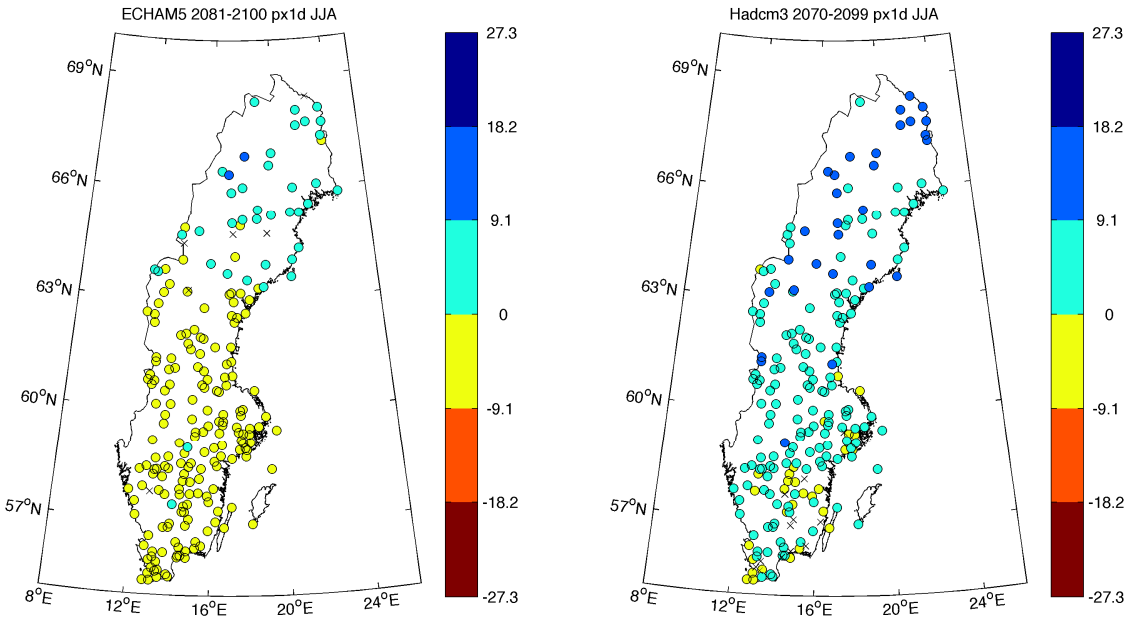

c)

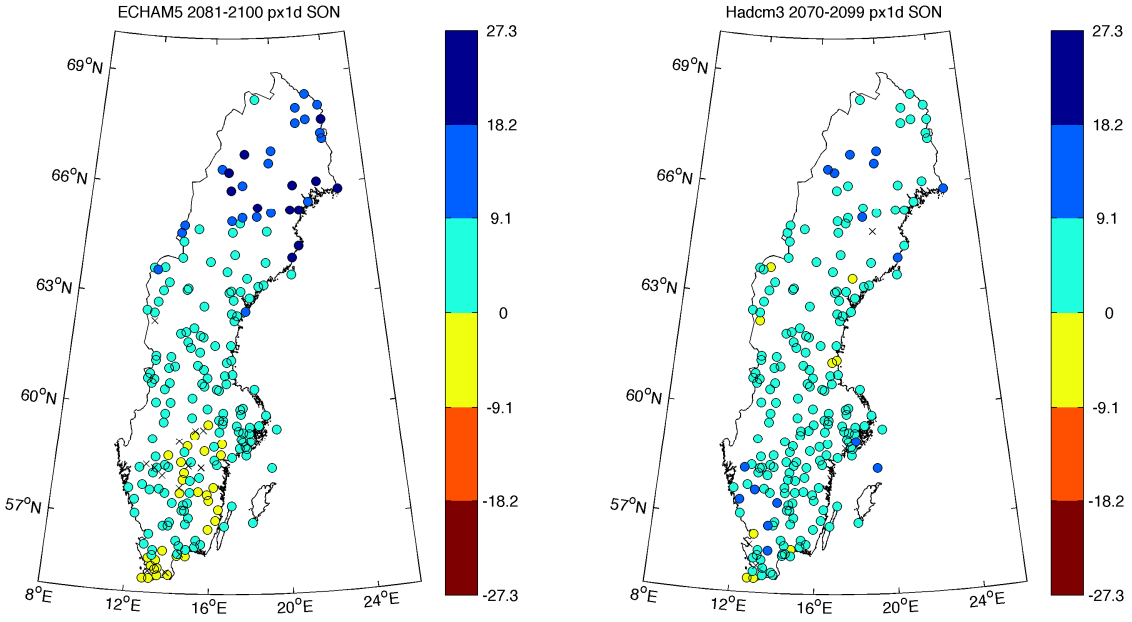

d)

Figure 3.49: Seasonal changes in *px1d* (in mm/day) at 220 stations in Sweden derived from WG-simulations based on the ECHAM5 scenario run for the years 2081 to 2100 (left column) and the HadCM3 scenario run for the years 2070 to 2099 (right column). The annual changes are calculated as 'future simulated climate minus observation'. Panel a): winter, b) spring, c) summer, d) autumn.

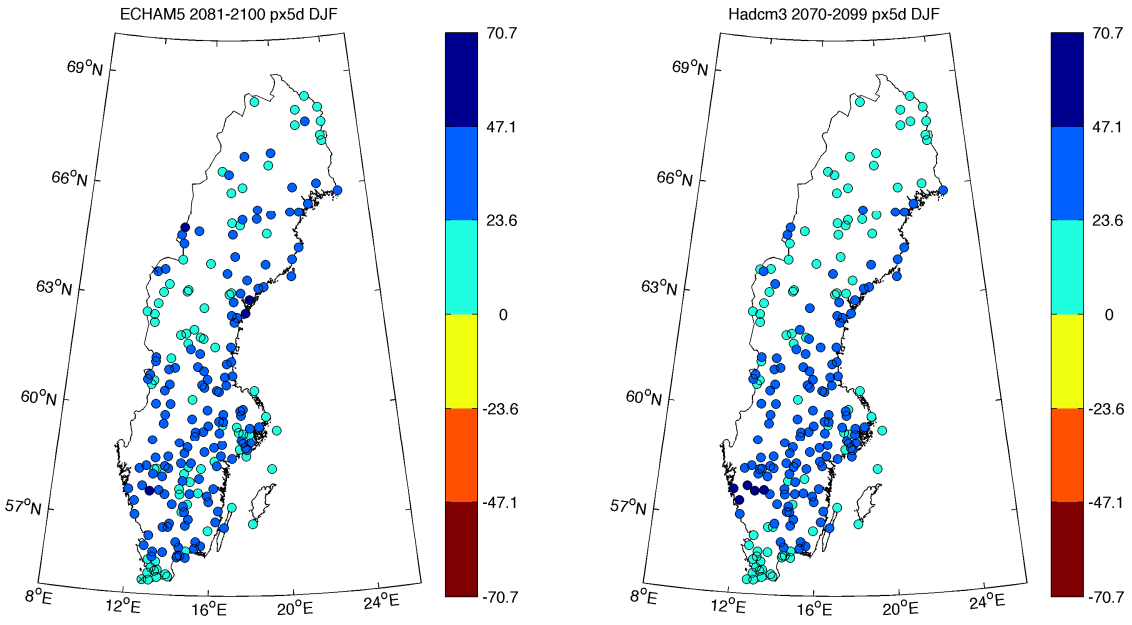
ECHAM5 2081-2100 px5d DJF
Hadcm3 2070-2099 px5d DJF
69°N
66°N
63°N
60°N
57°N
8°E
12°E
16°E
20°E
24°E
70.7
47.1
23.6
0
-23.6
-47.1
-70.7

a)

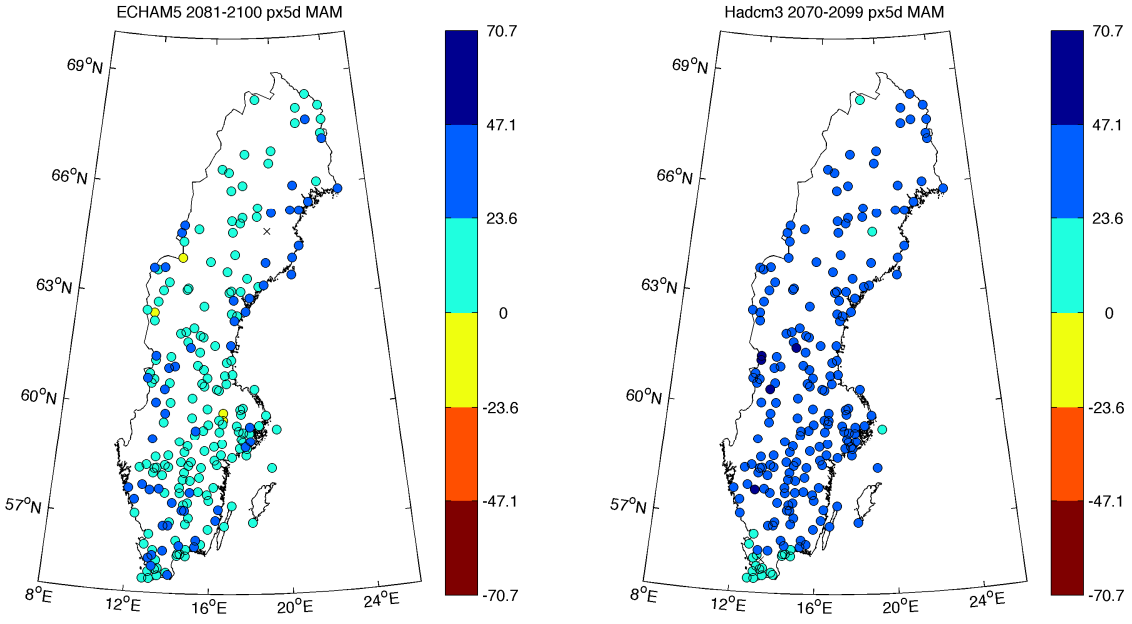
ECHAM5 2081-2100 px5d MAM
Hadcm3 2070-2099 px5d MAM
69°N
66°N
63°N
60°N
57°N
8°E
12°E
16°E
20°E
24°E
70.7
47.1
23.6
0
-23.6
-47.1
-70.7

b)

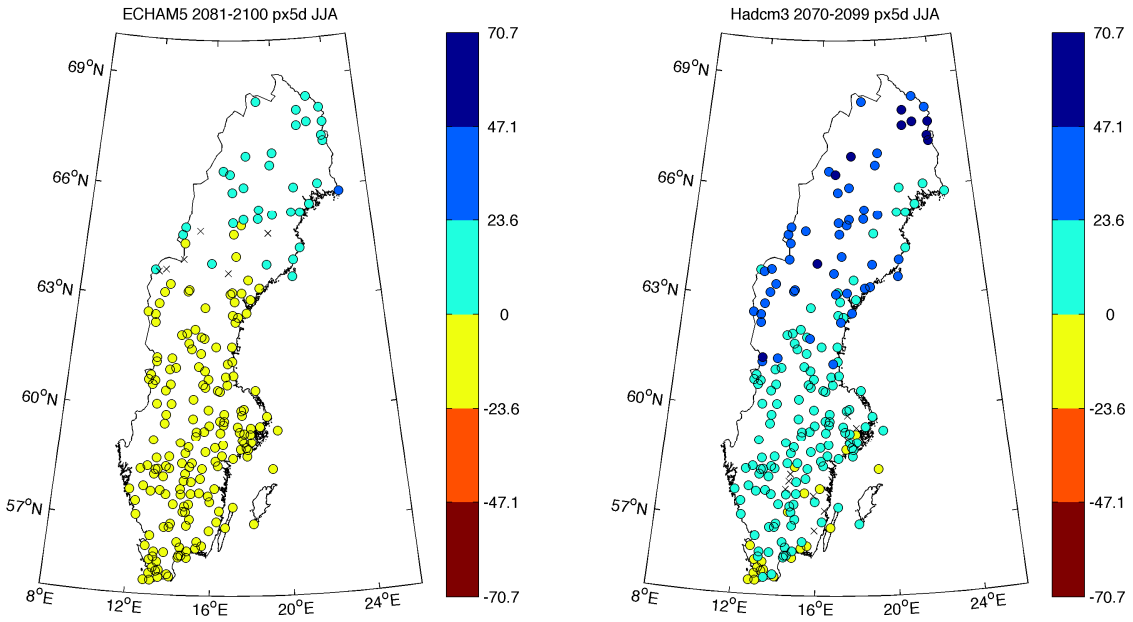

c)

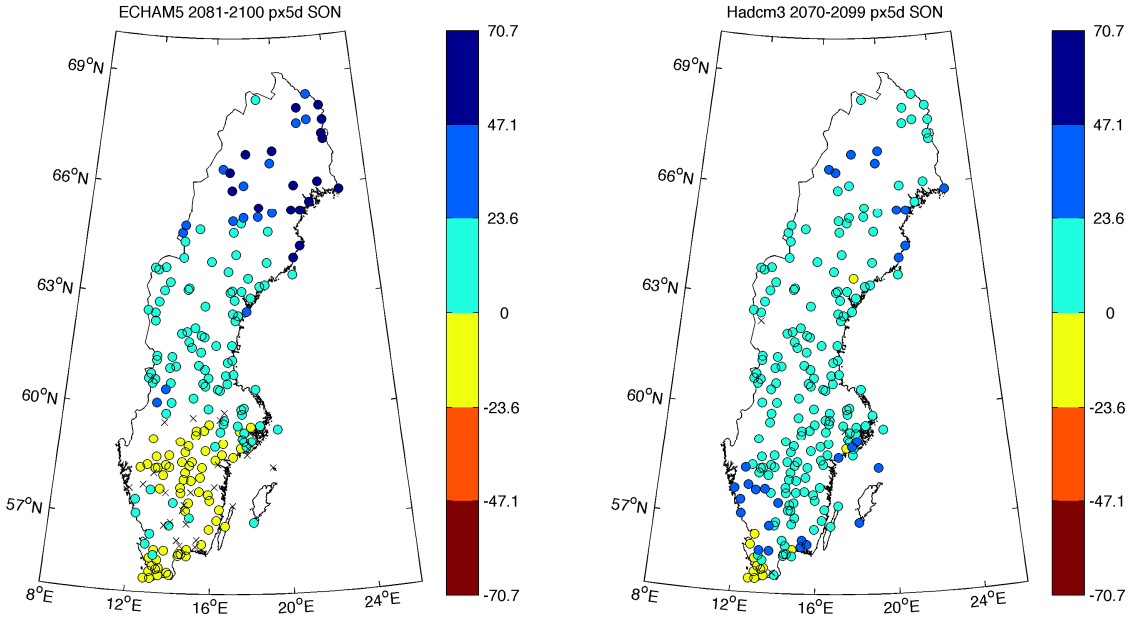

d)

Figure 3.50: Seasonal changes in *px5d* (in mm/5 days) at 220 stations in Sweden derived from WG-simulations based on the ECHAM5 scenario run for the years 2081 to 2100 (left column) and the HadCM3 scenario run for the years 2070 to 2099 (right column). The annual changes are calculated as 'future simulated climate minus observation'. Panel a): winter, b) spring, c) summer, d) autumn.

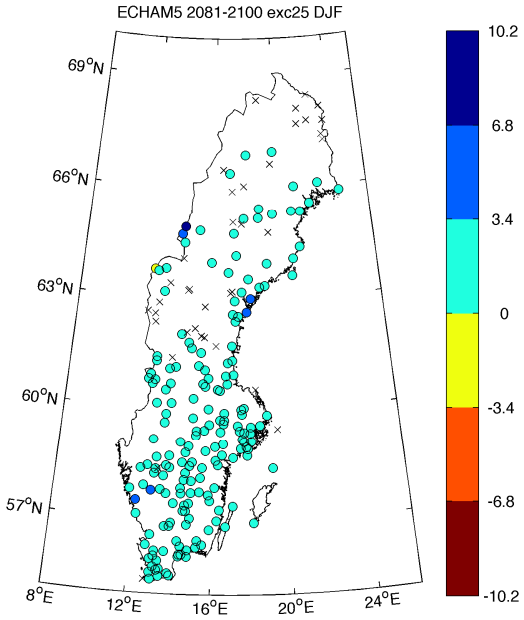
ECHAM5 2081-2100 exc25 DJF
69°N
66°N
63°N
60°N
57°N
8°E
12°E
16°E
20°E
24°E
10.2
6.8
3.4
0
-3.4
-6.8
-10.2

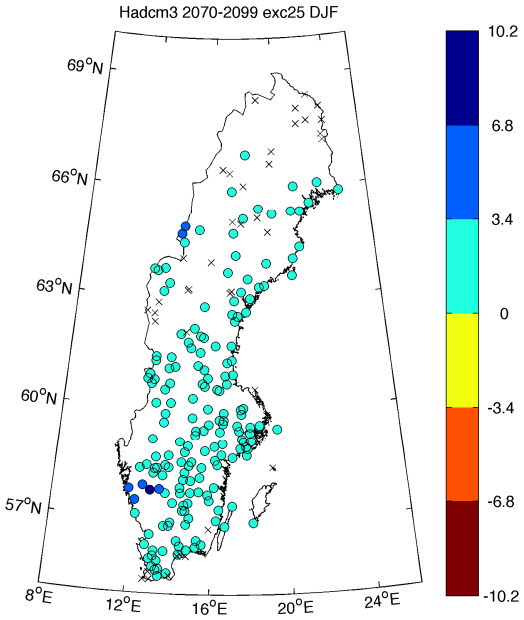
Hadcm3 2070-2099 exc25 DJF
69°N
66°N
63°N
60°N
57°N
8°E
12°E
16°E
20°E
24°E
10.2
6.8
3.4
0
-3.4
-6.8
-10.2

a)

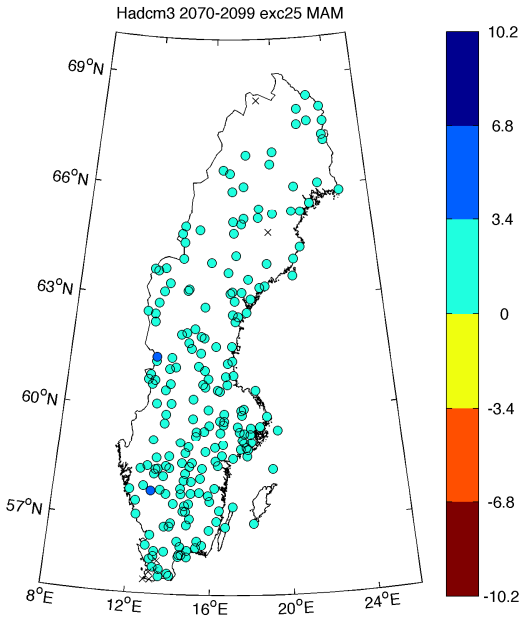
Hadcm3 2070-2099 exc25 MAM
69°N
66°N
63°N
60°N
57°N
8°E
12°E
16°E
20°E
24°E
10.2
6.8
3.4
0
-3.4
-6.8
-10.2

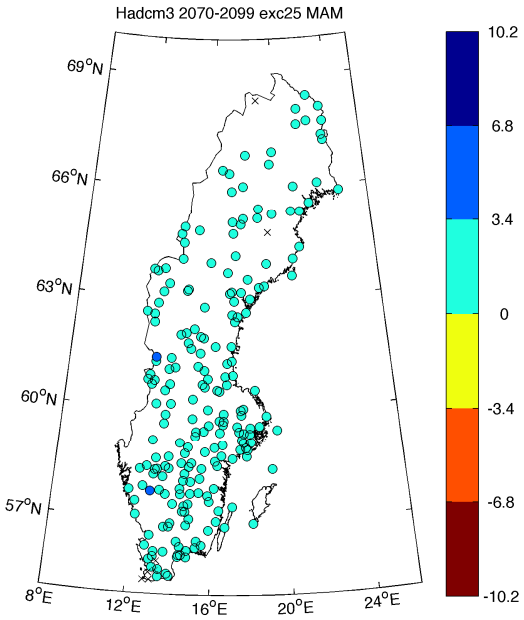
Hadcm3 2070-2099 exc25 MAM
69°N
66°N
63°N
60°N
57°N
8°E
12°E
16°E
20°E
24°E
10.2
6.8
3.4
0
-3.4
-6.8
-10.2

b)

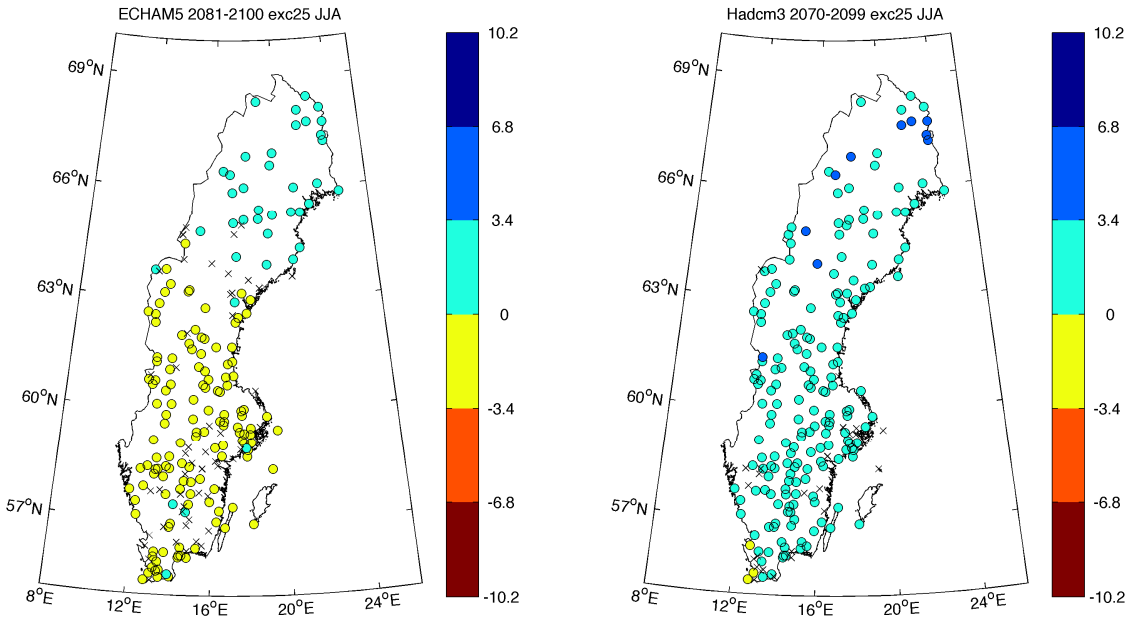

c)

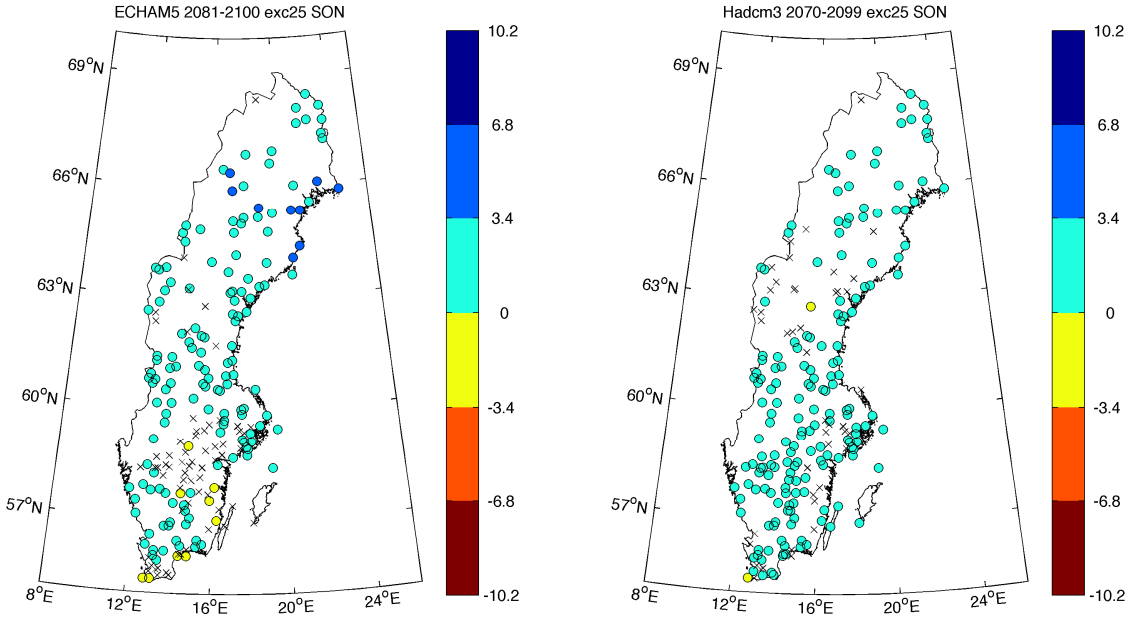

d)

Figure 3.51: Seasonal changes in *exc25* (in days) at 220 stations in Sweden derived from WG-simulations based on the ECHAM5 scenario run for the years 2081 to 2100 (left column) and the HadCM3 scenario run for the years 2070 to 2099 (right column). The annual changes are calculated as 'future simulated climate minus observation'. Panel a): winter, b) spring, c) summer, d) autumn.

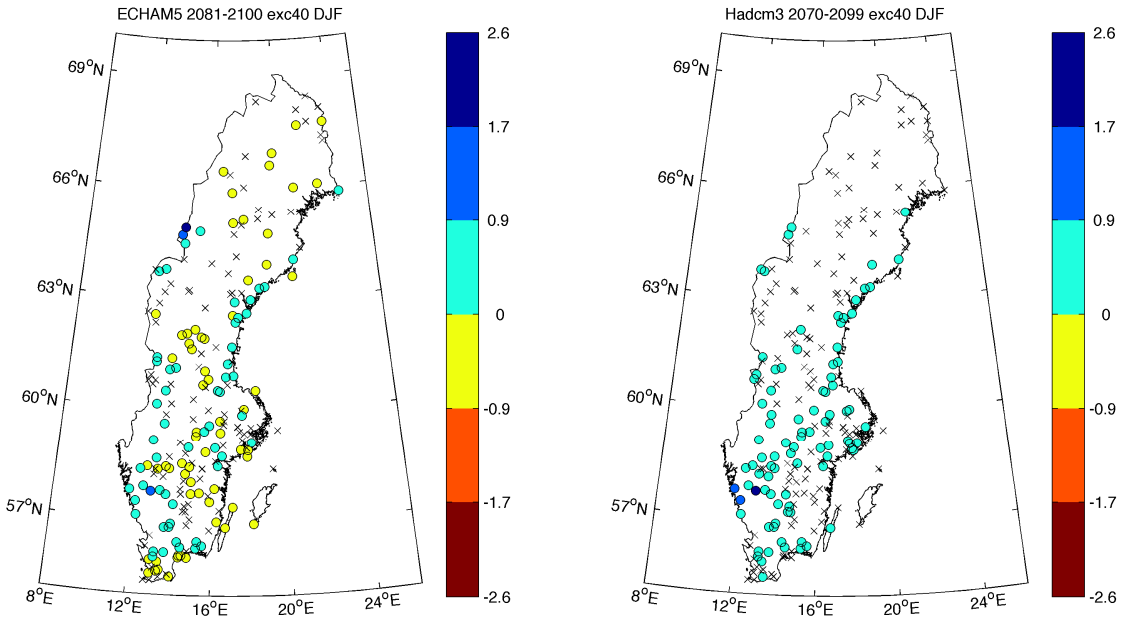
ECHAM5 2081-2100 exc40 DJF
Hadcm3 2070-2099 exc40 DJF
69°N
66°N
63°N
60°N
57°N
8°E
12°E
16°E
20°E
24°E
2.6
1.7
0.9
0
-0.9
-1.7
-2.6

a)

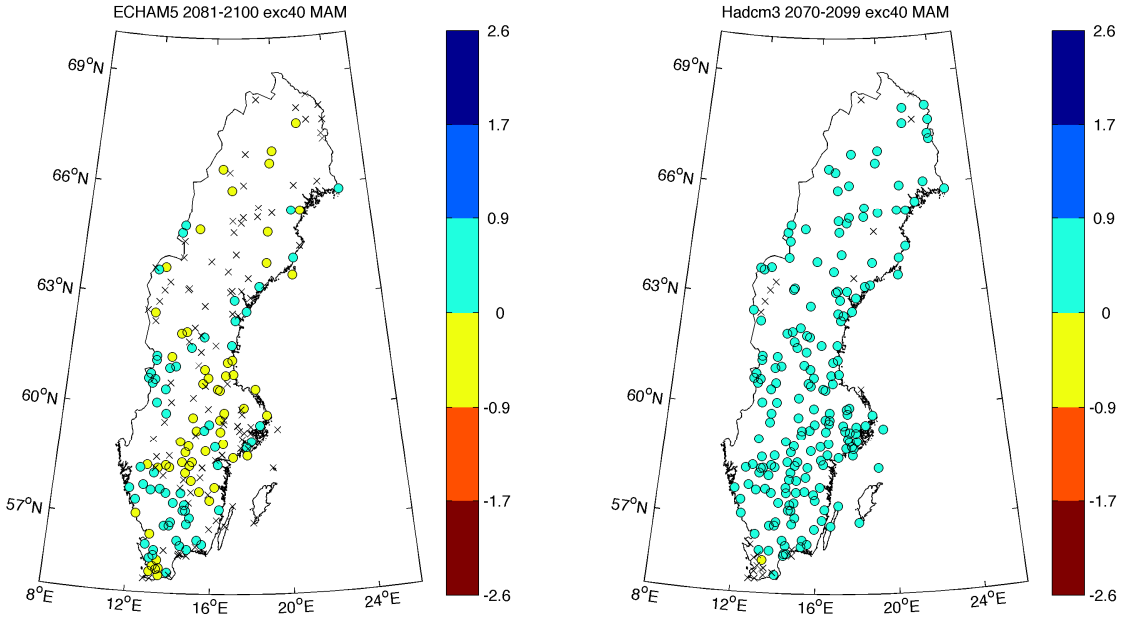
ECHAM5 2081-2100 exc40 MAM
Hadcm3 2070-2099 exc40 MAM
69°N
66°N
63°N
60°N
57°N
8°E
12°E
16°E
20°E
24°E
2.6
1.7
0.9
0
-0.9
-1.7
-2.6

b)

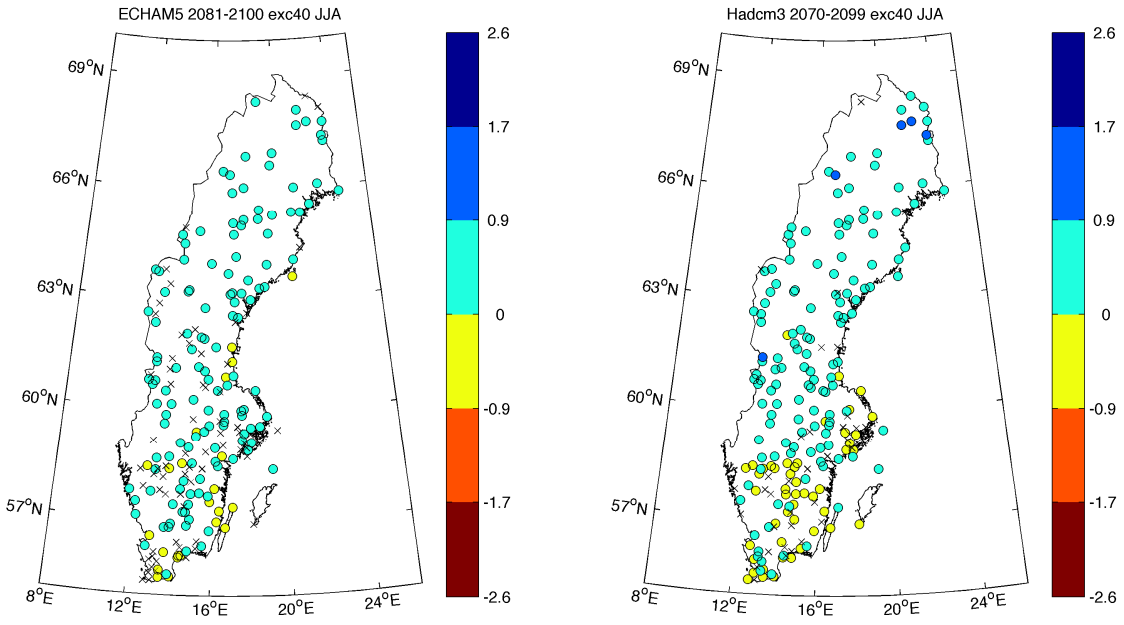

c)

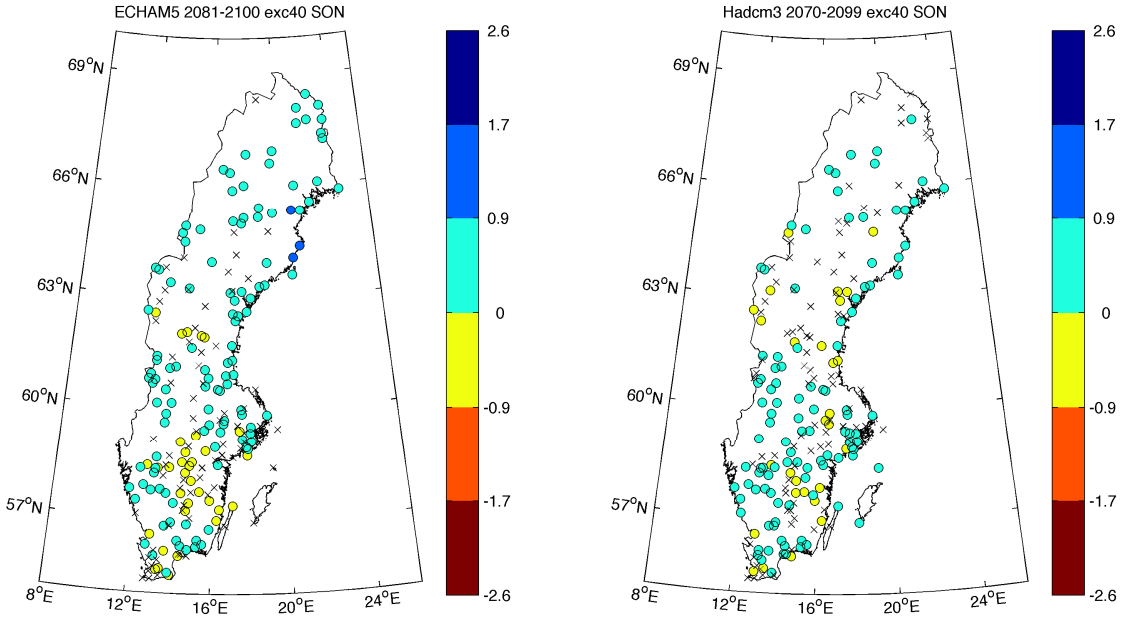

d)

Figure 3.52: Seasonal changes in *exc40* (in days) at 220 stations in Sweden derived from WG-simulations based on the ECHAM5 scenario run for the years 2081 to 2100 (left column) and the HadCM3 scenario run for the years 2070 to 2099 (right column). The annual changes are calculated as 'future simulated climate minus observation'. Panel a): winter, b) spring, c) summer, d) autumn.

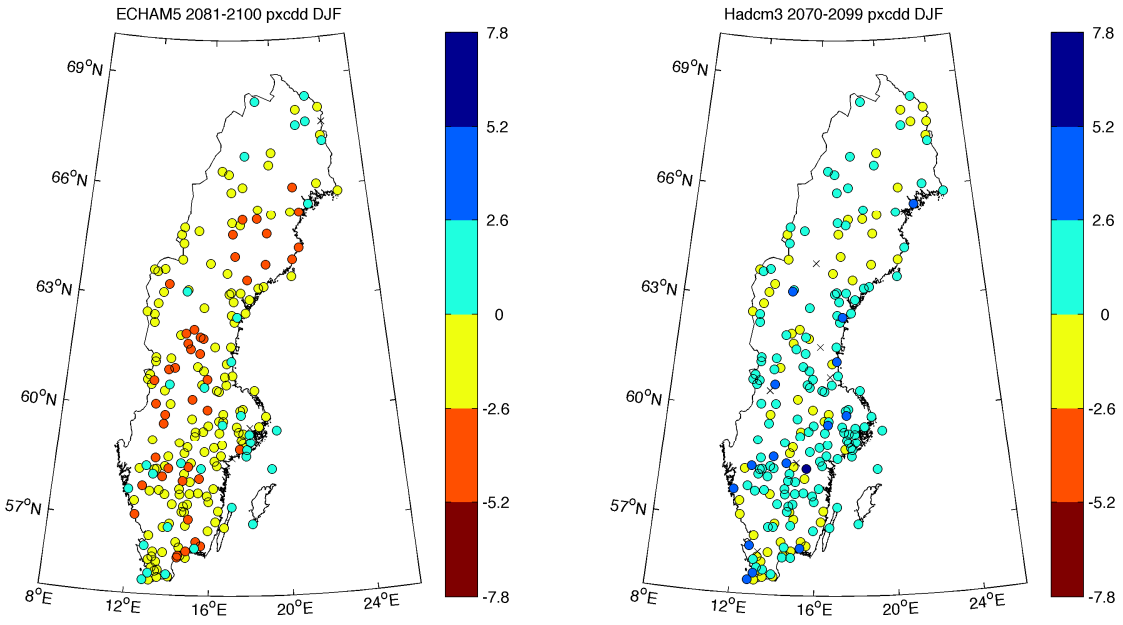
ECHAM5 2081-2100 pxcdd DJF
Hadcm3 2070-2099 pxcdd DJF
69°N
66°N
63°N
60°N
57°N
8°E
12°E
16°E
20°E
24°E
7.8
5.2
2.6
0
-2.6
-5.2
-7.8

a)

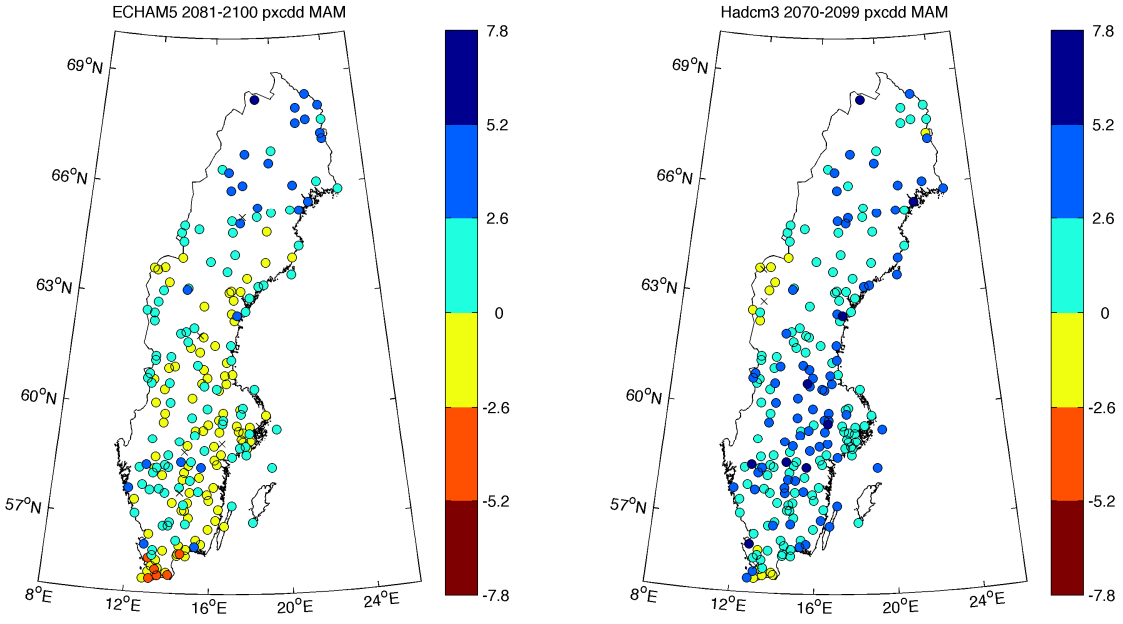
ECHAM5 2081-2100 pxcdd MAM
Hadcm3 2070-2099 pxcdd MAM
69°N
66°N
63°N
60°N
57°N
8°E
12°E
16°E
20°E
24°E
7.8
5.2
2.6
0
-2.6
-5.2
-7.8

b)

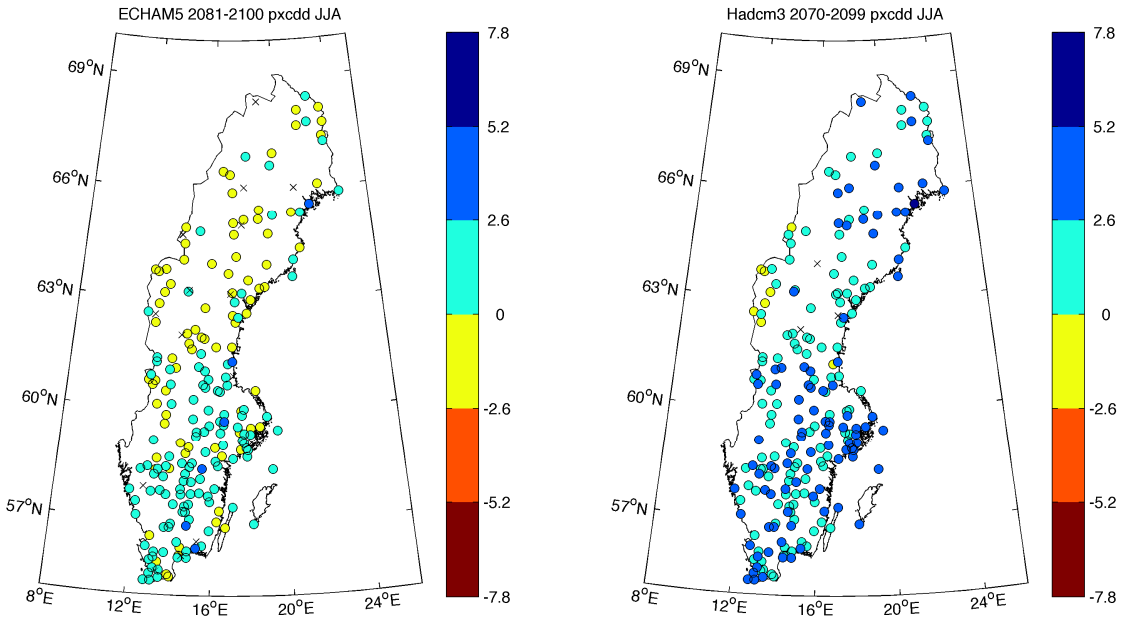

c)

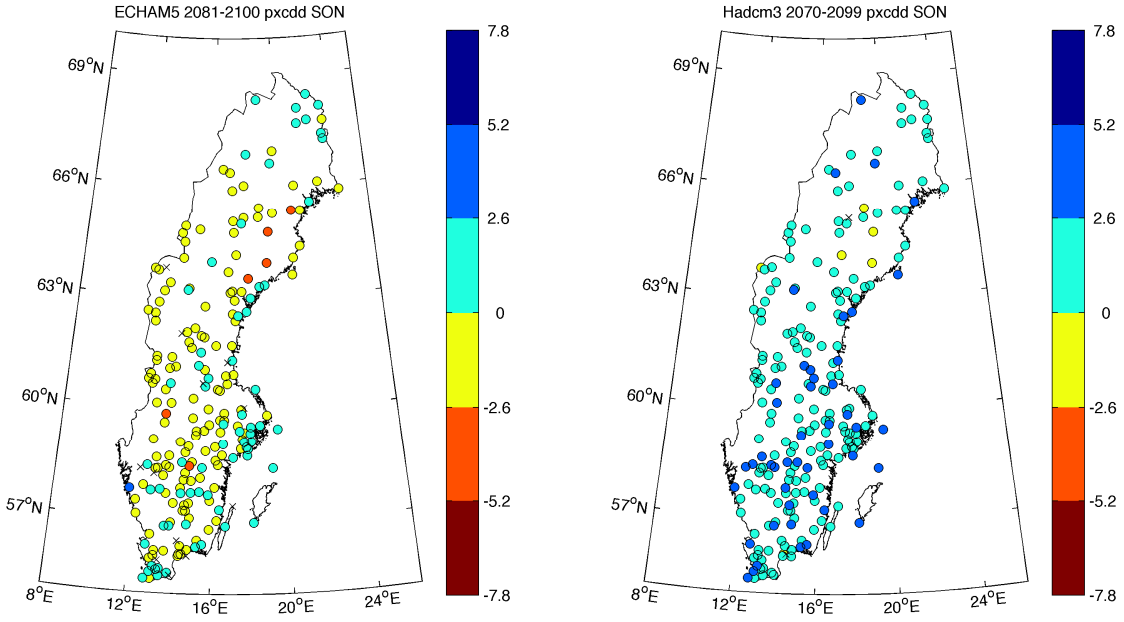

d)

Figure 3.53: Seasonal changes in *pxcdd* (in days) at 220 stations in Sweden derived from WG-simulations based on the ECHAM5 scenario run for the years 2081 to 2100 (left column) and the HadCM3 scenario run for the years 2070 to 2099 (right column). The annual changes are calculated as 'future simulated climate minus observation'. Panel a): winter, b) spring, c) summer, d) autumn.

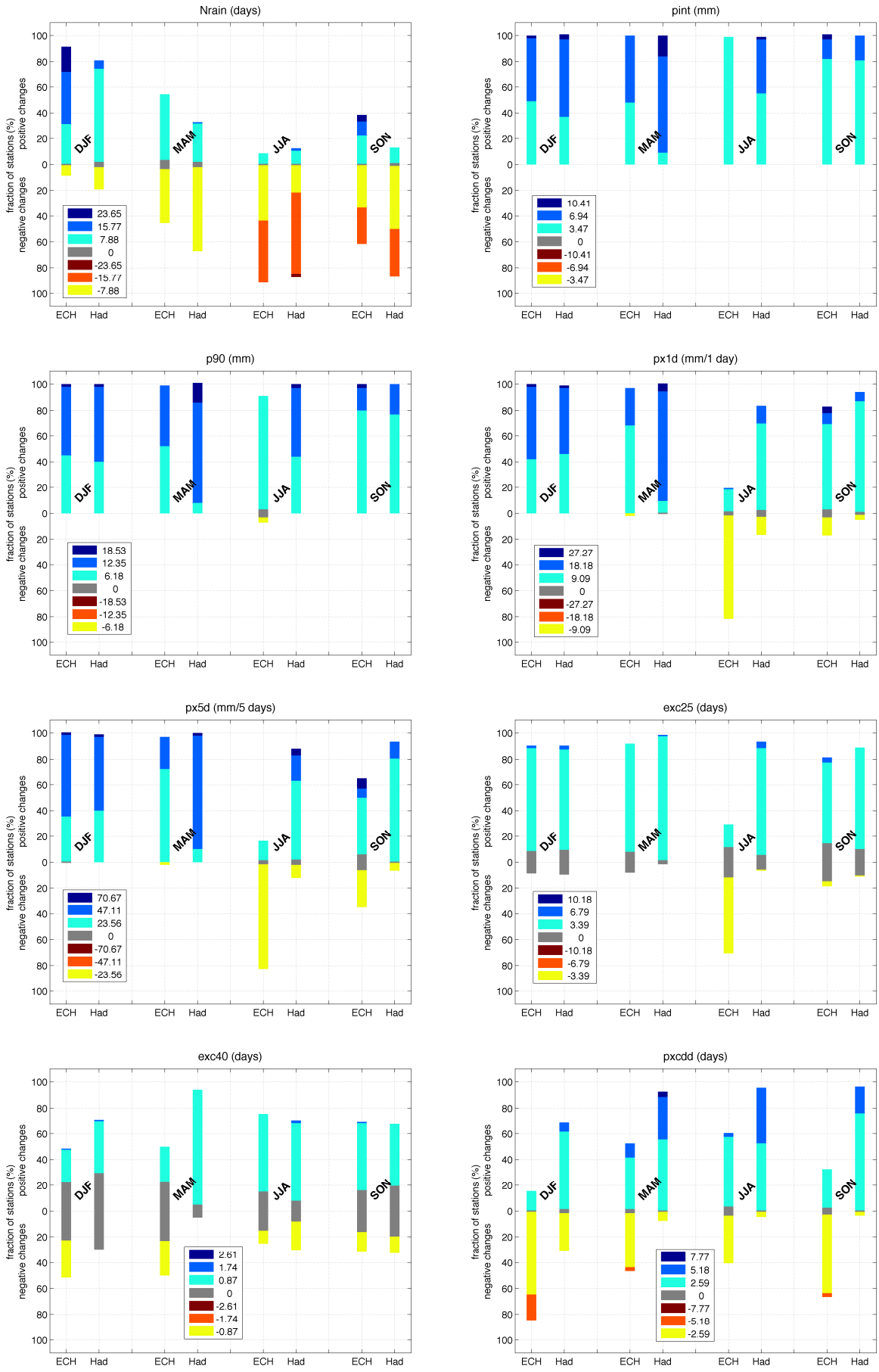

Figure 3.54 (Figure caption see next page).

Figure 3.54: Fraction of stations (%) with positive, zero or negative changes in the seasonal precipitation indices derived from WG-simulations based on the ECHAM5 scenario run for the years 2081 to 2100 and the HadCM3 scenario runs 2070-2099. The various indices are shown in individual panels. In these panels, each bar shows the fraction of stations where the changes are either positive, negative or zero. Positive and negative changes are divided into three classes. The intervals of the classes are given in the legend and their colours correspond to the ones used in Figure 3.46 to 3.53 (positive changes are indicated by bluish colours, negative changes are indicated by reddish colors). The fraction of stations remaining unchanged is indicated by grey. The length of each bar corresponds to 100%. There are two separate bars for each season, one for the ECHAM5-based simulations (left bar) and one for the HadCM3-based simulations (right bar). The various seasons are indicated by: DJF (winter), MAM (spring), JJA (summer) and SON (autumn).

Figure 3.54 and Table 3.2 summarize the results of the seasonal changes in the various indices. Both give the fraction of stations in percent having positive, negative or zero changes in the seasonal precipitation indices. Like in the maps displayed in Figure 3.46 to 3.43, the magnitude of the changes is divided into seven classes (three positive classes, three negative classes, one class for 'no change'). From Figure 3.54, similarities and differences in the local scenarios from the GCMs get obvious. The general picture emerges that the HadCM3-based simulations tend towards wetter conditions in the future. These scenarios partly produce larger changes and wetter conditions for a higher fraction of stations compared to the simulations using ECHAM5 (e.g., *pint, p90, px1d* and *px5d*). In the ECHAM5-based local scenarios, there is a relatively high fraction of stations with negative changes in summer in *px1d*, *px5d* and *exc25* and in all seasons for *pxcdd*. Both GCMs produce rather similar results for *Nrain*, *pint* and *p90*.

Table 3.2: Fraction of stations (%) with positive, zero or negative seasonal changes in the precipitation indices derived from WG-simulations based on the HadCM3 and ECHAM5 scenario climate. The magnitude of the change is divided into seven classes; three classes for negative and positive changes respectively, one class for zero change. The size of the "-" and "+" symbols indicate the various classes; the corresponding intervals and their unit are given in the row for each index.

Index and fraction of staton (%)	**-**	**-**	-	no change	+	+	+
***Nrain* (days)**	**-23.7**	**-15.8**	**-7.9**	**0.00**	**7.9**	**15.8**	**23.7**
H DJF	0	0	17	4	72	7	0
E DJF	0	0	8	1	31	40	20
H MAM	0	0	65	4	30	1	0
E MAM	0	0	42	7	51	0	0
H JJA	3	63	21	1	10	2	0
E JJA	0	48	43	1	8	0	0
H SON	0	37	49	2	12	0	0
E SON	0	28	33	1	22	11	5
***pint* (mm)**	**-10.4**	**-7.0**	**-3.5**	**0.00**	**3.5**	**7.0**	**10.4**
H DJF	0	0	0	0	37	60	4
E DJF	0	0	0	0	49	49	2
H MAM	0	0	0	0	9	75	16
E MAM	0	0	0	0	48	52	0
H JJA	0	0	0	0	55	42	2
E JJA	0	0	0	0	99	0	0
H SON	0	0	0	0	81	19	0
E SON	0	0	0	0	82	15	4
***p90* (mm)**	**-18.5**	**-12.4**	**-6.2**	**0.00**	**6.2**	**12.4**	**18.5**
H DJF	0	0	0	0	40	58	2
E DJF	0	0	0	0	45	53	2
H MAM	0	0	0	0	8	78	15
E MAM	0	0	0	0	52	47	0
H JJA	0	0	0	0	44	53	3
E JJA	0	0	4	6	88	0	0
H SON	0	0	0	0	77	23	0
E SON	0	0	0	0	80	17	3
***px1d* (mm/1-day)**	**-27.3**	**-18.2**	**-9.1**	**0.00**	**9.1**	**18.2**	**27.3**
H DJF	0	0	0	0	46	51	2
E DJF	0	0	0	0	42	56	2
H MAM	0	0	0	1	9	85	6
E MAM	0	0	2	0	68	29	0
H JJA	0	0	14	5	67	14	0
E JJA	0	0	80	3	17	1	0
H SON	0	0	4	2	86	7	0
E SON	0	0	14	6	66	9	5

Table 3.2 continuation

INDEX AND FRACTION OF STATION (%)	-	-	-	NO CHANGE	+	+	+
***px5d* (mm/5-days)**	**-70.7**	**-47.1**	**-23.6**	**0.00**	**23.6**	**47.1**	**70.7**
H DJF	0	0	0	0	40	57	2
E DJF	0	0	0	1	35	63	2
H MAM	0	0	0	0	10	88	2
E MAM	0	0	2	0	72	25	0
H JJA	0	0	10	4	61	20	5
E JJA	0	0	81	3	15	0	0
H SON	0	0	6	1	80	13	0
E SON	0	0	29	12	44	7	8
***exc25* (day)**	**-10.2**	**-6.8**	**-3.4**	**0.00**	**3.4**	**6.8**	**10.2**
H DJF	0	0	0	19	78	3	0
E DJF	0	0	0	17	80	2	0
H MAM	0	0	0	3	96	1	0
E MAM	0	0	0	16	84	0	0
H JJA	0	0	1	11	83	5	0
E JJA	0	0	59	23	18	0	0
H SON	0	0	1	20	79	0	0
E SON	0	0	4	29	63	4	0
***exc40* (day)**	**-2.6**	**-1.7**	**-0.9**	**0.00**	**0.9**	**1.7**	**2.6**
H DJF	0	0	0	59	40	1	0
E DJF	0	0	29	45	25	1	0
H MAM	0	0	0	10	89	0	0
E MAM	0	0	27	46	27	0	0
H JJA	0	0	22	16	60	2	0
E JJA	0	0	10	30	60	0	0
H SON	0	0	13	39	48	0	0
E SON	0	0	15	32	52	1	0
***pxcdd* (day)**	**-7.8**	**-5.2**	**-2.6**	**0.00**	**2.6**	**5.2**	**7.8**
H DJF	0	0	29	3	60	7	0
E DJF	0	20	64	1	15	0	0
H MAM	0	0	7	1	55	33	4
E MAM	0	3	42	3	40	11	0
H JJA	0	0	4	1	52	43	0
E JJA	0	0	37	7	54	3	0
H SON	0	0	3	1	75	21	0
E SON	0	3	61	5	30	0	0

4 Discussion

In this work, a WG was developed to create future daily precipitation series at the local scale for Sweden involving the following steps: 1) generate a site specific stochastic model (WG) simulating daily precipitation time series for the present climate at each of the 220 Swedish stations. Daily precipitation observations at these stations are used to calibrate the parameters of the model. 2) Present day climate simulation and future projections of daily precipitations for Sweden from two global climate models (GCMs), ECHAM5 and HadCM3, are extracted and used to get WG parameters for the present and future climates at the GCMs scale for Sweden. 3) The ratio of the weather generator parameters for the present climate simulated by the GCMs to those calculated for each station falling into the GCM grid box are computed for all the stations. 4) These ratios are assumed to be valid in the future climate. In this way the future parameters for each station under the projected future climate by GCMs can be calculated. 5) Using the estimated future parameters, the WG simulates the future daily precipitation at each station. 6) Finally the simulated daily precipitation for the future is used to compute the six indices. All working steps and the data sets used have their specific certainties and uncertainties, of which the most important ones will be discussed in the following.

The daily precipitation observations used in this study are obtained from the Swedish Meteorological and Hydrological Institute (SMHI) and are considered as certain. Only a very small fraction of the stations really had complete records. Since a large fraction of missing values in the records makes statistical analysis such as deriving extremes, temporal trends in the extremes or the estimation of the parameters for the WG uncertain, only stations having less than 10% missing values were included in the analysis. Finding a suitable threshold for the acceptable number of missing values in the records was therefore a trade off between keeping as many stations as possible and excluding the ones with too many holes.

Climate is permanently changing at various temporal and spatial scales. Changes in tomorrow's climate lying 50, 100 or several hundred years ahead are to be expected regardless what the reasons are for the changes. Studying past climate changes at various time scales allows us to learn about magnitude and rate of earlier changes, where and when they have taken place and eventually also why there was a change. The climate research community has therefore put enormous efforts into studying past climate variability all around the globe using a wide range of different data sources such as observational records as well as proxy data (IPCC, 2007). Knowledge about climate changes in the past allows us to put future changes estimated from climate models into a broader perspective. Prior to the development of the WG described in this report, spatial variability and changes in the Swedish precipitation climate during the past 40 to 50 years were studied within this project (Achberger and Chen, 2006). A large number of different indices describing various aspects of the precipitation climate such as means and extremes were calculated from the same precipitation data set used here. One of the main conclusions is that a clear majority of the stations show trends towards wetter conditions between 1961 and 2004. This finding is generally in line with results from other studies concluding that regions at middle and higher latitudes are becoming wetter and extremes are becoming more frequent and more intense. The past precipitation changes are thus considered as fairly certain. While these trends refer to a rather short period of time, precipitation variability over the past 150 years were studied within the EMULATE project ('European and North Atlantic daily to MULtidecadal climATE variability'). From daily precipitation observations in Southern Scandinavia starting in the beginning of the 19th century, it is obvious that the trend towards wetter conditions and stronger extremes persisted over at least the last 100 years (Moberg et al., 2006; Chen et al., 2006).

Another important result from Achberger and Chen (2006) is that there exists considerably spatial variability in the distribution of the precipitation indices across Sweden. Physiographic factors such as topography, land use, distance to the coast or larger water bodies and the shape of the coastline are factors influencing precipitation generation. Precipitation in connection with convective processes is usually limited to a rather restricted area. Since extremes, especially short time events such as 1-day maximum values or the exceedence of a certain threshold value within one day (i.e., *exc25, exc40*) are often caused by convective precipitation, these events are consequently very local in nature. From the previous analysis we know that Swedish precipitation and its changes are fairly local, which most likely will also be valid for the future.

The success of simulating future daily precipitation at local scale is dependent on several factors such as a) how well the WG-parameters estimated to calibrate the models correspond to the 'real' observed precipitation conditions (i.e., frequency distribution), b) how well the WG simulates rare events (extremes), c) the quality of the GCM used to derive future changes in the WG-parameters, d) the emission scenarios are realistic and e) the downscaling assumption is valid. Each of these points may introduce uncertainties in the simulated precipitation series. While it is impossible at this stage to put numbers on the various uncertainties, they can at least be discussed qualitatively.

Regarding the estimation of the Gamma-parameters, either the 'moment method' or the 'maximum-likelihood method' is usually used. Here, the latter approach was applied since it is generally considered as the statistically more reliable method. However, according to Watterson (2005), the maximum likelihood method tends to underestimate extremes, suggesting the preferred use of the moment method when extremes are to be derived from WG-simulations. If this applies also to Swedish precipitation conditions and to the simulations of this work is not known but could easily be tested. It was found in this work that the WG principally works fine but tends to underestimate extremes. Another way of improving the simulation of extremes could be to apply different probability distribution functions to parts of the distribution of observed daily precipitation. One could chose the Gamma function for all 'common' events up to a certain threshold and a separate second function taking care of the more rare events and extremes. This approach would also be worth testing, but it raises the question of what threshold should be used to divide the observed frequency distributions into the two parts.

A major concern in all studies involving data from climate models is the question to what degree the simulations are reliable and realistic. A range of different circumstances introduces uncertainties into the model results. Generally, all climate models simplify reality since it is impossible to completely simulate the extremely complicated climate system. Another problem is the restricted spatial resolution in the model, dividing the atmosphere, the Earth Surface and the oceans into a large number of model grid boxes of a certain size. Currently the typical size of a GCM box ranges between 1.2°lat x1.2°lon and 3.75°lat x 3.75°lon depending on GCM. Grid boxes of this size only allow are very coarse representation of the properties of the Earth's surface and the processes in the system, and the coarse resolution does not allow for variations of weather and climate within one grid box. Since many important processes in the atmosphere, for instance convective precipitation generation or cloud formation, take place at spatial scales much smaller than the grid boxes, all climate models apply parameterisations including these subgrid-scale processes in a simplified way. These are just a few examples of factors influencing results from climate models (a more comprehensive discussion can be found in Randall et al., 2007). Despite all these uncertainties, today's GCMs are able to realistically simulate features of the recent climate and past climate changes such as the large-scale distribution of e.g., temperature, precipitation and winds as well as the large-scale atmospheric circulation. Furthermore, they are considered to provide credible estimates of future climate changes at continental or larger scales (Randall et al., 2007).

Regardless of the GCM reliability projections of the future climate change are dependent on the emission scenarios used to describe the anthropogenic forcings of the climate system. Today, it is impossible to know in detail how future greenhouse gas emissions will develop in the future since they are highly dependent on demographic, technological and economic developments. Instead, scenarios are created as alternative images of how the future might look like and are useful tools to analyse how varies driving forces may influence future emission levels (IPCC, 2000). These scenarios cover a wide range of realistic assumptions regarding global population growth, economic and technological development. As a consequence, scenarios are to some extent uncertain, even based on the most plausible assumptions. Usually, GCMs are run with several (or two rather different) emission scenarios to simulate a large part of possible future climate changes.

Finally, there are uncertainties associated with the downscaling procedure. Here, the GCM scenarios are downscaled by scaling the GCM-derived WG-parameters to the specific sites using the relationship between the WG-parameters representative for an area of the size of a GCM-grid box and the WG-parameters of the individual sites located within this grid box. In a strict sense, such a relationship between the local scale (i.e., the station sites) and the regional scale (i.e., the GCM grid box scale) is only valid for that period of time for which the relationship was established. A fundamental assumption in statistical downscaling relies on the idea that an empirically established relationship between the two scales even is valid in the future (IPCC, 2001). Whether this is true or not is impossible to test, as there are no ‘observations’ for the future. One way to check the plausibility of this assumption, however, is to divide the period with observations into several shorter records for which the relationships are found individually. If these relationships are close to each other one can conclude that the relation between scales is stable over time. This does not prove that the assumption is valid in the future, but gives a hint about the variability in the relationship.

5 Summary and Conclusion

This report describes the development of a weather generator (WG) to create future daily precipitation series at the local scale for Sweden. WG models were created and simulations of the future precipitation climate were carried out for 220 meteorological stations in Sweden, for which synoptic observations existed for the period 1961 to 2004. The large-scale climate change signal for the simulations of the future local precipitation climate were taken from scenario runs from two GCMs, ECHAM5 and HadCM3. One important objective of the work was to quantify future precipitation extremes, which was done by means of selected indices quantifying extreme intensities and frequencies. These indices were derived from the WG simulations of future local precipitation. A large part of the report therefore focuses on these indices, their changes at annual and seasonal scale as well as how well they are simulated by the WG.

The local precipitation scenarios based on the two GCMs show a general change towards increased precipitation across Sweden on annual scale and in different seasons. In parallel with the decrease in the number of wet days (*Nrain*) on annual scale, daily precipitation intensity (*pint*) increases and there is a clear trend towards stronger extremes in the future. However, the magnitude of the changes depend on index. Deviations from this general rule emerge depending on GCM used and season. Future large-scale changes in the precipitation conditions, as estimated from the difference between the GCM control and scenario runs, are manifested by changes in the parameters of the Gamma-distribution and the four transition probabilities. Changes in the Gamma-parameters indicate an overall increase in precipitation. By means of the site-specific WG-models, this change is translated to the local scale.

To sum up, the most important conclusions from this study are given below:

Local precipitation scenarios:

- The local precipitation scenarios based on HadCM3 and ECHAM5 show that the Swedish precipitation climate – on annual and seasonal scale – becomes generally wetter in the future.
- The magnitude of the change and its geographical distribution varies with index, season and the GCM used for the WG simulation.
- The frequency of wet days (*Nrain*) decreases at many stations on annual scale. In winter, *Nrain* increases almost everywhere, in summer, *Nrain* drops everywhere except in northernmost Sweden (ECHAM5) and in North-West Sweden (HadCM3).
- Daily precipitation intensities *pint* together with the moderate extremes *p90* increase at all stations on annual and seasonal scale. The local scenarios based on the both GCMs give very similar results.
- The one-day (*px1d*) and five-day (*px5d*) maximum amounts increase at the majority of all stations on annual scale as well as in spring and winter. There is a difference in the magnitude of change depending on GCM used.
- The heavy precipitation events *exc25* and *exc40* increase at the majority of all stations on annual scale.
- The seasonal changes in *exc25* and *exc40* vary with GCM. According to HadCM3, *exc25* increase at the majority of all stations in all seasons, *exc40* in spring, summer, and autumn (*exc40*). The ECHAM5-based simulations estimate at many stations either a drop in *exc40* or a zero change in winter, spring and autumn.

- The annual and seasonal changes in the number of consecutive dry days (*pxcdd*) vary with GCM. Especially the ECHAM-based scenarios suggest a decrease in *pxcdd* in autumn and winter, while a rise in *pxcdd* occurs in summer at stations in Southern Sweden. Using HadCM3, *pxcdd* increases at the majority of all stations in all seasons.
- The local scenarios based on HadCM3 often give a larger change (wetter conditions) than the ECHAM5-based scenarios.

GCM precipitation scenarios and changes in GCM-derived WG-parameters:

- Both GCM control runs considerably overestimate annual total precipitation compared to the observations. The difference is related to a significant higher frequency of rainy days in the simulations.
- According to both GCMs, annual precipitation totals increase in the future. This change is related to rising daily precipitation intensities.
- Gamma-α decreases and Gamma-β increases according to the scenario simulations of both GCM. This implies a small increase in daily intensities exceeding 5-7 mm/day.
- The changes in the transition probabilities depend on season and GCM. According to ECHAM5, *p01* (wet day follows a dry day) increases in summer and autumn. HadCM3 suggests a decrease in *p10* (dry day follows a wet day) in all seasons.
- Generally, the changes at local scale agree with the changes at large scale derived from the GCMs.

Development and verification of the weather generator:

- The transition probabilities *p00* and *p11* vary across Sweden in all seasons. *p11* is higher along the Swedish west coast and in parts of Southern and central Sweden. *p00* decreases from South to North (implying more consecutive dry days in Southern Sweden).
- The transition probabilities *p00* and *p11* vary with season: *p00* is higher and *p11* is lower during spring and summer. In autumn and winter, the pattern is reversed.
- The Gamma-parameters vary considerably over the course of the year: α is higher and β is lower during autumn and winter, in spring and summer, the pattern is reversed.
- The agreement between simulated and observed daily precipitation is in general very good but varies slightly depending on month. Deviations are larger in summer and autumn.
- The WG is able to simulate very heavy rainfall events like *exc40*, but tends to underestimate the number of such events.
- The agreement in the spatial distribution of observed and simulated precipitation indices is generally good. Positive as well as negative deviations occur for all indices implying that the differences are not systematic.
- The WG works well in all parts of Sweden.

Acknowledgement

This study is supported by the Swedish Rescue Services Agency through a grant “Extreme rainfall events in Sweden and their importance for local planning”. Additional support to Deliang Chen for this work is provided by the Swedish Science Council (VR) through the project “Past and future extreme climates in relation to atmospheric circulation over Europe: The role played by anthropogenic forcing”. This work is the contribution No.20 from TELLUS, the centre of Earth System Science at University of Gothenburg.

We are grateful to the reference group consisting of Barbro Näslund, Babaro Johansson, Birgit Willner, and Matin Nelden. We have benifted much from the inspiring discusions and practical suggestions during the reference group meetings.

References

Achberger, C. and D. Chen, 2006: Trend of extreme precipitation in Sweden and Norway during 1961-2001. Earth Sciences Centre, C72. Earth Sciences Centre, Göteborg University, Gothenburg, 58 pp.

Benestad, R. E. D. Chen, and I. Hanssen-Bauer, 2008: Empirical-Statistical Downscaling. World Scientific Publishing Co. Pte. Ltd., Singapore, pp 297 (in press).

Beniston, M., and D. B. Stephenson, 2004: Extreme climatic events and their evolution under changing climatic conditions. Global and Planetary Change, 44, 1-9

Beniston, M., 2004: The 2003 heat wave in Europe. A shape of things to come? Geophysical Research Letters, 31, 2022-2026

Brown, B.G. and R.W. Katz, 1995: Regional analysis of temperature extremes: Spatial analog for climate change? Journal of Climate, 8, 108-119.

Chen, D. and A. Walther, A. Moberg, P.D. Jones, J. Jacobeit, D. Lister (2006): Trend Atlas of the EMULATE indices. Research Report C73. Earth Sciences Centre, Göteborg University, Gothenburg, Sweden, 798 pp.

Christensen, J.H., B. Hewitson, A. Busuioc, A. Chen, X. Gao, I. Held, R. Jones, R.K. Kolli, W.-T. Kwon, R. Laprise, V. Magaña Rueda, L., Mearns, C.G. Menéndez, J. Räisänen, A. Rinke, A. Sarr and P. Whetton, 2007: Regional Climate Projections. In: Climate Change 2007: The Physical Science Basis. Contribution of Working Group I to the Fourth Assessment Report of the Intergovernmental Panel on Climate Change [Solomon, S., D. Qin, M. Manning, Z. Chen, M. Marquis, K.B. Averyt, M. Tignor and H.L. Miller (eds.)]. Cambridge University Press, Cambridge, United Kingdom and New York, NY, USA.

Easterling D.R., Meehl G. A., Parmesan C., Changnon S. A., Karl T. R. and L. O. Mearns 2000:. Climate extremes: Observations, modeling, and impacts. Science 289:2068-2074.

Fowler, H.J. and C. G. Kilsby 2003: A regional frequency analysis of United Kingdom extreme rainfall from 1961-2000. International Journal of Climatology, 23, 1313-1334

Frich, P., Alexander L.V., Della-Marta P., Gleason P., Haylock M., Klein-Tank, A. and T. Peterson 2002: Observed coherent changes in climatic extremes during the second half of the 20th Century. Climate Research, 19:193-212.

Groisman, P.Y., Karl, T.R., Easterling, D.R., Knight, R.W., Jamason, P.F., Hennessy, K.J., Suppiah, R., Page, C., Wibig, J., Fortuniak, K., Razuaev, V., Douglas, A., Førland, E. and Zhai, P.: 1999: Changes in the probability of heavy precipitation: important indicators of climatic change. Climatic change, 42, 243-283

Hanssen-Bauer, I., C. Achberger, R. Benestad, D. Chen, and E. Førland, 2005: Empirical-statistical downscaling of climate scenarios over Scandinavia: A review, Climate Research Vol. 29, 255-268.

Haylock, M.R. and C.M. Goodess, 2004: Interannual variability of European extreme winter rainfall an links with mean large-scale circulation. International Journal of Climatology, 24, 759-776

Hundecha, Y. and A. Bardossy, 2005: Trends in daily precipitation and temperature extremes across western Germany in the second half of the 20th century. International Journal of Climatology, 25, 1189-1202

Hutchinson, M., 1995: Stochastic Space-Time Weather Models from Ground-Based Data. Agricultural and Forest Meteorology, 73, 237–265.

IPCC, 2001: Climate Change 2001: The Scientific Basis (J.T. Houghton et al., Eds.) Intergovernmental Panel on Climate Change, Cambridge University Press, 881pp.

Karl, T.R., N. Nicholls and A. Ghazi, 1999: CLIVAR/GCOS/WMO workshop on indices and indicators for climate extremes: Workshop summary. Climatic Change, 42, 3-7.

Katz, R. W. and B. G. Brown, 1992: Extreme events in a changing climate: Variability is more important than averages. Climatic Change, 21, 289-302

Klein Tank, A.M.G. and G.P. Können 2003: Trends in indices in of daily temperature and precipitation extremes in Europe, 1946-1999. Journal of Climate, 16, 3665-3680

Mearns, L.O., R.W. Katz and S.H. Schneider, 1984: Extreme high temperature events: changes in their probabilities and changes in mean temperature. Journal of Climate and Applied Meteorology, 23, 1601–1613

Moberg, A., P.D. Jones, D. Lister, A. Walther, M. Brunet, J. Jacobeit, O. Saladie, J. Sigro, E. Aguilar, P. Della-Marta, J. Luterbacher, P. Yiou, L.V. Alexander, D. Chen, A.M.G. Klein Tank, H. Alexandersson, C. Almarza, I. Auer, M. Barriendos, M. Begert, H. Bergström,R. Böhm, J. Butler, J. Caesar, A. Drebs, D. Founda, F.-W. Gerstengarbe, M. Giusi, T. Jónsson, M. Maugeri, H. Österle, K. Pandzic, M. Petrakis, L. Srnec, R. Tolasz, H. Tuomenvirta, P.C. Werner, H. Linderholm, A. Philipp, H. Wanner, E. Xoplaki, 2006: Indices for daily temperature and precipitation extremes in Europe analysed for the period 1901-2000, /Journal of Geophysical Research/,111, D22106, doi:10.1029/2006JD007103.

Moberg, A. & Jones, P.D. 2005: Trends in indices for extremes in daily temperature and precipitation in central and Western Europe, 1901-99. International Journal of Climatology, 25, 1149-1171.

Nicholls, N. and W. Murray, 1999: Workshop on Indices and Indicators for climate extremes, Asheville, NC, USA, 3-6 June 1999. Breakout Group B: Precipitation. Climatic Change, 42, 23-29.

Randall, D.A., R.A. Wood, S. Bony, R. Colman, T. Fichefet, J. Fyfe, V. Kattsov, A. Pitman, J. Shukla, J. Srinivasan, R.J. Stouffer, A. Sumi and K.E. Taylor, 2007: Climate Models and Their Evaluation. In: Climate Change 2007: The Physical Science Basis. Contribution of Working Group I to the Fourth Assessment Report of the Intergovernmental Panel on Climate Change [Solomon, S., D. Qin, M. Manning, Z. Chen, M. Marquis, K.B. Averyt, M.Tignor and H.L. Miller (eds.)]. Cambridge University Press, Cambridge, United Kingdom and New York, NY, USA.

Richardson CW (1981) Stochastic simulation of daily precipitation, temperature, and solar radiation. Water Resources Research, 17:182–190.

Semenov M.A. and Barrow, E. M. 1997: Use of a stochastic weather generator in the development of climate change scenarios. Climatic Change, 35:397-414.

Schmidli, J. and C. Frei, 2005: Trends in heavy precipitation and wet and dry spells in Switzerland during the 20th century. Int. J. Climat., 25, 753-771

Trenberth, K.E. 1999: Conceptual framework for changes of extremes of the hydrological cycle with climate change. Climatic Change, 42, 327-339.

Watterson, I.G. 2005: Simulated changes due to global warming in the variability of precipitation, and their interpretation using a gamma-distributed stochastic model. Advances in Water Resources 28, 1368-1381.

Wigley, T.M.L. 1985: Impact of extreme events. Nature 316: 106-107

Wilks D.S., 1992: Adapting stochastic weather generation algorithms for climate change studies. Climatic Change 22, 67-84.

Wilks, D.S. and R.L. Wilby, 1999: The weather generation game: a review of stochastic weather models, Progress in Physical Geography.23: 329-357.